INFORMATION TO USERS

This manuscript has been reproduced from the microfilm master. UMI films the text directly from the original or copy submitted. Thus, some thesis and dissertation copies are in typewriter face, while others may be from any type of computer printer.

The quality of this reproduction is dependent upon the quality of the copy submitted. Broken or indistinct print, colored or poor quality illustrations and photographs, print bleedthrough, substandard margins, and improper alignment can adversely affect reproduction.

In the unlikely event that the author did not send UMI a complete manuscript and there are missing pages, these will be noted. Also, if unauthorized copyright material had to be removed, a note will indicate the deletion.

Oversize materials (e.g., maps, drawings, charts) are reproduced by sectioning the original, beginning at the upper left-hand corner and continuing from left to right in equal sections with small overlaps. Each original is also photographed in one exposure and is included in reduced form at the back of the book.

Photographs included in the original manuscript have been reproduced xerographically in this copy. Higher quality 6" x 9" black and white photographic prints are available for any photographs or illustrations appearing in this copy for an additional charge. Contact UMI directly to order.

UMI

A Bell & Howell Information Company
300 North Zeeb Road, Ann Arbor MI 48106-1346 USA
313/761-4700 800/521-0600

PATTERN AND PROCESS IN VOLCANO SEISMOLOGY

A

THESIS

Presented to the Faculty

of the University of Alaska Fairbanks

in Partial Fulfillment of the Requirements

for the Degree of

DOCTOR OF PHILOSOPHY

By

John Paul Benoit, B.S.

Fairbanks, Alaska

May 1998

PATTERN AND PROCESS IN VOLCANO SEISMOLOGY

By

John Paul Benoit

RECOMMENDED:

Prof. Max Wyss

Prof. John Eichelberger

Dr. Roger Hansen, State Seismologist

Research Prof. Stephen McNutt,
Advisory Committee Chair

Associate Prof. Paul Layer,
Department Head

APPROVED:

Prof. Paul Reichardt,
Dean, College of Natural Science,
Engineering, and Mathematics

Prof. Joseph Kan,
Dean of the Graduate School

6-2-95

Date

ABSTRACT

The patterns of occurrence and the underlying processes of two important seismological phenomena at volcanoes, earthquake swarms and volcanic tremor, were investigated. A global database of volcanic earthquake swarm parameters was compiled and was used to evaluate the March 10-14, 1996 seismo-volcanic crisis at Akutan Volcano, Alaska. Earthquake swarm durations and magnitudes were compared with eruptive activity using this database. Trends identified using the database suggest that the Akutan swarm was not precursory and, no eruption occurred. We postulate that a deep intrusion with a large opening component occurred under the flanks of Akutan. The global swarm database has provided an important baseline and has proved to be useful in preparing eruption scenarios for public information releases.

The duration-amplitude distribution or frequency-size scaling of volcanic tremor was also examined. The hypothesis tested was that the duration-amplitude distribution may be approximated by an exponential function. The exponential model, implying a scale-bound source process, is found to be a better fit to data then a power-law (scale invariant) model. The exponential model gives a satisfactory description of tremor associated with a wide range of volcanic activity. We propose that exponential scaling of tremor amplitude is due to fixed source geometry driven by a variable excess pressures. This implies that the characteristic amplitude of the duration-amplitude distribution is proportional to a geometric dimension of the source.

Broadband seismic data recorded at Arenal volcano, Costa Rica, provide new constraints on tremor source processes. Arenal's tremor contains as many as seven harmonics, whose frequencies vary temporally. This source is inferred to be a shallow, 200-660 m-long resonator, radiating seismic energy from displacement antinodes. We infer that the resonator is gas-charged magma with variable bubble concentration within the conduit and also changes as a function of time, thereby changing the acoustic velocity and the boundary conditions. Polarization analyses for the fundamental mode show particle motion azimuths abruptly rotating, which may be explained by a decrease in incidence angle near the recording site. We suggest that energy for this mode is radiated predominantly from a displacement antinode that is changing position with time.

Table of Contents

Chapter 1

Thesis Introduction

Chapter 2

Use of a global database of volcanic earthquake swarms during the 1996 seismo-volcanic crisis at Akutan volcano, Alaska

Appendix 2A

Development and Description of the Global Volcanic Earthquake Swarm Database

Chapter 3

The Duration-Amplitude Distribution of Volcanic Tremor

Appendix 3A

Appendix 3B

Appendix 3C

Chapter 4

New Constraints on Source Processes of Volcanic Tremor at Arenal Volcano, Costa Rica, Using Broadband Seismic Data

Appendix 4A

Chapter 5

Thesis Conclusion

List of Figures

Chapter 2

Chapter 3

Chapter 4

List of Tables

Chapter 2

Chapter 3

Acknowledgements

This thesis would not be possible without a great deal of support and encouragement from many people. I sincerely thank my primary advisor and committee chairman, Dr. Stephen McNutt, for his sound scientific guidance, unending encouragement, and most of all, for his friendship. I also thank him for my introduction to the wonders of flying red rocks, a moment that I will never forget.

I extend my sincere gratitude to my advisory committee Drs. Max Wyss, John Eichelberger, Roger Hansen, and Juergen Kienle, whom have contributed in many ways to this body of work and to my experience in Alaska. I thank Drs. David Stone, Douglas Christensen, and Paul Layer for the many discussions at the lunch table and on Friday afternoons, which has taught me many things, including, not all science is done behind a computer.

My special thanks go to my friends and cohorts of the third floor of the Geophysical Institute. In particular Stefan Wiemer, Zhong Lu, Hilary Fletcher, Arthur Jolly, Kent Lindquist, Guy Tytgat, Vicki McConnell, John Power, Milton Garces, and Mitch Robinson deserve special mention for helping me, in their own ways, complete this body of work.

To my family whom has continually supported me in all of my endeavors, I extend my sincere appreciation. I am especially indebted to Rubai Xie, whom enabled me to finish this thesis before the turn of the millennium. Finally, I thank my dear Katherine, without her support and encouragement none of this could be possible.

I acknowledge the Alaska Volcano Observatory for my continuous support throughout my thesis work.

Chapter 1

Thesis Introduction

1.0 General Introduction

A primary goal of Volcanology is to provide an assessment of the hazards posed by the world's volcanoes, and of particular societal importance is the question of forecasting the time, type, and magnitude of volcanic eruptions. To accomplish this objective, a basic understanding of the physical processes involved in the ascent of magma to the surface is required. The science of Volcanology is still relativity young and a theoretical framework of the physical processes has been sketched out in only the most general terms. At this young stage, much remains to be gained through observational studies and exploratory analyses of the data collected at the world's volcanoes.

Geological studies can provide important constraints on the size, types of eruptive activity, and eruption mechanisms. However, these studies are of limited use for the short-term forecasting of an eruption. Geophysical monitoring of active volcanoes can provide the data necessary to forecast these events. Experience gained at well-monitored volcanoes clearly indicate that most, perhaps all, eruptions are preceded and accompanied by measurable geophysical changes in the state of the volcano [*Tilling*, 1989]. Several monitoring strategies have been employed to detect these changes, including: seismology, ground deformation, geochemistry, thermal, and potential fields methods. Seismological monitoring has the longest and most successful history of detecting precursory changes before eruptions. Beginning with the pioneering work by *Omori* [1914] in Japan and *Wood* [1915] in Hawaii, significant changes in

seismicity were shown to occur before eruptions. Since these early works, seismology has emerged as the primary tool for volcano monitoring. Today, about one out of three volcanoes that has erupted in historical time is monitored by some type of seismic instrumentation [*McNutt*, 1996].

Seismic monitoring is most effective when it can be continuously carried out through entire eruptive cycles, including periods of quiescence, precursors, and eruptions [*Swanson et al.*, 1983; 1985]. Unfortunately, very few volcanoes have been monitored over an entire eruptive cycle with a full array of seismic instrumentation. This situation presents a common scenario; unrest begins at a long-inactive and unmonitored volcano and the lack of background data renders results difficult to interpret, even after monitoring has begun. The interpretation of the data is further hindered by the lack of adequate theoretical models of the physical processes associated with the ascent of magma. The most successful prognoses for monitoring are based on recognition of patterns seen earlier [*Swanson et al.*, 1983; 1985], and given that many characteristics are common to many volcanoes, a compilation and analysis of case histories of unrest may reveal these patterns. An understanding of these patterns can then be used to construct models of the physical processes involved. Finally, these models can be tested against forecasts of future activity. The results of these tests can then be analyzed and used to improve the models.

This thesis will explore in detail the patterns of occurrence of two commonly recorded seismological phenomena at volcanoes, earthquake swarms and volcanic tremor. The presence and characteristics of both swarms and tremor have been shown to be useful towards the goal of forecasting of the time, type, and magnitude of an eruption [e.g. *McNutt*, 1996], in addition to being scientifically interesting in their own right. Earthquake swarms are defined as series of earthquakes occurring closely in space and time without a single outstanding main shock [*Mogi*, 1963], and are pervasive in volcanic areas. These swarms are perhaps the most important

indicator of an impending eruption, yet they have rarely been studied systematically. Volcanic tremor is a continuous seismic signal that accompanies virtually all eruptions. The source processes of volcanic tremor is related to pressure fluctuations associated with transport and degassing of magma. Tremor is therefore a prime target to gain understanding of the processes associated with the ascent of magma and refine forecasts of both the types and magnitudes of eruptions.

1.1 An overview of the chapters

This thesis is divided into five chapters: this general introduction, three journal article manuscripts, and general conclusions. Each of the journal article manuscripts is preceded by an introduction and followed with conclusions specific to that chapter. The progression of chapters is intended to move from a very broad global study to a very specific topical study and does not reflect the order in which the work was completed.

The first manuscript (Chapter 2) explores the relationships between volcanic earthquake swarms and volcanic activity. Global data from 1979 to 1989 pertaining to volcanic earthquake swarms have been compiled into a relational database. This database is composed of three parts: a section containing general information on volcanoes, a section containing earthquake swarm data (such as dates of swarm occurrence and durations), and a section containing eruption information. The primary objective of this study is to generate a global baseline for comparison with future seismic activity, to quantify the duration of volcanic earthquake swarms, and to expose general relationships between volcanic swarms and eruptions. These relationships are then tested during a seismo-volcanic crisis that occurred on Akutan Island in March 1996. This chapter was submitted (December 1997) to the *Journal of Volcanology and Geothermal Research*.

Part of this project is exploratory in nature, a hypothesis-generating project. Through the act of compiling such a data set several patterns have emerged. New hypotheses can be defined and subsequently tested with the collection of new data. For example, the repose period between eruptions appears to be related to the duration of the preceding swarm [*Benoit and McNutt*, 1996a]. For a subset of swarms, the longer the repose period between eruptions, the longer the duration of the preceding swarm. A second example is the Generic Volcanic Earthquake Swarm Model [*McNutt and Benoit*, 1995], which outlines a series of processes and their associated seismicity throughout an eruption cycle. This model emerged from the examination of hundreds of swarms and will provide a framework with which to more fully evaluate seismic unrest.

Due to the large size of the swarm database, over 350 pages, I chose not to include the entire database within this thesis. However, two parts of the database are included in Appendix 2A for reference. The appendix is excerpted from a US Geological Survey Open-file Report [*Benoit and McNutt*, 1996b], and describes in detail, the structure of the database and how the swarm data were complied. The third section of the database, the eruption table, is also included. The data contained in the eruption table compares eruptive activity with parameters measured for earthquake swarms.

In the next chapter, (Chapter 3) we investigate the patterns of occurrence of volcanic tremor. This chapter focuses on modelling a fundamental property of tremor, the relationship between its frequency of occurrence and size. This frequency-size distribution is tested against two statistical models: a power-law and an exponential model. The exponential model, implying a scale-bound source process, is compared with a power-law (scale invariant) model. The models are tested at several volcanoes for tremor associated with a range of volcanic activity, including tremor associated with magmatic and phreatic eruptions, shallow and deep source regions, and geothermal sources. This study then examines and provides evidence against the hypothesis that

tremor is composed of a series of low-frequency events spaced closely in time. Finally, we suggest that these scaling parameters may prove to be useful to distinguish eruptive from non-eruptive tremor.

Three appendices follow chapter 3. The first appendix defines the normalized metric (reduced displacement) used in this study and how it is estimated from other amplitude measures. The second appendix outlines a technique to measure tremor amplitudes more accurately, and the third appendix shows duration amplitude measurements for acoustic data recorded at Arenal volcano. This chapter, less the appendices, will be submitted to the *Journal of Geophysical Research.*

Chapter 4 is a topical study that examines the spectral and polarization characteristics of tremor recorded at Arenal volcano, Costa Rica. From this analysis we developed a new model for the generation of tremor at Arenal. This model provides constraints on shallow degassing processes within the shallow conduit. Spectral and polarization analyses are performed on broadband seismic recordings made by us at Arenal volcano in the spring of 1994. Analyses of the tremor associated with small explosive eruptions clearly show patterns in the spectra and particle motion polarizations. The proposed model suggests that these patterns are the resonance modes of a gas-charged magma-filled conduit and the rapid changes are due to degassing of the magma at shallow depths within the conduit.

The main body of Chapter 4 is published in *Geophysical Research Letters* [*Benoit and McNutt*, 1997]. This manuscript was expanded to include forward modeling of surface waves. Appendix 4A outlines the method and source code used to calculate the Love-wave dispersion curves.

The final chapter (Chapter 5) presents the general conclusions of this thesis, along with an outline for future research directions.

1.2 References

Benoit, J. P. and S. R. McNutt, New constraints on source processes of volcanic tremor at Arenal volcano, Costa Rica, using broadband seismic data, *Geophys. Res. Lett.*, 24, 449-452, 1997.

McNutt, S. R. and J. P. Benoit, Generic Earthquake Swarm Model, (extended abs.), *Periodico di Mineralogia*, 64, 229-230, 1995.

McNutt, S. R., Seismic monitoring and eruption forecasting of volcanoes: A review of the state-of-the-art and case histories, *in*: Monitoring and mitigation of volcano hazards, R. Scarpa and R. I. Tilling eds., Springer-Verlag, Berlin, 99-146, 1996.

Omori, F., The Sakura-jima eruptions and earthquakes, *Bull. Imp. Earthquake Invest. Comm.*, 8, No. 1-6, 525 p., 1914.

Swanson, D. A., T. J. Casadevall, D. Dzurisin, S. D. Malone, C. G. Newhall, and C. S. Weaver, Predicting eruptions at Mount St. Helens, June 1980 through December 1982, *Science*, *221*, 1369-1376, 1983.

Swanson, D. A., T. J. Casadevall, D. Dzurisin, R. T. Holcomb, C. G. Newhall, S. D. Malone, and C. S. Weaver, Forecasts and prediction eruptive activity at Mount St. Helens, U.S.A.: 1975-1984, J. *Geodynamics*, 3, 397-423, 1985.

Tilling, R. I., *Volcanic hazards*, Tilling, R. I., ed., American Geophysical Union, Washington D.C., 123 p., 1989.

Wood, H. O., The seismic prelude to the 1914 eruption of Mauna Loa, Bull. Seismol. Soc. Am., 5 39-50, 1915.

Chapter 2

Use of a global database of volcanic earthquake swarms during the 1996 seismo-volcanic crisis at Akutan volcano, Alaska[1]

2.0 Abstract

We compiled a global database of volcanic earthquake swarm parameters to study the relationship between swarms and eruptions. We used the database to evaluate the March 10-14 1996 seismo-volcanic crisis at Akutan Volcano, (54N08', 165W58'), Alaska. In particular, we compared volcanic earthquake swarm durations and magnitudes of the largest earthquakes with eruptive activity using the swarm database. We also used the database as a tool to develop and constrain eruptive scenarios during the Akutan crisis. For precursory earthquake swarms, durations and magnitudes were compared to the Volcanic Explosivity Index (VEI) of the associated eruption. We tested the hypothesis that longer, more energetic swarms precede larger, more explosive eruptions. We find that swarms preceding eruptions last longer than those not associated with eruptions. The median swarm durations are 9 and 3.7 days respectively. The distributions of the magnitudes of the largest earthquakes within precursory swarms show no significant difference with non-precursory swarms. We examined the distributions of both durations and magnitudes within each VEI category. For less explosive eruptions (VEI 0-3), there appears to be no clear relationship between the swarm duration and the VEI. However, when larger, more explosive eruptions are considered (VEI 3-6), the mean of swarm durations increases as the explosivity of the eruptions increases. A similar positive correlation is apparent when the magnitude of the largest earthquake within a swarm (M_{max}) is compared to the VEI. For eruptions of VEI 2 or greater, the mean magnitude of the largest precursory earthquake shows an increase with increasing explosivity. The largest shock and the duration of a precursory swarm are parameters reflecting the total seismic energy released. For more explosive eruptions (VEI 3-6) the above results support the hypothesis that more energetic earthquake swarms precede more explosive eruptions.

---

[1]Benoit, J. P. and S. R. McNutt, submitted to *Journal of Volcanology and Geothermal Research*, December 1997.

A strong earthquake swarm consisting of two pulses occurred at Akutan on March 10-11 and 13-14, 1996. No eruption followed these swarms. The strength of the Akutan swarms was much larger than global observations of volcanic swarms. Within 4 days local residents felt over 3000 earthquakes. The largest events were a $m_b = 4.7$ ($M_L = 5.1$), and a $m_b = 4.6$ ($M_L = 5.3$), and the swarms contained at least 18 events with $m_b > 4.0$. To assess the character of these swarms, we compared the Akutan swarm with the global database. The comparison yielded only 3 out of 700 cases with similar numbers of felt events and only 21 cases with shocks of equal or larger magnitudes. The M_{max} of these swarms are not a reliable indicator of the likelihood of occurrence of an impending eruption. However, the database shows that flank eruptions are more often preceded by large shocks. Assuming that an eruption was imminent at Akutan, from these trends we would forecast a large flank eruption. The durations of the Akutan swarms (24 and 18 hrs. of intense activity and 3.5 days in total duration) are relativity short when compared to global data. The database durations thus suggest that the Akutan swarm was not precursory. We postulate that a deep intrusion with a large opening component occurred under the flanks of Akutan. The global swarm database has provided an important baseline and has proved to be very useful in preparing eruption scenarios for public information releases. This is especially true for volcanoes, such as Akutan, which had little or no monitoring history at the time of the March 1996 swarm.

2.1 Introduction

Earthquake swarms are pervasive at volcanoes, but have seldom been studied systematically. Most swarms that are described in the literature are those that occurred in association with eruptions; indeed, earthquake swarms are the most reliable method of forecasting eruptions. Because swarms are such a common and important phenomenon, we undertook a systematic and comprehensive study of swarms at volcanoes. An eleven-year period (1979-1989) was chosen, and summary parameters from over 700 swarms were compiled. We term the result the Global Volcanic Earthquake Swarm Database (GVESD). The database and a detailed description of parameters are given in *Benoit and McNutt*, [1996a; 1996b].

One of the primary goals of the swarm database is to provide a basic monitoring tool for volcanoes with little or no seismological monitoring history. At such a volcano, the evaluation of a swarm can prove to be problematic. Is the swarm unusual? How does this swarm compare to other swarms at similar volcanoes? Did eruptions follow the similar swarms? If an eruption did follow the swarm, what type of eruption and how big? The GVESD can provide constraints or a range of possible outcomes to these types of questions. A query of the database quickly gives a list of case histories that share some attribute with the swarm in question. These queries can be complex involving many relationships across the database. For example, we can query the database for precursory swarms that occurred at a stratovolcano, lasted longer than 3 days, and contained a M5 earthquake. Such a set of case histories from a global data set can be valuable during a crisis response because they can be used as a basis for constructing eruptive scenarios. These data are not only useful to form a probabilistic judgement during a crisis but also provide constraints for more detailed studies of the underlying processes.

On March 11, 1996 a vigorous swarm of felt earthquakes began at Akutan volcano (54N08', 165W58') in Alaska's Aleutian Islands. A crisis quickly developed as more than 3000 earthquakes were felt by the residents of Akutan village 13 km east of the summit. No local instrumental seismic monitoring of the volcano existed at the onset of the crisis, so there was no baseline of data for comparison. Instead, this crisis provided a field test of the utility of the swarm database. As the crisis developed, the database was repeatedly queried and the results were compared to the observations at Akutan. These results and previous work with the database became an important component in evaluating the crisis and building possible eruptive scenarios for the residents of Akutan village and the emergency response community.

In this paper we review the data included within the GVESD and how they were compiled. We next examine several relationships between swarm parameters and eruptive activity, and

finally, we show how the GVESD was used during the March 1996 seismo-volcanic crisis at Akutan volcano, Alaska.

2.2 Global Volcanic Earthquake Swarm Database (GVESD)

The GVESD is compiled from 11 years (1979-1989) of data as reported in the Bulletin of Volcanic Eruptions (BVE) of the Volcanological Society of Japan. We chose BVE as our primary data source for several reasons. First, it contains data on many swarms that were never reported in the reviewed literature. This is because most papers report eruptions, and swarms are included only if they were associated with eruptions. In other words, the reviewed literature is biased in favor of swarms followed by eruptions, whereas BVE more fully reports a variety of activities during times of no eruptions. Second, BVE is prepared once per year, which gives investigators the opportunity to summarize data on a broad time scale. Monthly reports, such as the Smithsonian Institution Global Volcanism Network Bulletin often focus more narrowly on the necessarily short (one month) time scale. Third, the BVE includes a section devoted to miscellaneous information. The miscellaneous information section includes many reports of seismic activity at volcanoes that were not in eruption that year. Finally, BVE includes a supplement, which is used to provide additional information on previous years' activity. This systematic updating provides an additional element of quality control, which is not found in most standard reports.

The time period, 1979 to 1989, was chosen to include several well-studied swarms that occurred at Mt. St. Helens, Etna, Kilauea, Augustine, Redoubt, O-Shima, and Izu-Tobu. A cogent effort was made not only to focus on the well-studied swarms, but also to include smaller, less well known swarms and swarms not associated with eruptions. Since very large eruptions occur

relatively infrequently, swarms associated with very large eruptions were poorly represented in the database. This gap was filled by adding selected swarms and associated eruptions (e.g., Sakurajima 1914 and 1955, Paricutin 1943, Bezymianny 1955, Shevelluch 1964, and Pinatubo 1990) which occurred outside the 1979-89 time window.

The GVESD is composed of three main tables. The first table contains general information on volcanoes that were active during the study period. This table includes the location, elevation, morphology, and the range of eruptive products. The second table contains earthquake swarm data. The parameters included are: dates of swarm occurrence, swarm duration, numbers of events (felt and unfelt), event type, magnitude of the largest event, maximum felt intensity, energy (rate released and cumulative), average b-values, and basic instrumental information (e.g. detection threshold) as well as errors associated with some of these parameters. A third parallel table contains information pertaining to eruptive activity, including dates of activity, eruption intensity, and the character of the eruption.

It was our initial intention to perform a full multi-parametric study of the database. However, it quickly became apparent that durations and the magnitudes of the largest earthquake (M_{max}) were the most widely reported parameters, whereas many other parameters were poorly reported (e.g., energy, cumulative seismic energy release, detection threshold, b-value). Thus we have focused our initial efforts on understanding the distributions of swarm durations and M_{max}, and their relation to eruptive activity.

2.3 Results from the GVESD

Out of a total of 700 swarms, the database lists 385 cases which include swarm duration and 180 cases which include the M_{max}. These large samples give robust estimates of the mean,

median, and standard deviation of the duration and M_{max} distributions. These parameters then were sub-divided according to their relationships to eruptions.

2.3.1 Swarm duration

Earthquake swarms are generally defined as a sequence of events closely clustered in time and space without a single outstanding shock [*Mogi*, 1963]. Our working definition follows Mogi's general outline and also requires a significant increase in the rate of local volcanic earthquakes above the background rate. We take volcanic earthquakes to be of any type, for example A, B, [Minakami, 1960], high frequency, low frequency, short period, long period, [*Koyanagi et al.*, 1987], volcano tectonic, [*Latter*, 1981], explosion events, etc., but they must occur within an arbitrary near distance to the volcano (typically < 15 km). We do not identify a significant increase over the background rate in a strict statistical sense, but accept the experience and point of view of each reporter. In other words, if the reporter feels that an increase in seismicity is significant enough to report, then we include that report as a swarm record along with a quality modifier. We also do not consider seismic crises (peak seismicity rates within a swarm), obvious mainshock-aftershock sequences, or tremor episodes as swarms.

This working definition was developed through the systematic examination of over 700 swarms. One single fixed definition or algorithm is preferable, but is not feasible due to the widely varying qualities and formats of the data. Future studies would greatly benefit from standardized reporting and the strict application of an algorithm to distinguish the starts, ends and durations of swarms [e.g., *Evison and Rhoades*, 1993].

Swarm duration varies from very short, intense swarms lasting less than an hour, such as those reported at Piton de la Fournaise and Kilauea, to swarms lasting several years, such as those recorded at Long Valley and Usu calderas (Usu at 1682 days is the longest swarm in the

database). The median duration of 385 swarms was found to be one week [*Benoit and McNutt*, 1996b].

Swarm durations were then separated based on their relationship to eruptive activity: those that preceded eruptions (precursory) and those not associated with eruptions (non-precursory). Occasionally, eruptions begin some time after a swarm ends. For example, the 1989 Izu-Tobu eruption commenced ~2 days after the end of a 6 day long volcano-tectonic swarm. Approximately one quarter of all precursory swarms in the database display a seismicity rate decrease or quiescence before the onset of an eruption. To account for these cases, we consider swarms precursory when an eruption begins within three months after a swarm ends. The three month cut-off was determined by examining the interval between the end of swarms and the beginning of eruptions. In two-thirds of swarms showing quiescence, an eruption occurred within 10 days, and 80% occurred within 3 months. The three months cut-off interval is also used in the *Volcanoes of the World*, a global catalog of volcanoes and eruptions, [*Simkin and Seibert*, 1994] to distinguish eruptive episodes from eruptions.

The durations of the precursory swarms tend to be longer than non-precursory swarms (Figure 2.1). The median duration of precursory swarms was found be more than twice that of non-precursory swarms, 9 and 3.7 days respectively. The distributions mean durations are 8 and 3.5 days, with a standard deviations of 0.79 and 0.91 log-days, and 95% confidence limits of 0.11 and 0.15 log-days for precursory and non-precursory swarms, respectively. The mean of these distributions were found to be significantly different from one another (at the 95% confidence level using a t-test), in other words the durations of each swarm type are drawn from different parent populations [*Benoit and McNutt*, 1996b].

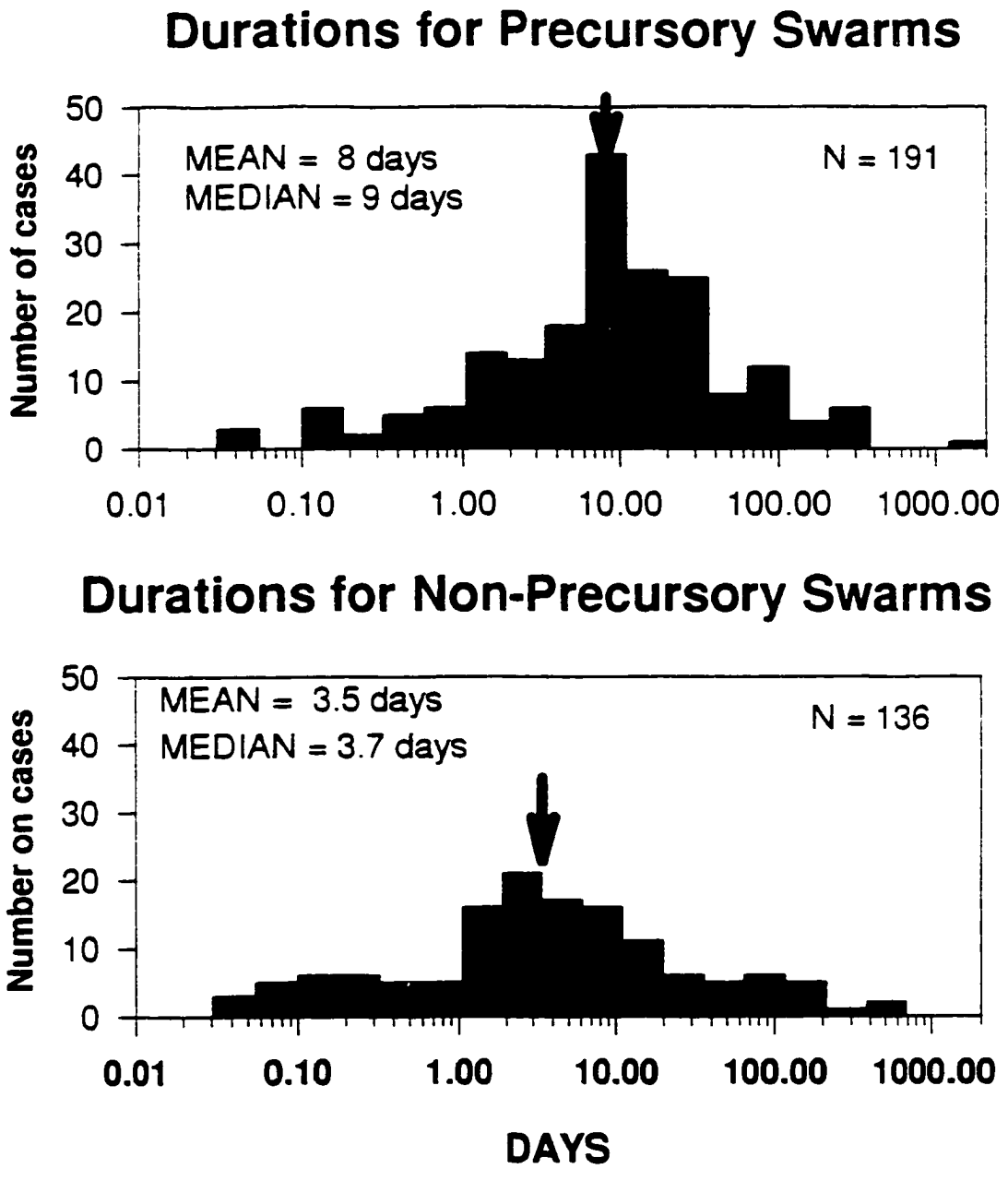

Figure 2.1 Earthquake swarm durations and their association with eruptions. Comparison of the distribution of 191 swarm durations that precede eruptive activity (precursory) and 136 durations that are not associated with eruptive activity (non-precursory). The geometric means are 8 and 3.5 days (marked with bold arrows), and the medians 9 and 3.7 days for precursory and non-precursory swarms, respectively.

2.3.2 Swarm duration and eruption explosivity

The durations of precursory swarms were then compared to the explosivities of the following eruptions. We wish to know whether swarm durations vary significantly with eruption size. The Volcanic Explosivity Index (VEI) [*Newhall and Self*, 1982] is used to parameterize the explosivity (size) of the eruptions which followed swarms; note that each increase of one unit in VEI corresponds to one order of magnitude in tephra volume. Figure 2.2 gives the number of cases, and the mean, median, and quartiles for each distribution. Additional descriptive statistics are given in Table 2.1. The distribution of swarms preceding VEI 0 eruptions is the most compact as measured by the 95% confidence limits. This distribution is primarily composed of cases from Kilauea volcano and therefore mainly represents effusive basaltic eruptions at Kilauea. The VEI 1 and 2 classes span Strombolian eruptions. Slightly longer swarms precede the larger Strombolian eruptions, however the distributions are similar. VEI 3 and larger eruptions are basically all sub-Plinian to Plinian eruptions involving larger volumes of erupted material. For swarms preceding VEI 3 and larger eruptions, the mean durations show a positively correlated trend with the VEI. Unfortunately, the trend is not statistically significant due to the small number of cases for the largest eruptions. More data are needed on VEI 5 and greater eruptions to establish formal significance of the correlation.

Table 2.1 **Swarm duration statistics by the size of the following eruption.**

VEI	*number of cases*	*median (days)*	*mean (days)*	*std. dev. (log days)*	*95% conf. interval (log days)*
0	45	11	7.9	0.54	0.16
1	50	6	4.8	0.86	0.27
2	30	12	6.1	0.88	0.37
3	26	9	6.7	1.02	0.44
4	5	45	30	0.44	0.55
5	2	41	41	-	-
6	1	-	-	-	-

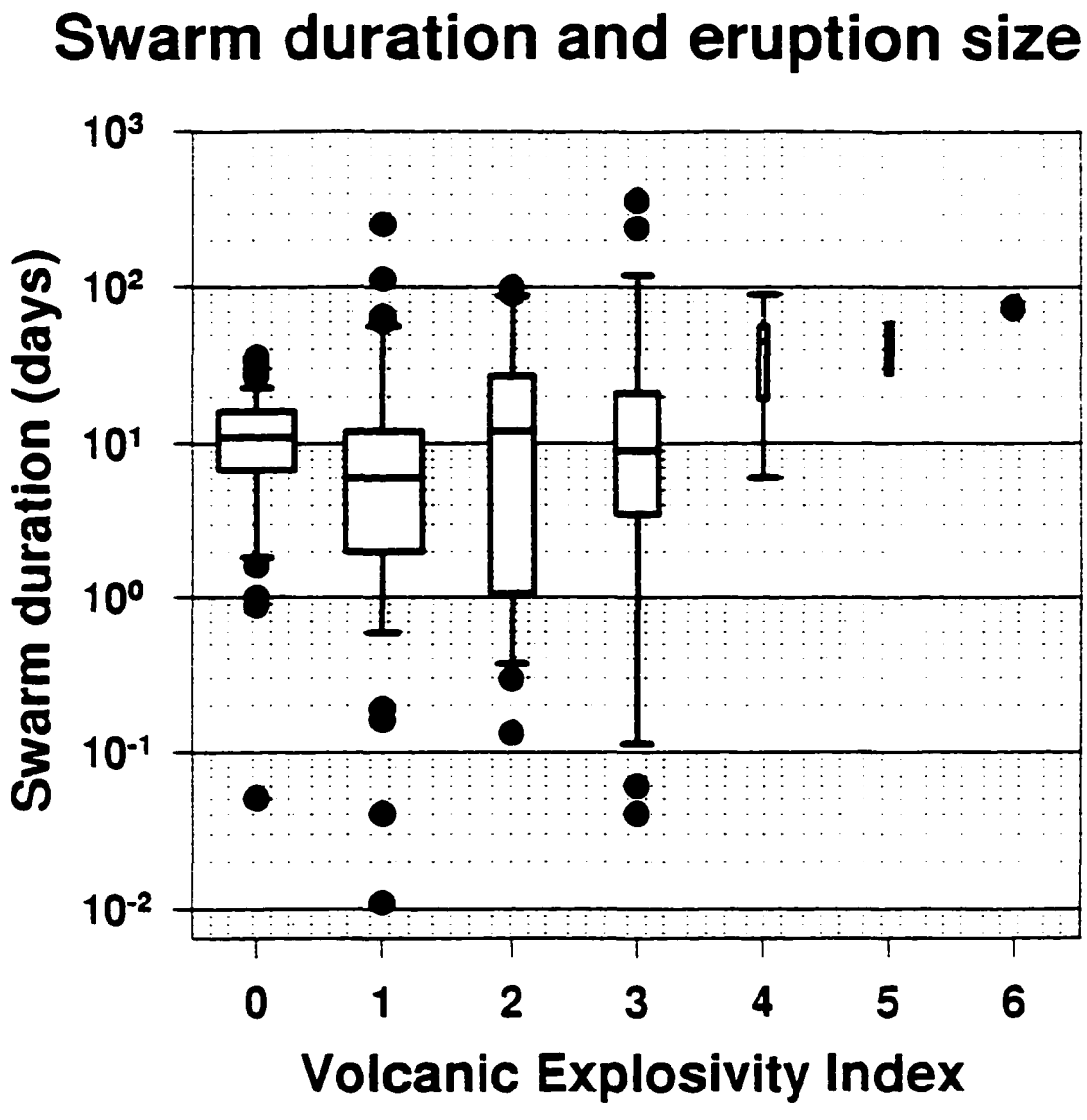

Figure 2.2 Box plots of precursory swarm durations and the size of eruptions. These data suggest that for larger eruptions (VEI > 3) the median duration of swarms is longer than those for smaller eruptions. The median for each distribution is shown as line drawn through the box. The lower and upper fences of the box plot mark the 10th and 90th percentiles of each distribution, respectively. The lower and upper hinges show the 1st and 3rd quartiles of each distribution, respectively. The values outlying the upper and lower fences are plotted individually.

2.3.3 Event type and swarm duration

Volcanoes produce a wide variety of seismic signals. Many swarms are composed of two or more distinct types of earthquakes. For example, a common sequence is a swarm of high-frequency events followed by low-frequency events, tremor, explosion events, and finally deep earthquakes [*McNutt and Benoit*, 1995]. To further describe the nature of the seismicity that makes up a swarm we added an event type(s) field to the database. The event type field attempts to reflect this complexity by listing (in the order of occurrence, if reported) all the event types that occurred during the swarm. Some swarms are defined and reported by event type. At Kilauea, for example, swarms are reported by location and event type. We separated swarms reported at this level of detail into individual swarm records. Most reports do not provide this level of detail, therefore, most swarm records contain more than one event type.

To examine the dependence of swarm duration on event type we divided swarms into two broad groups: high- and low-frequency events. Worldwide terminology varies substantially in describing seismicity at volcanoes. Thus, these terms may have specific meanings and uses at each observatory. Nevertheless we grouped together swarm durations with A-type, high frequency, and volcano-tectonic events for this comparison. Within this paper these swarms are referred to as "high-frequency swarms." Similarly, B-type, low frequency, long period, and tornillo events are also grouped together and referred to as "low-frequency swarms."

Figure 2.3 shows histograms comparing the durations for these two groups. The median duration of high-frequency swarms (11 days) is more than twice as long as the duration of low-frequency swarms (5 days). The significant difference in the mean durations is not totally unexpected because the underlying processes are probably different. High-frequency swarms are generally thought to be the brittle failure of the country rocks in response to a concentrated source

of stress, such as the intrusion magma or other fluid. In contrast, low-frequency swarms reflect many processes including: the exsolution of magmatic volatiles, the interaction of magma with groundwater, fluid pressurization, transport, resonance, and other superficial processes (all occurring at relatively shallow depths, generally less than 4 km).

2.3.4 The largest shock within a volcanic earthquake swarm (M_{max})

The database contains over 180 records in which the magnitude of the largest shock (M_{max}) within the swarm is recorded. The M_{max} values range from 0.5 to 6.2. The largest events in the database, M_s6.2 at Miyake-jima in 1983 and M6.0 at Oshima in 1986, occurred in association with large fissure eruptions. The M_s6.2 event at Miyake-jima and a M5.6 event at Soputan in 1985 are the largest events preceding an eruption included in the database. The largest events without a following eruption within 3 months are: a M_{JMA}5.7 at Unzen in 1984 (an eruption occurred in 1990); and a M6.2 at Long Valley Caldera in 1980 (no eruption as of this writing).

Many magnitude scales are used in reporting these events. M_L, M_{JMA}, m_b, and M_C are roughly equivalent to M (moment magnitude) in the range of 4 to 6.5 [*Bakun*, 1984; *Boore and Joyner*, 1982; *Katsumata*, 1983; *Jackson*, 1994]. The Russian energy class measurements were converted for comparison. The Russian energy scale K_s was converted to M using: $M = (K_s - 4.6) / 1.5$ [*Gorelchik*, 1989].

Figure 2.4 shows a comparison of the M_{max} for precursory and non-precursory swarms. The mean of the M_{max} distribution for precursory swarms is not significantly different from the mean of non-precursory swarms. The mean M_{max} is 3.4 for precursory swarms and 3.2 for non-precursory swarms. The precursory distribution shows a slightly larger spread than the non-precursory distribution. The standard deviations of the distributions are 1.3 and 1.1 magnitude units for precursory and non-precursory swarms, respectively.

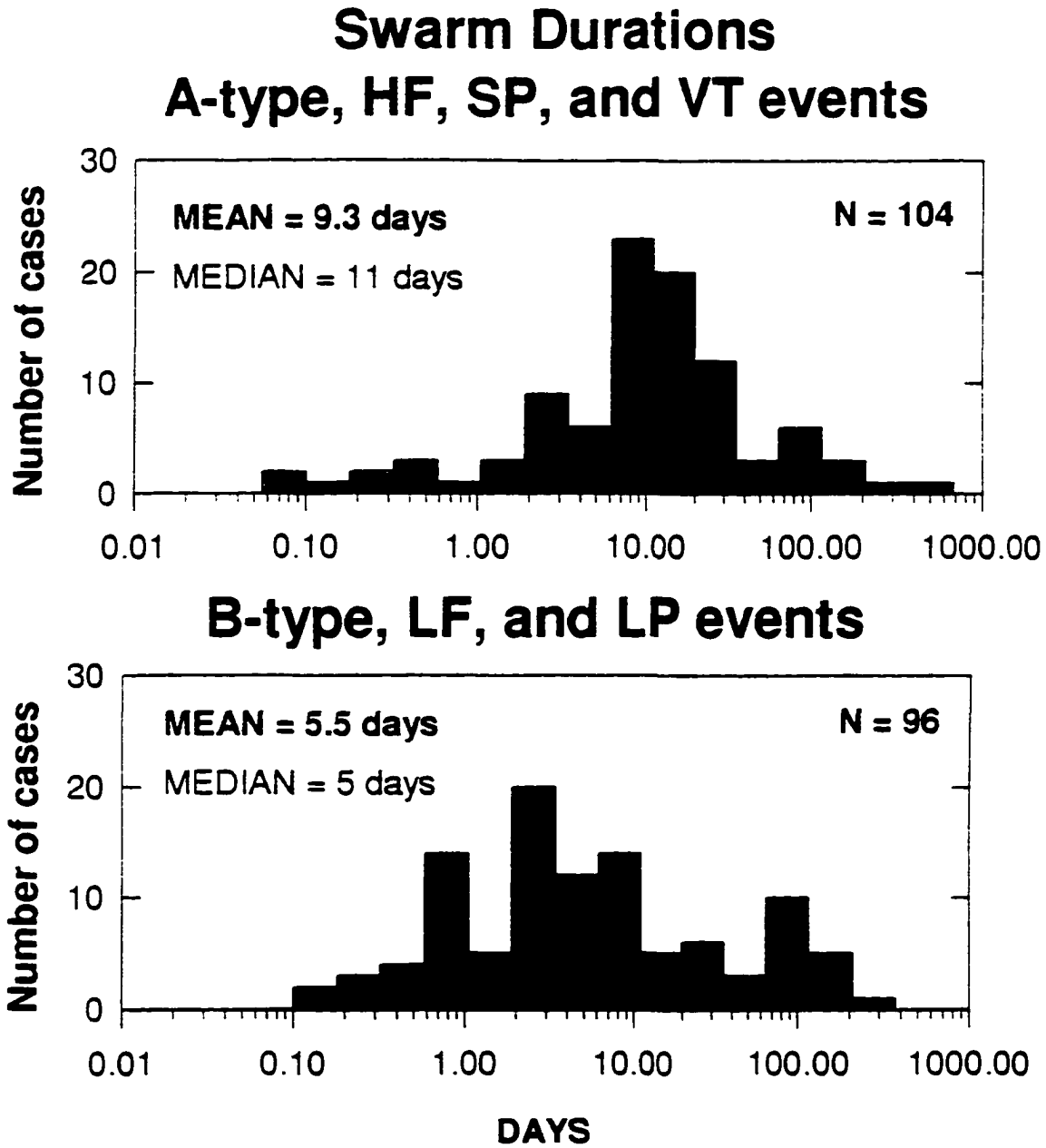

Figure 2.3 Histograms of swarm durations based on event type. The top histogram shows 104 swarms that contain A-type, high-frequency, short-period or volcano-tectonic events, and the bottom histogram shows 96 swarms that contain B-type, low-frequency, or long-period events. The geometric means are 9.3 and 5.5 days, and the medians 11 and 5 days for high-frequency and low-frequency swarms respectively.

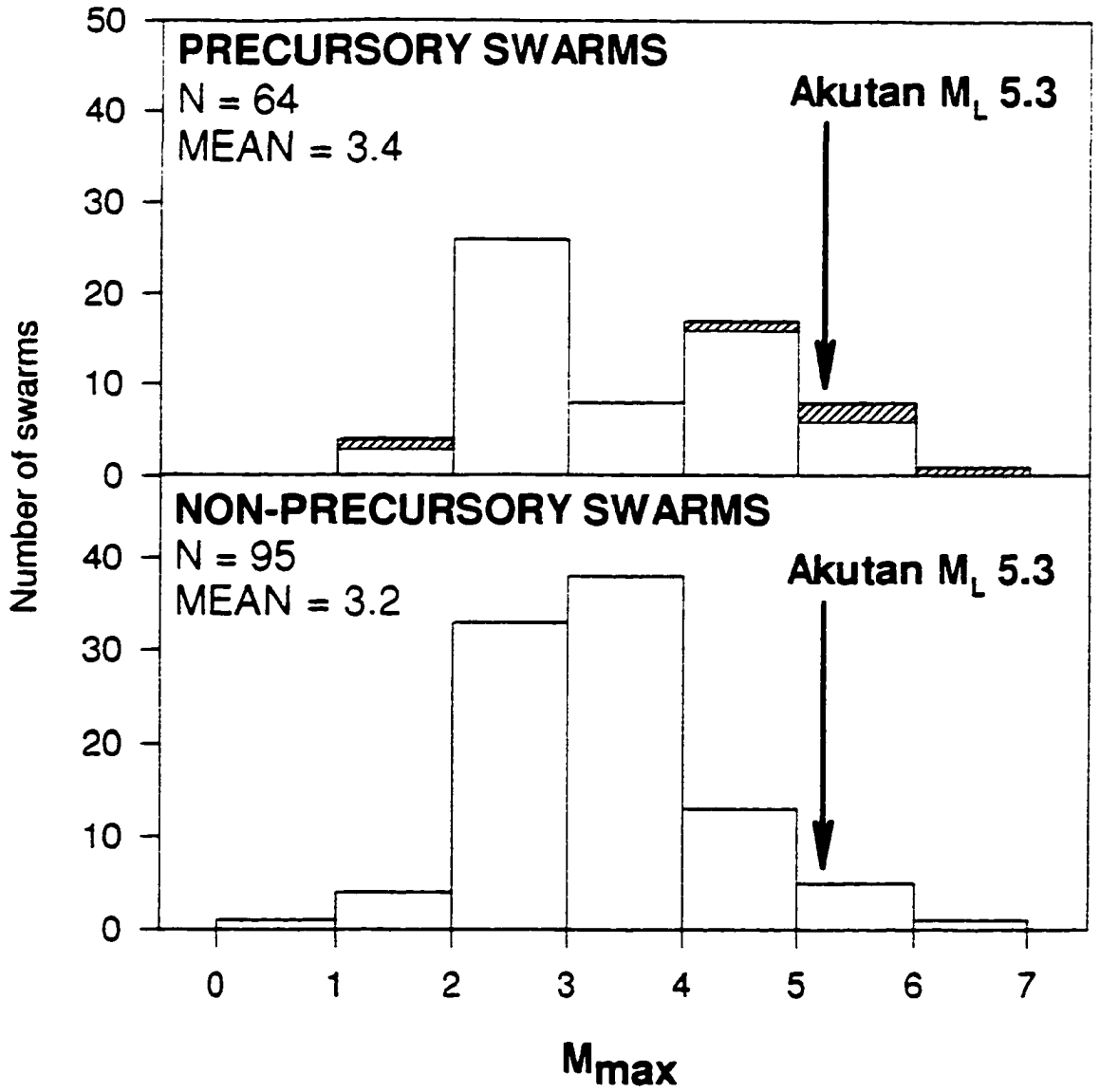

Figure 2.4 Histograms of maximum magnitude (M_{max}). Comparison of the distributions of magnitude of the largest shock within 64 precursory swarms and 95 non-precursory swarms. The means of the distributions are M3.4 and M3.2 for precursory and non-precursory swarms, respectively. The largest shock of the Akutan swarms is marked on both histograms. For precursory swarms the open bars are events that preceded central vent eruptions, while the striped bars are from swarms that preceded flank or radial fissure eruptions.

The eruption location is then used to further subdivide the precursory swarms. Two broad groups were constructed, "central vent" and "flank or radial fissure" eruptions. The open bars on the top histogram of Figure 2.4 show events that preceded central vent eruptions, while the striped bars are from swarms that preceded flank or radial fissure eruptions. With one exception (Nyamuragira 1981), eccentric and radial fissure eruptions are preceded by larger shocks than central vent eruptions.

2.3.5 M_{max} and the explosivity of the following eruption

Values of M_{max} from precursory swarms are compared to the size of the following eruptive activity. Figure 2.5 shows a box plot of precursory swarm M_{max} versus the VEI of the following eruption. Descriptive statistics for each distribution are given in Table 2.2. Similar to the duration-VEI plot (Figure 2.2), the M_{max} for VEI 0 represents effusive basaltic Hawaiian eruptions. Only two precursory M_{max} values are recorded in the database for this VEI class and are therefore not representative. The mean M_{max} values are similar for VEI 1-2 or Strombolian eruptions. For VEI greater than or equal to 3, the VEI is positively correlated with the mean M_{max}. However, this correlation is not significant due to the lack of the number of cases in the largest eruption classes. Once again, more data are needed on VEI 5 and greater eruptions to establish the formal significance of this correlation.

Table 2.2 **M_{max} statistics by the size of the following eruption.**

VEI	*number of cases*	*median*	*mean*	*std. dev.*	*95% conf. interval*
0	2	-	-	-	-
1	10	2.4	2.7	1.4	1.0
2	12	2.6	2.9	1.2	0.7
3	18	3.0	3.2	1.4	0.7
4	8	3.9	3.8	1.2	1.0
5	3	4.4	4.5	0.5	1.2
6	1	-	-	-	-

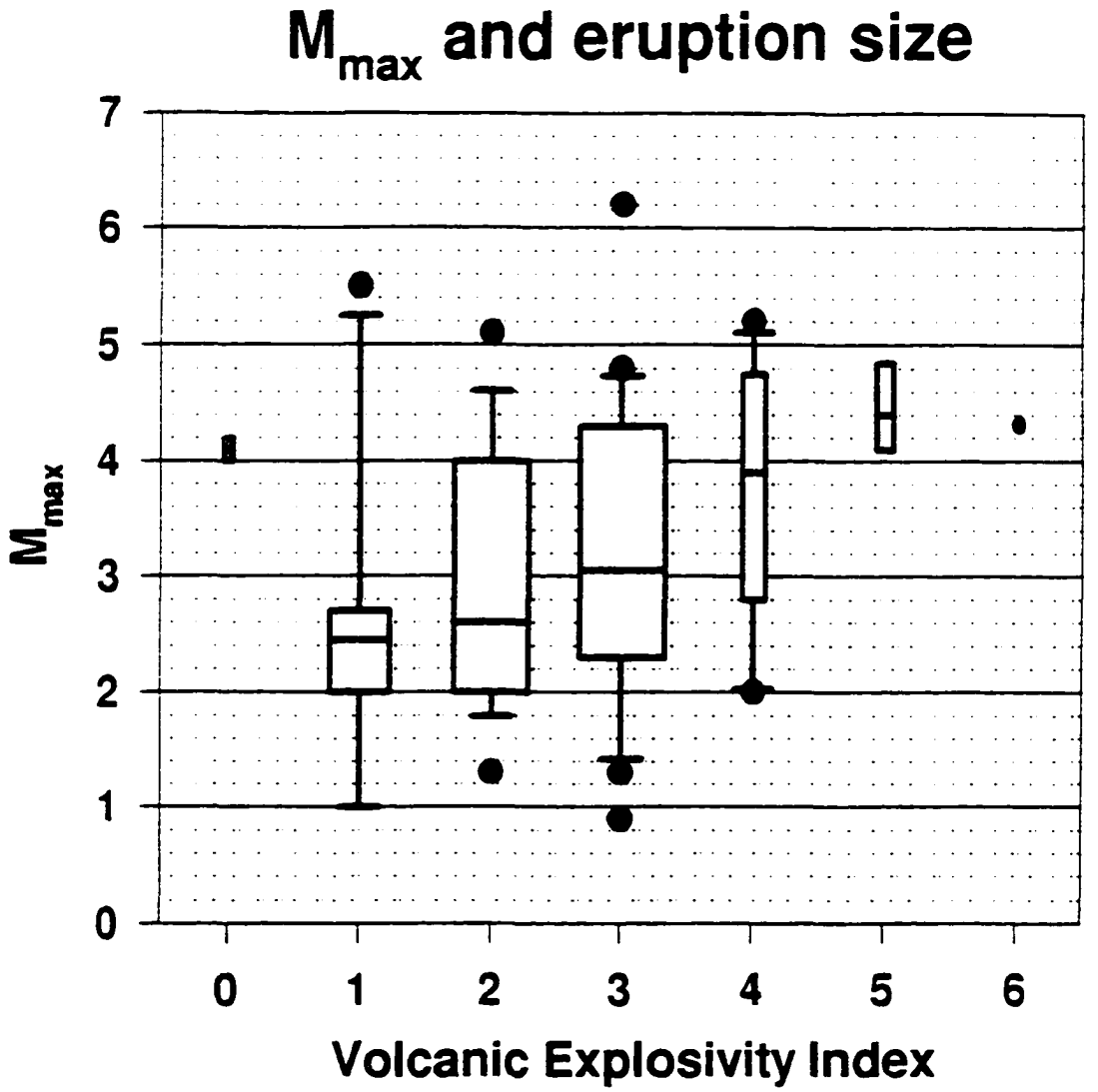

Figure 2.5 Box plots of precursory swarm M_{max} and the size of following eruptions. These data suggest that for larger eruptions (VEI > 3) the median M_{max} of swarms is longer than those for smaller eruptions. The median for each distribution is shown as line drawn through the box. See Figure 2.2 for description of the box plot hinges and fences.

2.4 A case study: Using the GVESD during the 1996 Akutan crisis

2.4.1 Description of the Akutan swarms

The onset of the seismic crisis at Akutan Island (Figure 2.6) was marked by a vigorous, 24 hour long swarm starting March 10, 1996 at about 7:30 PM AST (GMT - 09:00). The largest event in this swarm occurred at 9:10 PM AST and had a magnitude of 4.7 m_b (National Earthquake Information Center, NEIC) 5.1 M_L (Alaska Tsunami Warning Center, ATWC) and was felt as far as Dutch Harbor about 60 km to the southwest. Eight other events with magnitudes of 4.0-4.3 m_b were located by the NEIC within 20 km of the summit of Akutan volcano (Table 2.3). The rate of activity peaked about 6 hours after the onset, when more than 40 events/hour (Figure 2.7) were recorded at seismic station DTN, located 250 km to the northeast (Figure 2.6). Residents of Akutan described the effects of this activity as nearly continuous, low intensity motion punctuated by large individual shocks.

A second swarm of 18 hours duration began on March 13, 1996 at about 4:45 PM AST. The largest event of this swarm occurred at 8:43 PM AST and had a magnitude of $m_b = 4.6$ (NEIC) $M_L = 5.3$ (ATWC). This event was also felt in Dutch Harbor at an intensity of MMIII. The second swarm included 9 events with magnitudes in the range 4.0-4.6 m_b (NEIC) (Table 2.3). The rate of earthquakes observed at station DTN built up quickly and remained relatively constant throughout the second swarm (Figure 2.7). Starting one hour after the swarm began; rates of 15-30 events per hour were recorded at station DTN for 13 hours. The residents of Akutan village (13 km from the volcano's summit) felt an estimated 3000 events during these two swarms (R. Rozier, written comm., 1996). A list of all the events located by the NEIC within 25 km of Akutan volcano is given in Table 2.3. Local magnitudes were contributed by the ATWC.

Note, on average the local magnitudes (M_L) are 0.6 units greater than the body-wave magnitudes (m_b). During the first days of the swarm the closest station to Akutan available in real-time was SND at 370 km and only a few additional stations were available within a 600 km radius for which local magnitude is defined. The lack of data is probably the largest contributing factor to the discrepancy between the magnitude scales.

On March 12th the first seismometer was installed on Akutan Island, and by March 18th a four-station temporary network was installed and earthquakes were being routinely located. All of the events were high frequency or volcano-tectonic events, and no long-period events or volcanic tremor were recorded. After the temporary network was established the level of seismicity continually declined. Within 3 months the seismicity rate had dropped to 3-7 locatable events per week [*Power et al.*, 1996]. The total seismic moment released by the two swarms is estimated at 2.7×10^{18} Nm using coda duration magnitudes at station DTN (J. Power, writ. comm. 1997). A second estimate of the total moment release of 5.5×10^{16} Nm was calculated using the m_b given in Table 2.3 and relations between m_b and M_s [*Abe and Kanamori*, 1980] and M_s and M_o [*Kanamori*, 1977]. The moment calculated from the body-wave magnitudes is almost two orders of magnitude less than the value estimated from coda-duration magnitudes. This discrepancy is caused partly by the systematic difference in m_b and M_L. The two estimates are used as upper and lower bounds. For comparison, the moment released at Akutan (10^{16}-10^{18} Nm) is similar to the moment released during the 1980 eruption at Mount St. Helens (1.1×10^{17} Nm) [*Weaver et al.*, 1981; *Mori et al.*, 1996].

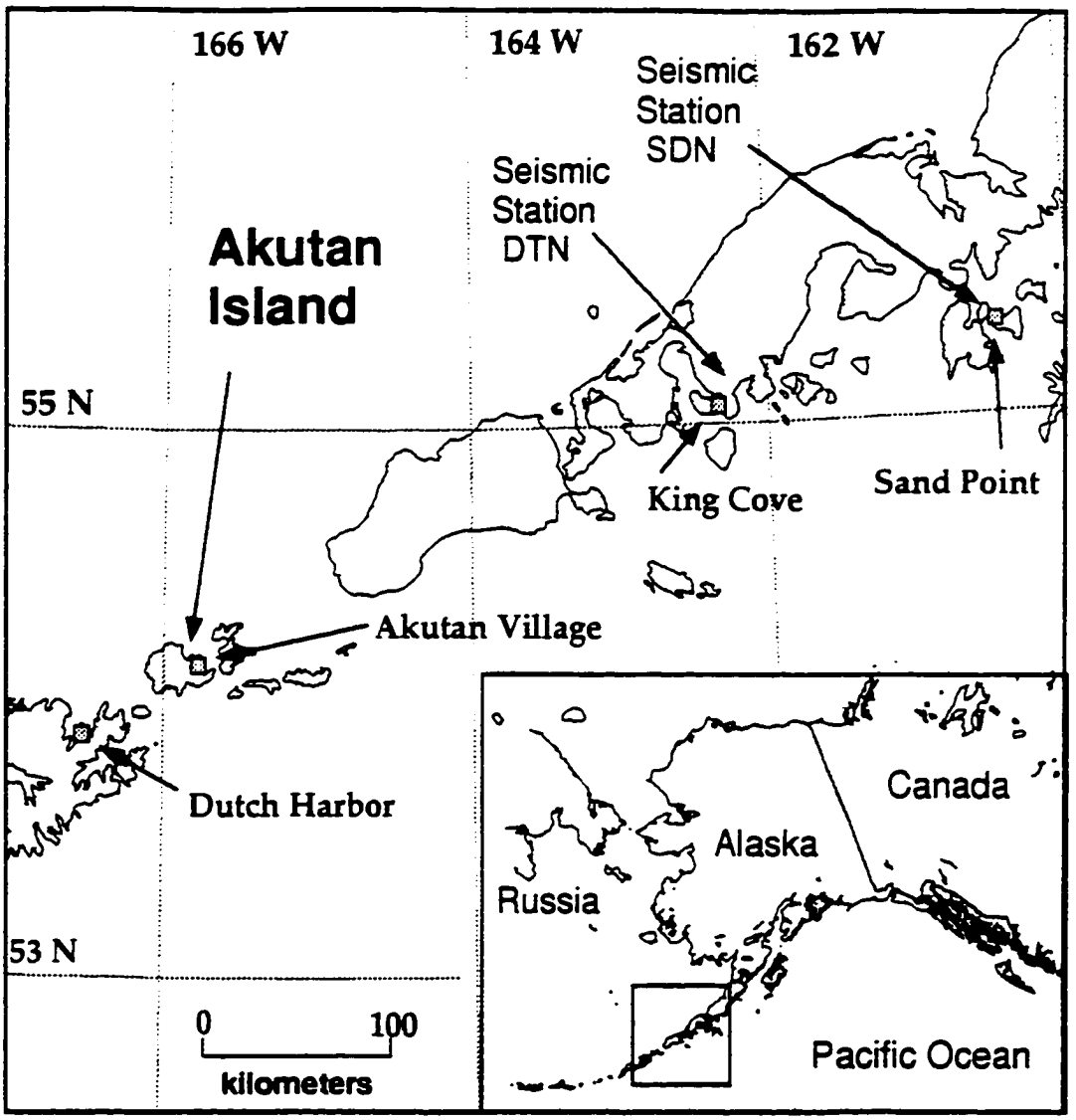

Figure 2.6 Location map of Akutan Island and the nearest permanent seismic stations (DTN and SND).

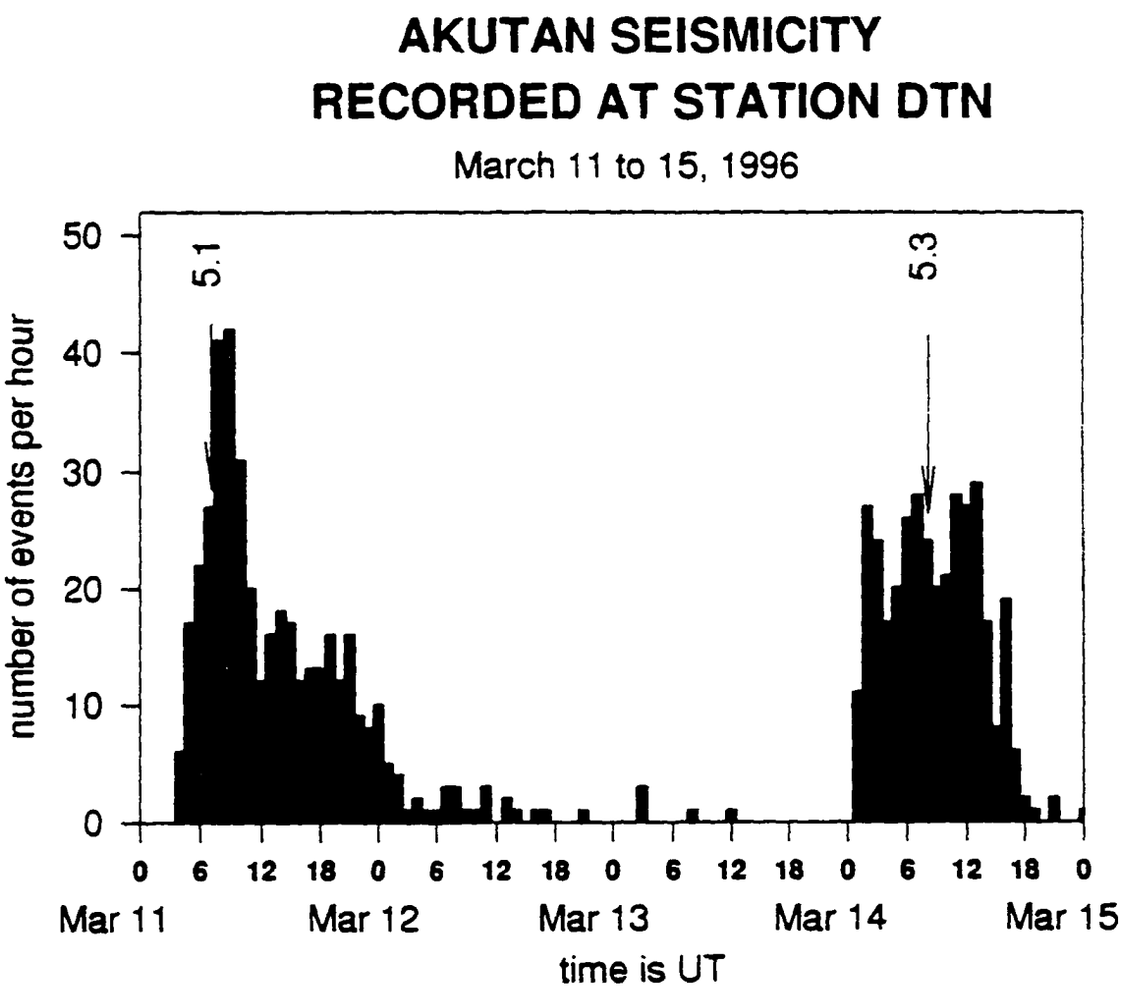

Figure 2.7 Histogram of the number of earthquakes per hour recorded at station DTN (250 km to the northeast) for the March 11-14, 1996 Akutan swarm. The occurrences of events greater than or equal to M 5 are marked with arrows.

Table 2.3 Locations and magnitudes for the largest earthquakes of the Akutan swarms.

date	origin time UT	lat	lon	mb	Ml	intensity
3/11/96	05:41:51.59	54.133	-166.043	4.1	4.4	IV
	06:10:18.08	54.231	-166.087	4.7	5.1	IV
	07:09:55.53	54.269	-166.077	4.4	4.7	IV
	07:14:14.60	54.238	-166.092	4.2	4.4	IV
	08:17:16.42	54.282	-166.219	4.3	4.4	IV
	08:30:48.35	54.180	-165.995	4.0	4.5	IV
	08:52:44.58	54.204	-166.107	4.2	4.6	IV
3/12/96	00:32:17.95	53.991	-166.170	3.4	4.3	IV
	02:06:22.25	54.184	-165.967	4.0	4.8	IV
3/13/96	03:38:38.27	54.071	-166.207	3.9	4.7	IV
3/14/96	03:55:36.17	54.220	-166.003	4.0	4.8	IV
	05:43:53.65	54.204	-166.001	4.6	5.3	V*
	07:19:11.83	54.236	-165.765	3.9	4.7	IV
	07:28:44.28	54.313	-166.101	3.9	4.6	IV
	09:07:51.81	54.197	-165.894	3.8	4.6	IV
	09:18:10.20	54.076	-165.917	3.8	4.5	IV
	10:00:18.21	54.230	-165.963	4.2	4.7	IV
	10:31:43.41	54.260	-165.965	3.5	4.4	IV
	10:51:15.38	54.209	-165.984	4.2	4.6	IV
	11:21:20.85	54.129	-165.878	3.7	3.5	IV
	11:56:13.90	54.125	-165.826	4.3	5.0	IV
	12:35:07.13	54.229	-165.795	3.8	4.4	IV
	13:13:38.09	54.114	-165.990	4.3	4.9	IV
	13:17:57.68	54.177	-166.139	4.0	4.4	IV
	14:58:16.91	54.047	-165.881	3.9	4.3	IV
	15:21:21.32	54.156	-165.906	4.3	5.0	V
	16:09:45.01	54.035	-165.929		4.4	IV
	16:13:51.60	54.134	-165.844	4.6	5.2	V
	17:00:08.38	54.181	-165.997	3.9	4.6	IV
	17:29:59.36	54.245	-165.982	3.4	4.4	IV
	18:23:20.23	54.136	-165.993	3.7	4.5	IV
	19:27:57.85	54.117	-166.123	4.2	5.0	IV

Felt intensities are from Akutan
*Felt (III) on Unalaska.

2.5 Discussion

As the crisis at Akutan progressed, the duration and the M_{max} of the swarms were repeatedly compared to the previously prepared histograms and box plots (Figure 2.1 and Figure 2.5). Specific queries were constructed and the resulting case histories and the comparisons with the global distributions were assessed. This information was quickly synthesized with the available geological information (i.e. 200 years of recorded eruptive history) [e.g. *Simikin and Seibert*, 1994; *Finch*, 1935] to build a broad range of eruptive scenarios. On March 14th at 2:00 PM, the Alaska Volcano Observatory released an information update stating three possibilities:

> Based on the frequency, number and locations of recorded earthquakes, the following scenarios are considered possible at this time:
>
> (1) Earthquake activity diminishes and no eruption occurs
>
> (2) Eruption of a lava flow from a vent on the flank or within the summit caldera, accompanied by ash plumes and explosions
>
> (3) Significant, explosive eruption producing ash plumes to altitudes of 30,000' ASL or higher.

These very broad statements encompassed just about anything that could happen at a volcano. These types of statements nonetheless are helpful for the emergency response community and are needed as soon as possible. A more detailed analysis followed in the weeks after the swarm. An attempt was made to assign some likelihood or probability to each of the above scenarios. The remainder of this discussion details how these data were assessed and their physical implications. Each of the swarm parameters discussed in general above are now directly compared to the Akutan case.

The durations of the Akutan swarms were 18 and 24 hours. The combined duration of the sequence was about 3.5 days, the same as the mean of non-precursory swarms. Considering the duration parameter alone, the relatively short Akutan swarms would be considered non-precursory. In other words, shorter lasting swarms are less likely to precede eruptions. However, if the activity re-intensified or continued for several more days these swarms would have a higher likelihood of being precursory.

The observation that precursory swarms are about twice as long as non-precursory swarms may be simply explained as the greater ascent of magma to the surface by longer lasting swarms, while intrusions or failed eruptions (less ascent) are manifested by shorter swarms [*Benoit and McNutt*, 1996b]. Factors such as the rate at which magma can enter the swarm volume, and the rate and extent of magma transfer between adjacent dikes, may also control the duration of a swarm [*Hill*, 1977]. The extent of the magma transfer between dikes is necessarily greater for magma that reaches the surface than for an intrusion, which stops short. Several other factors, not directly related to the movement of magma, may also control the duration of shorter swarms. Volcanic and geothermal areas have been shown to be sensitive to small strains such as; earth and tidal stresses [*McNutt and Beavan*, 1981; *Rydelek et al.*, 1988], surface waves from regional or teleseismic earthquakes [*Hill et al.*, 1993], seasonal ocean-loading [*McNutt and Beavan*, 1987] or changes in barometric pressure [*Rinehart*, 1980]. The periods of such strains, which can be forcing functions, may partly control swarm durations.

The Akutan swarms were almost exclusively composed of high-frequency events. Only one low-frequency event was detected on March 15, 1996 during the crisis. Nine other low-frequency events were located in the next three months. Poor quality locations put the events several kilometers to the southeast of the island. Due to their locations the events were not

considered to be associated with the volcano, but may be related to superficial processes such as small submarine landslides. No volcanic tremor was detected at Akutan.

A commonly observed sequence of event types during a precursory swarms is as follows; high-frequency events, low-frequency events, tremor, explosion events, and finally deep earthquakes [*McNutt and Benoit*, 1995]. Over 40 cases in the database show all of these event types in the above relative order. Many other precursory swarms show two or more components, again in the same relative order. The Akutan swarms possessed only the first component of this generic sequence. Using this generic precursory swarm sequence as a guide, the lack of both low-frequency events and tremor suggests that the Akutan swarms were not yet leading to an eruption. If an eruption were to occur, we would expect to detect at least one other event type, e.g. low-frequency events or tremor, before an eruption would begin. Low-frequency events and tremor generally represent processes occurring at relatively shallow depths ($\leq$ 4km) within the crust. If a magmatic intrusion was driving the Akutan swarms, the lack of low-frequency events and tremor provides some evidence that the intrusion had not yet risen to very shallow depths.

When the descriptive statistics of all of the generic sequences' component distributions are well determined (e.g. the data presented in Figures 2.1-2.5 and Tables 2.1-2.2) a probabilistic eruption forecasting scheme could be developed. This scheme or algorithm could compare durations of an ongoing earthquake sequence with the generic sequence and give probabilistic assessments of possible outcomes. This task has not yet been done and is beyond the scope of the present paper.

The largest events in the Akutan swarms were $m_b = 4.7$ ($M_L = 5.1$) and $m_b = 4.6$ ($M_L = 5.3$). There is not a significant difference between the distributions of M_{max} for precursory and non-precursory swarms (Figure 2.4). Therefore, the size of the M_{max} alone does not give a clear

indication that a swarm is likely to lead to an eruption. Many of the events of the Akutan swarms were felt. The database was searched using the question: "Are there any comparable swarms with over 3000 felt earthquakes within a period of a few days?" Out of 700 swarms, the answer was no. The number was lowered to $\geq$ 500 felt events and the database returned only 3 cases (Table 2.4). Two of these swarms occurred before and during eruptions and the third occurred 5 years before an eruption. Usu volcano, with 2145 felt events, came the closest to the Akutan swarms. The felt events at Usu occurred over several years, not in only a few days as in the Akutan case. This small data set does not indicate whether or not the swarm is precursory, but with respect to the numbers of felt events, the Akutan swarms are quite extraordinary.

Table 2.4 Swarms with greater than 500 felt earthquakes.

volcano	*swarm start date*	*number felt*	*number detected*	*activity*	*references*
Akutan	11-Mar-96	>3000	777	no eruption	this paper
Usu	6-Aug-79	2145	11526	during eruption	BVE no 17, p 49-53; BVE no 23, p 61
Tacana	7-May-86	1000	4000	before eruption	BVE no 25, p 65; BVE no 26, p 64-65
Unzen	15-May-84	519	10544	no eruption	BVE no 24, p 65

If we assume the Akutan swarms were precursory we can compare the M_{max} with the VEI of the following eruption (Figure 2.5). Using m_b=4.7 as the M_{max} for the Akutan swarms the most likely VEI categories are VEI 4 and 5. In other words, if the Akutan swarms were precursory, the large earthquakes suggest that a flank eruption or a large explosive eruption through the central vent were probable.

In general, volume changes within the crust produce shear stresses, which are released by earthquakes. *McGarr* [1976] proposed a direct relation between total seismic moment release and volume changes within mines. *Abe* [1992] applied this relation to a volcanic setting. Abe compared the volume of the Katmai caldera and the total moment released in association with the formation and found it to be in good agreement with McGarr's relation. This general relationship is also supported by the data shown in Figure 2.5; larger more explosive eruptions tend to be preceded by larger earthquakes. Using this scaling relationship the change in volume was estimated for the Akutan swarms. Following *Abe* [1992], the moment can be interpreted in terms of a model of shear faulting or a volume source. For the volume source the swarm occurs in response to shear stresses induced by change in a volume of material [*McGarr*, 1976]. The moment is written as

$$M_o = \mu V, \tag{2.1}$$

where M_o is the total moment, μ is the rigidity, and V is approximated by total volume of material added to the region. Taking $\mu = 3 \times 10^{10}$ N/m^2, we obtain $V = 1.6 \times 10^6$ m^3 from the body-wave derived total moment and $V = 9.0 \times 10^7$ m^3 from the coda-duration derived total moment. This volume of material would correspond to a VEI 2-3 eruption. These volume estimates are probably both lower bounds since the formulation assumes the volume change is accommodated entirely within the seismogenic crust. Magma at such depths would contain few vesicles, in contrast to tephras whose volumes are measured to determine VEI.

The database was queried for specific swarm case histories with magnitude 4.5 or greater shocks. The query returned a list of 26 swarms with $M_{max} \geq 4.5$, out of 188 swarms where the M_{max} was recorded in the database. Twelve of the swarms preceded eruptions (Table 2.5), while 14 did not precede eruptions within the following three months (Table 2.6). Of the precursory

swarms, half of the cases preceded eruptions from flank or radial fissure vents. Two cases, Izu-Tobu and Paricutin, preceded fissure eruptions that created new volcanoes. The relationship, if any, of the M_s5.3 earthquake near On-Take to the following eruption is unclear. The remaining cases, Soputan, Sheveluch, and Colo (Una Una), preceded central vent eruptions. Of note, both the Sheveluch and the Colo swarms preceded large explosive eruptions (VEI 4).

Table 2.5 **Precursory swarms with M_{max} greater than or equal to M4.5.**

volcano	*swarm start date*	*M_{max}*	*comment*	*reference*
Miyake-Jima	3-Oct-83	M_s6.2	About 1.5 hours of seismicity preceded eruption of a 4.5 km long fissure on the SW flank.	BVE no 23, p 29-32
Soputan	15-Mar-85	M5.6	After 65 days of increased seismicity and then felt shocks an eruption began.	BVE no 25, p 26 USGS Bull 1855, 1988
Izu-Tobu	30-Jun-89	M_{JMA}5.5	An eruption from a new volcano occurred after 11 days of increased seismicity.	BVE no 29, p 47-54
On-Take	15-Aug-76	M_s5.3	Large distance between hypocenters and eruption vent. No direct relation between eruptions and earthquakes.	BVE no 19, p 49-50 BVE no 20, p 55-56
Sakura-Jima	10-Jan-14	M_s5.2	Explosive eruption from the W, E, and SE flanks began after 3 days of felt earthquakes	Abe, 1979
Usu	22-Jul-10	M_s5.1	An eruption from a radial fissure occurred on the N flank after 4 days.	Abe, 1979
Tacana	15-Dec-85	M5.0	A small phreatic flank eruption occurred after 72 days of increased semicity.	BVE no 25, p 65 BVE no 26, p 64-65
St. Helens	20-Mar-80	M5.0	A flank eruption occurred after 59 days of precursory seismicity.	BVE no 20, p 71-79 USGS Prof. Paper, 1250, 1984
Sheveluch	2-Nov-64	M4.9	A VEI 4 eruption was preceded by swarm of earthquakes and accompanied by continuous tremor.	Tokarev, 1985
Lonquimay	7-Dec-88	M4.6	After 18 days of increasing seismicity a eruption began through a new vent on the NE flank of the volcano.	BVE no 28, p 83 Barrientos & Acevedo-Aranguiz, 1992
Colo (Una Una)	4-Jul-83	M4.6	A VEI 4 eruption was preceded by 2 weeks of felt earthquakes.	BVE no 23, p 20-21
Paricutin	7-Jan-43	M4.5	The formation of a new volcano was preceded by more than 45 days of increased seismicity.	Yokoyama and de la Cruz-Reyna, 1990

Table 2.6 Non-precursory swarms with M_{max} greater than or equal to M4.5.

volcano	*swarm start date*	M_{max}	*comment*	*reference*
Don Joao de Castro Bank	21-Nov-88	M5.8	The earthquakes were centered 53km SE of the Don Joao de Castro Bank along the Sete Cidades fault.	BVE no 28, p 107-108
Unzen	15-May-84	M_{JMA}5.7	Over nine months 519 earthquakes were felt. No anomalous fumarolic activity was observed.	BVE no 24, p 65
Long Valley Caldera	4-Oct-78	M5.7	Major swarm 15km SE of the caldera. Activity migrated to the NE and concentrated at the S tip of the caldera.	BVE no 21, p 90-93 Ryall and Ryall, 1981
Long Valley Caldera	7-Jan-83	M_L5.2	Intial swarm 4km SE of Mammoth. Activity expanded to fill an elliptical area 7km futher to ESE along the S moat.	BVE no 22 p 107-108; Savage and Cockerham, 1984
Norikura	7-Mar-86	M5.1	After this earthquake activity increased 5-10km SSW of the volcano. No extra-ordinary volcanic activity was observed.	BVE no 29 p 100-101
Rabaul	Jan-82	M5.1	Seismicity essentially consists of shallow short period volcano tectonic earthquakes originating at 6km depth.	BVE no 22, p 98-101
Rabaul	22-Apr-84	M5.1	Almost all events are high-frequency tectonic-like earthquakes.	BVE no 24, p 63-64
Rabaul	15-Sep-83	M_L5.0	Greater numbers of events in successive swarms.	BVE no 23, p 58 BVE no 25, p 58
Kirishima	28-Apr-86	M4.9	The epicenter was 15km SW of the volcano. Three events were felt. Ground cracks and small landslides were reported.	BVE no 26, p 82
Tecapa	21-Apr-85	m_b4.7	A 8km long 0.8-1km wide graben with 30cm vertical offset formed on the NW flank.	BVE no 25, p 65
Kilauea	10-Aug-81	M4.5	Associated with an intrusion in the SW rift zone.	BVE no 21, p 65-66 Klein et al., 1987
Hakkoda	10-Aug-86	M4.5	An earthquake swarm occurred at the NW foot of the volcano.	BVE no 26, p 83
Bandai	16-Jun-87	M4.5	Many earthquakes were located 10km SW of the summit. 14 events were felt and accompanied by rumblings.	BVE no 27 p 85
Liamuiga	24-Oct-88	m_b4.5	A swarm in the vicinity of the volcano included at least 5 events that were felt by all on St. Kitts.	BVE no 28, p 106-107

In summary, for the precursory swarms, most of the case histories with shocks ≥ 4.5 precede flank, radial fissure eruptions, or the formation of new volcanoes. These types of eruptions are relatively uncommon; most eruptions occur through a central vent. Globally, only about 5% of all eruptions in the Smithsonian's *Volcanoes of the World* [*Simkin and Siebert*, 1994] data file are classified as flank or radial fissure eruptions. The link between the large earthquakes and flank eruptions may be due to the spatial variations in rock strength near volcanoes. The environment immediately surrounding the conduit may be relatively weak and incapable of generating large earthquakes. Changes in volume there may be accommodated aseismically. Intrusions propagating away from the primary eruptive locus may encounter stronger country rock capable of supporting larger precursory earthquakes. Directly below volcanic centers the deepest seismicity tends to shoal. This is presumably due to heating of the country rock above a magma body [e.g. *Hill*, 1992]. This effectively decreases the seismogenic thickness directly below the volcano. The seismogenic thickness also will limit the maximum size of earthquakes. Intrusions moving out to the flank of a volcano will encounter presumably cooler rocks and a thicker seismogenic layer capable of supporting larger earthquakes.

Most of the largest shocks ($M \geq 5.0$) of the non-precursory swarms occurred at Long Valley and Rabaul calderas, each of which had several episodes of unrest in the 1980's. The largest non-precursory event in the database, M5.8, occurred 53 km away from the Don Joao de Castro Bank submarine volcano on a branch of the Azores-Gibraltar fracture zone. However, it is unclear how or if this swarm is related to volcanic activity. At least two of the non-precursory swarms, Kirishima and Tecapa (Table 2.6) were associated with surface deformation. Ground cracks and small landslides were observed near Kirishima volcano and an 8 km long graben was formed on the northwest flank of Tecapa volcano.

At Akutan a series of very recent ground cracks were discovered during the 1996 summer field season. The cracks trended northwest and southeast of the crater (Figure 2.8) and geological evidence showed that these cracks were formed within the last year and presumably during the March seismic swarms (P. Stelling writ. comm., 1996).

For many of the non-precursory cases (in Table 2.6), the earthquake activity is not focused directly below a central vent but instead is located several kilometers away on the volcano's flank. Some of these swarms may be related to intrusions but others may be tectonic swarms that happen to be near an active volcano. The problem of determining whether a swarm is volcanic or tectonic in origin certainly deserves further study. Perhaps the addition of geodetic data may provide an important constraint in making the distinction between tectonic and volcanic swarms. In the database we have used an arbitrary distance of 15 km as a cut-off between volcanic and tectonic swarms. However, further work is needed to determine the underlying physical processes.

In summary, for the non-precursory swarms the case histories fall into two groups; swarms associated with calderas and swarms occurring at stratovolcanoes some distance away from the primary eruptive center. In general, calderas are larger structures and therefore capable of supporting larger events. For the cases occurring at stratovolcanoes and linked to a magmatic intrusion, a similar reasoning can be applied for the precursory swarms as for the non-precursory swarms. The only difference is that the intrusion stopped short of the surface for the non-precursory swarms.

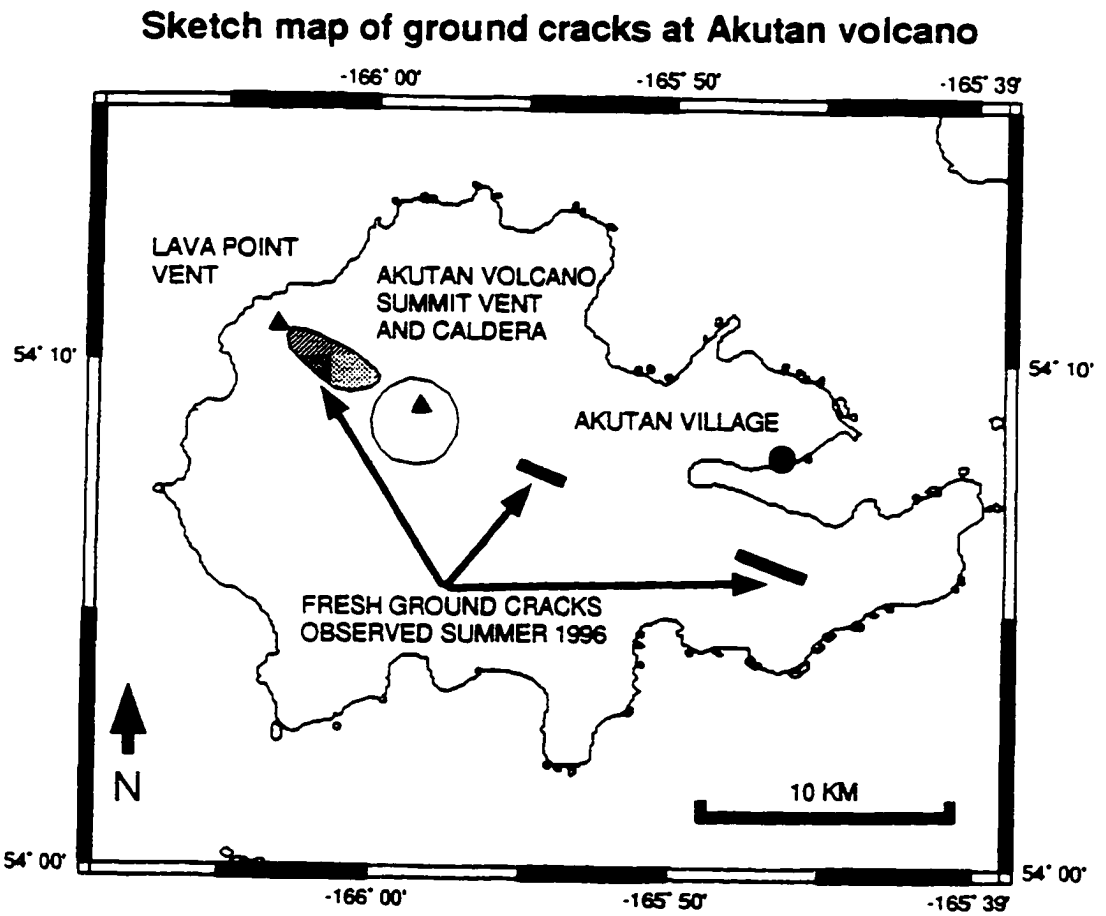

Figure 2.8 Sketch map of ground cracks on Akutan Island. The cracks were discovered and mapped during the 1996 summer field campaign. Three zones of fresh on echelon ground cracks were observed. The northeastern zone was the most extensive. The historically active eruptive centers, the summit caldera vent and Lava Point flank vent are shown as black triangles.

2.6 Conclusions

Very few volcanic earthquake swarms have had such large numbers of felt events in such a short time as the March 1996 Akutan swarms. When taken in isolation, the magnitude of the largest shock within a swarm has limited predictive value, but if an eruption were imminent, trends observed in the database suggest two scenarios; 1) these large shocks tend to precede explosive eruptions, and 2) most of the largest shocks precede eruptive breakouts through flank or radial fissure vents. The durations of the Akutan swarms were relatively short, 24 and 18 hours. The combined total duration is 3.5 days, the same as the mean duration for non-precursory swarms, suggesting that the activity was not precursory. At the time of the crisis, these results were considered along with the available eruptive history, and eruptive scenarios were constructed and communicated to the hazard response community [*Keith, et al.*, 1996].

During July 1996 fieldwork at Akutan, very fresh ground cracks were discovered northwest and southeast of the crater (Figure 2.8 and Figure 2.9). The cracks on the northwest flank were the most extensive. En echelon groups of cracks defined a zone 300 to 500 m wide and approximately 3 km long on the northwest flank between the summit caldera and the historically active Lava Point flank vent [ca. 1910; *Finch*, 1935]. Vertical displacements of 30 to 80 cm were measured in the local graben structures, but no consistent lateral offsets were observed. Two other zones of fresh ground rupture were observed on the southwest flank approximately 1 and 2 km long coincident with mapped Holocene faults [*Power et al.*, 1996]. The rupture of the previous season's snow pack showed that the cracks occurred within the last year and presumably during the March seismic swarms (P. Stelling, writ. comm. 1996). No heat, steam

or other evidence of near-surface magma was observed in the cracks (T. E. C. Keith, writ. comm., 1996).

The observation of ground cracks, which are extensional structures, suggests a near-surface intrusion. However, no seismic evidence was detected for an intrusion reaching very shallow depths (≤4km), such as low-frequency events or tremor. To reconcile these observations, we propose that a deep intrusion occurred with a large opening component. This would result in surface cracks without magma interaction with the water table or exsolution of magmatic volatiles. Based on a systematic study using the database, the Akutan swarms shared the most attributes with the 1985 swarm at Tecapa, El Salvador. At Tecapa an 8 km-long graben was formed on the northwest flank of the volcano after four days of felt earthquakes including a m_b4.7. The graben was 0.8-1 km wide with 30 cm of vertical offset. The seismicity then declined and no eruption occurred [*McClelland et al.*, 1989].

During the March 1996 seismo-volcanic crisis at Akutan Volcano, the Global Volcanic Earthquake Swarm Database proved to be valuable in evaluating possible scenarios. For the Akutan case an eruption was not likely, however, based on the magnitude data, if an eruption were to occur, a flank eruption was more likely then a summit eruption. Field observations conducted five months later showed extensive ground cracking suggesting that this forecast was indeed accurate.

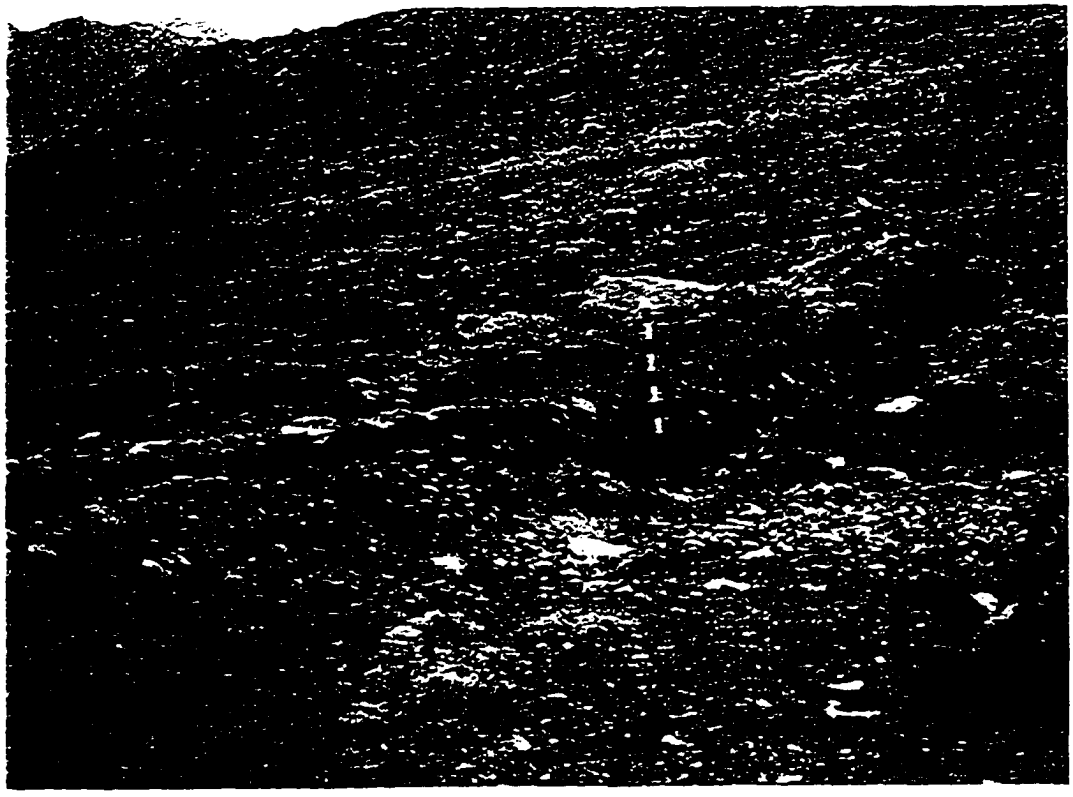

Figure 2.9 Photograph of a ground crack, believed to have formed during the March 1996 earthquake swarm. The maximum vertical displacement in this photograph is ~50 cm, no consistent lateral offsets were observed. This crack could be traced approximately 1 km along strike. The view is looking east-northeast about 5-km east-southeast of the summit. (Photograph and description courtesy H. Fletcher)

2.7 Acknowledgments

For many thought stimulating discussions in the heat of the crisis and afterwards we thank J. Power, C. Stephens, J. Lahr, S. Wiemer, R. Hansen, and K. Lindquist. We also thank J. Power for sharing the seismic moment calculations, P. Stelling for unpublished maps of the ground cracks, H. Fletcher for the photograph of the ground cracks, and M. Wyss for his comments, which have improved this manuscript. This work was supported by the Alaska Volcano Observatory under the US Geological Survey Volcano Hazards and Geothermal Studies Program, and by additional funds from the State of Alaska.

2.8 References

Abe, K., 1979. Magnitudes of major volcanic earthquakes of Japan 1901 to 1925, *J. Fac. Sci., Hokkaido Univ., 6*: 202-212.

Abe, K., 1992. Seismicity of the caldera-making eruption of Mount Katmai, Alaska in 1912, *Bull. Seis. Soc. Am., 82*: 175-191.

Abe, K., and H. Kanamori, 1980. Magnitudes of great shallow earthquakes from 1953 to 1977, *Tectonophys.*, 62: 191-203.

Bakun, W.H., 1984. Seismic moments, local magnitudes, and coda-duration magnitudes for earthquakes in central California, *Bull. Seis. Soc. Am., 74*: 439-458.

Barrientos, S. E., and P. S. Acevedo-Aranguiz, 1992. Seismological aspects of the 1988-1989 Lonquimay (Chile) volcanic eruption, *J. Volc. Geotherm. Res.*, 53: 73-87.

Benoit, J.P., and S.R. McNutt, 1996a. Global volcanic earthquake swarm database 1979-1989, U.S. Geol. Survey Open File Report 96-69, Fairbanks 333 pp.

Benoit, J.P., and S.R. McNutt, 1996b. Global volcanic earthquake swarm database and preliminary analysis of volcanic earthquake swarm duration, *Annali de Geofisca, 39*: 221-229.

Boore, D.M., and W.B. Joyner, 1982. The empirical prediction of ground motion, *Bull. Seis. Soc. Am., 74*: S43-S60.

Bulletin of Volcanic Eruptions (BVE), 1977. no. 17.

Bulletin of Volcanic Eruptions (BVE), 1979. no. 19.

Bulletin of Volcanic Eruptions (BVE), 1980. no. 20.

Bulletin of Volcanic Eruptions (BVE), 1981. no. 21.

Bulletin of Volcanic Eruptions (BVE), 1982. no. 22.

Bulletin of Volcanic Eruptions (BVE), 1983. no. 23.

Bulletin of Volcanic Eruptions (BVE), 1984. no. 24.

Bulletin of Volcanic Eruptions (BVE), 1985. no. 25.

Bulletin of Volcanic Eruptions (BVE), 1986. no. 26.

Bulletin of Volcanic Eruptions (BVE), 1988. no. 28.

Bulletin of Volcanic Eruptions (BVE), 1989. no. 29.

Evison, F.F., and D.A. Rhoades, 1993. The precursory earthquake swarm in New Zealand: hypothesis test, New Zealand *J. Geo. Geophys., 36*: 51-60.

Finch, R. H., 1935. Akutan volcano, *Zeitschrift fur Vulkanologie, 16*: 155-160.

Gorelchik, V.L., 1989. Seismological study of the Kliuchevskoi flank eruption of 1983 (Kamchatka), *J. Volc. Geotherm. Res.*, *78*: 8591-8622.

Hill, D. P., 1977. A model for earthquake swarms, *J. Geophys. Res.*, *82*: 1347-1352.

Hill, D. P., 1992. Temperatures at the base of the seismogenetic crust beneath Long Valley Caldera, California, and the Phlegrean Fields, Caldera, Italy, *in* Volcanic Seismology, ed. P. Gasparini, R. Scarpa, K. Aki, p 432-461, Springer-Verlag, Berlin, 572 pp.

Jackson, S.M., 1994. Magnitudes of earthquakes associated with basalt dike intrusion for use, *in* INEL seismic hazards evaluations, Idaho National Engineering Laboratory.

Kanamori, H., 1977. The energy release in great earthquakes, *J. Geophys. Res.*, *82*: 2981-2987.

Katsumata, A., 1983. Comparison between the JMA magnitude and the moment magnitude and estimation of the attenuation function for the maximum displacement amplitude on the basis of moment magnitude, *in* Internation workshop on strong motion data, , Port Harbour Research Institute of Japan and United States Geological Survery, USA, 127-144 pp.

Keith, T. E. C., C. J. Nye, J. C. Eichelberger, T. P. Miller, J. A. Power, 1996. March 1996 seismic crisis at Akutan Volcano, Central Aleutian arc, Alaska (abs.), *EOS Trans*, *77*: F815.

Koyanagi, R.Y., B. Chouet, and K. Aki, 1987. The origin of volcanic tremor in Hawaii: Part 1, Data from the Hawaiian Volcano Observatory 1969-1985, *in* Volcanism in Hawaii, edited by R.W. Decker, Wright, T. L., and Stauffer, P. H., , U.S. Geological Survey, 1221-1258 pp.

Latter, J.H., 1981. Volcanic earthquakes, and their relationship to eruptions at Ruapehu and Ngauruhoe volcanoes, *J. Volc. Geotherm. Res.*, *9*: 293-309.

McClelland, L., T. Smikin, M. Summers, E. Nielsen, T. C. Stein eds., 1989. *Global volcanism* 1975-1985, Prentice-Hall, Englewood Cliffs, New Jersey, 655 pp.

McGarr, A., 1976. Seismic moments and volume change, *J. Geophys. Res.*, *81*: 1487-1494.

McNutt, S.R., and J.P. Benoit, 1995. Generic earthquake swarm model (extended abs.), *Periodico di Mineralogia*, 64: 229-230.

Minakami, T., 1960. Fundamental research for predicting volcanic eruptions (part 1): Earthquakes and crustal deformations originating from volcanic activities, *Bull. Earthquake Res. Inst., 38*: 497-544.

Mogi, K., 1963. Some discussions on aftershocks, foreshocks, and earthquake swarms--The fracture of a semi-infinite body caused by an inner stress origin and its relation to the earthquake phenomena, *Bull. Earthquake Res. Inst., 41*: 615-658.

Mori, J., R. A. White, D. H. Harlow, P. Okubo, J. A. Power, R. P. Hoblitt, E. P. Laguerta, A. Lamuza, and B. C. Bautista, 1996. Volcanic earthquakes following the 1991 climactic eruption of Mount Pinatubo: Strong seismicity during a waning eruption, *in* Fire and mud: eruptions and lahars of Mount Pinatubo, C. G. Newhall and R. S. Punongbayan eds., Univ. Washington Press, p. 339-350.

Newhall, C. G. and S. Self, 1981. The volcanic explosivity index (VEI): an estimate of the explosive magnitude for historical volcanism, *J. Geophy. Res., 87*: 1231-1238.

Power, J. A., J. F. Paskievitch, D. H. Richter, R. G. McGimsey, P. Stelling, A. D. Jolly, H. J. Fletcher, 1996. 1996 seismicity and ground deformation at Akutan volcano, Alaska, *EOS Trans, 77*: F514.

Simkin, T. and L. Seibert, 1994. *Volcanoes of the world* 2nd ed., Geoscience Press, Tuscon, 349 pp.

Tokarev, P. I., 1985. The prediction of large explosions of andesitic volcanoes, *J. Geodyn.*, 3: 219-244.

Weaver, C. S. W. C. Grant, S. D. Malone, and E. T. Endo, 1981. Post-May 18 seismicity: Volcanic and tectonic implications, *in* The 1980 eruptions of Mount St. Helens, Washington, P. W. Lipman and D. R. Mullineaux, eds., USGS Prof. Paper 1250, p. 102-122.

Yokoyama, I., and de la Cruz-Reyna, 1990. Precursory earthquakes of the 1943 eruption of Paricutin volcano, Michoacan, Mexico, *J. Volc. Geotherm. Res.*, *44*: 265-281.

Appendix 2A

Development and Description of the Global Volcanic Earthquake Swarm Database[2]

2A.1 Introduction

Earthquake swarms are pervasive at volcanoes, but have seldom been studied systematically. Most swarms that are described in the literature are those that occurred in association with eruptions; indeed, earthquake swarms are the most reliable method of forecasting eruptions. For the purpose of this report, a swarm is defined as many earthquakes of the same size occurring in a small volume. Swarms are different in these two ways from a mainshock-aftershock sequence or a foreshock-mainshock-aftershock sequence (fig. 2A.1). Swarms are especially common in volcanic areas.

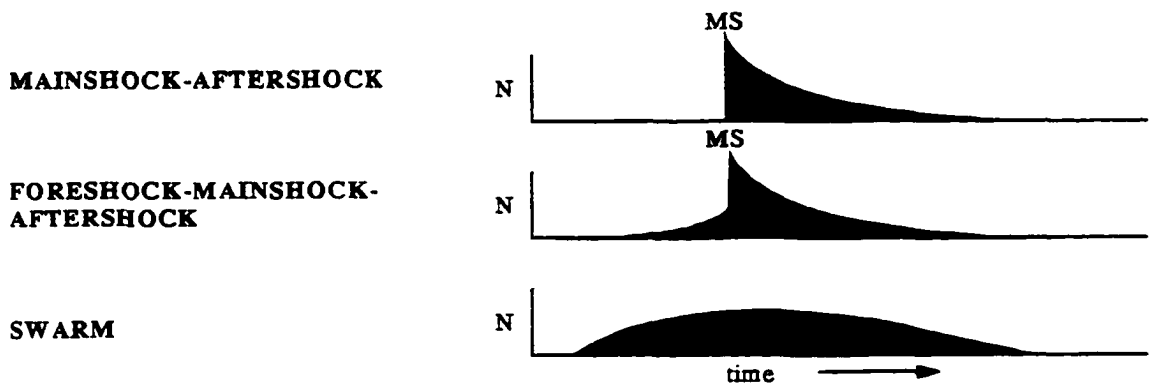

Figure 2A.1 The number of events (N) per unit time versus time is schematically shown for the three types of earthquake sequences. The mainshock (MS) indicates the sharp increase in rate for the upper two distributions.

[2] This appendix is excerpted from: Benoit, J. P. and S. R. McNutt, Global volcanic earthquake swarm database 1979-1989, US Geological Survey Open-File Report 96-69, 333 p., 1996.

Because swarms are such a common and important phenomenon, we undertook a systematic and comprehensive study of swarms at volcanoes using modern commercially available database software. We term the result the Global Volcanic Earthquake Swarm Database (GVESD). This report describes the database and how it is structured.

We chose BVE as our primary data source for several reasons. First, it contains data on many swarms that were never reported in the open literature. This is because most papers report eruptions, and swarms are included only if they were associated with eruptions. In other words, the open literature is biased in favor of eruptions, whereas BVE more fully reports a variety of activity during times of no eruptions. Second, BVE is prepared once per year, which gives investigators the opportunity to summarize data on a broad time scale. Monthly reports, such as the Smithsonian Institution Global Volcanism Network Bulletin, often focus more narrowly on the necessarily short (one month) time scale. Third, BVE is organized by time, so the 1980 issue, for example, contains data on many volcanoes for 1980. This makes it easy to select a sample, which includes known large (or small) eruptions, whereas the open literature often has a significant delay between an event and the report. Fourth, BVE data are organized systematically, which greatly aids the preparation of data for entry into the electronic database. Fifth, the BVE includes a section devoted to miscellaneous information. The miscellaneous information section includes many reports of seismic activity at volcanoes that were not in eruption that year. Finally, BVE includes a supplement, which is used to provide additional information on previous years' activity. This systematic updating provides an additional element of quality control, which is not found in most standard reports.

In spite of the generally high quality of BVE data, there are a number of limitations in those data as well as in the very nature of the problem we have chosen for study. In many respects this has been an exercise in the study of messy data. We have been faced with the difficult task of converting the judgments and measurements of many other scientists, which are often reported in words, into numerical data. We have thus been faced with a myriad of decisions and have struggled to maintain consistency and high quality control. A most basic decision is the start time of an earthquake swarm. In most cases this has been reported by a remote observer, but the units vary widely from "10:23 on July 24" to "late July." In some cases we have had to read data from a graph or histogram, so we have had to decide whether a factor of 2 or 3 increase above background

marks the onset of a swarm. The sections below on the structure of the database provide many examples of such decisions.

It was our initial intention to perform a full multi-parametric study of the database. However, it quickly became apparent that durations of earthquake swarms were the most widely reported parameter whereas many other parameters were poorly reported (e.g., energy, cumulative seismic energy release, detection threshold, b-values). Thus we have focused our initial efforts on understanding the distribution of the swarm duration with respect to eruptive activity.

2A.2 *Database Structure and Description*

The GVESD consists of three main tables: a volcano table (VOLCAT), a volcanic earthquake swarm table (SWARMCAT), and an eruption table (ERUPTCAT). The volcano table contains general information on 149 volcanoes active between 1979-1989. This table also serves as the parent table for the rest of the database. A sample record of the volcano and swarm table is shown in figure 2A.2.

KUSATSU-SHIRANE Honshu-Japan 36.62N 138.55E *VOTW num.*:0E03-12=
Morphology: strato or composite *Tectonic framework:* Convergent (arc)
Elevation above m.s.l.: 2176 m *Edifice relief:* 500 m
Range of eruptive products: andesite *Last known eruption after:* 1964

SWARM DATE: 82/10/22 ±0.5 Dur. (days): 1.5 ±1 Type: 1aq Event type(s): VE,t Grade: B

Max. Magnitude:
Max. Intensity: MM at
Depth (km): ±
Detection threshold: 1.2
Cum. energy release:
EQ total: 23
Felt total:
b-value:
Repose (yr.): 6
Previous swarms:
Seismograph: permanent
Dist. to vent 1.1 km
Type: electromagnetic
Component: 3
Natural period: 1 s
Magnification: 5 K
OTHER REPORTED OBSERVATIONS
Tremor: Y Migration:
Deformation: Focal mech:
Gravity: Y EQ families:
Magnetic: Y Rumbling: Y
Geothermal: Y

Key phrase: Prior to eruptions, frequency of volcanic earthquakes increased on Oct. 22 (23 events).

The exact time of occurrence of these phreatic explosions was not well known. However, at 08:55 continuous volcanic tremors (amplitude = 0.2 um), possibly due to eruptive activity, commenced and was recorded at 1.1 km NE of Yugama crater and the amplitude became 5 um through about 11:00. Then, the amplitude of continuous volcanic tremors decreased; 1 um after 12:30, 0.3 um after 00:00 on Oct. 27. 0.1 um after 16:15 and stopped at 01:24 on Oct. 30.

Prior to eruptions, the frequency of volcanic earthquakes increased on Oct. 22 (23 events) and one volcanic tremor was recorded volcanic earthquakes swarmed from 21:45 (Oct. 26) to 07:38 (Oct. 27) but frequency suddenly decreased after that.

Figs: seismic activity before and after phreatic explosion of Oct. 26.

BVE No. 22, p. 47-50.

Figure 2A.2 An example record from the Global Volcanic Earthquake Swarm Database. The top box shows the information contained in the volcano table. The middle portion shows one

swarm record from the swarm table. The bottom portion shows text excerpted from the original reports.

2A.2.1 Volcano Table

The volcano name, geographical region, latitude, longitude, and volcano number used within the database are drawn directly from Volcanoes of the World Data File 1992, an update of Volcanoes of the World (Simkin and others, 1981; Simkin and Siebert, 1994). The Volcanoes of the World Data File was expanded to include the volcano elevation, edifice height, morphology, compositional range of erupted products, tectonic framework, and a short geologic summary of each volcano (time is local unless otherwise stated). This supplemental information was taken from the List of the World Active Volcanoes, a special issue of the BVE, (Katsui and others, 1971), and Volcanoes of North America, (Wood and Kienle, 1990).

2A.2.2 Earthquake Swarm Table

The volcanic earthquake swarm table holds over 600 records containing summary information related to each swarm and includes the dates of occurrence, durations, and the uncertainties in these measurements. Other parameters related to swarms such as the swarm type (see definitions below), the event type, the magnitude and intensity of the largest shock, the number of felt and unfelt events, and a short summary of the seismic instrumentation are included with each swarm record. This summary information is supplemented with an extended field that contains text excerpted from the original reports. A reference list is included with each record. See figure 2A.2 for an example.

2A.2.3 Eruption Table

The eruption table contains summaries of over 160 eruptions associated with well-documented earthquake swarms. It includes information pertaining to eruptive activity, such as dates of activity, eruption intensity (Volcano Explosivity Index), and character of the eruption. This information is drawn from the BVE and the Smithsonian Institution's Global Volcanism Program eruption data file. The eruption table does not include all eruptions that occurred during the time period covered by the database.

The following sections contain detailed descriptions of parameters in each of the above tables.

2A.3 VOLCAT Organization and Parameter Description

The conventions for the volcano name, geographical region, latitude, longitude, and volcano number used within the GVESD are the same as in the Volcanoes of the World (Simkin, and others, 1981). The order of presentation is by geographic region and follows the organization of the Catalog of Active Volcanoes of the World, IAVCEI, 1951- present. Table 2A.1 shows the regional organization, the number of swarm records in each region, and the starting page for each region in the GVESD. Table 2A.2 is an alphabetical listing of the volcanoes, the number of swarm records at each volcano, and the volcano number.

Table 2A.1 Regional Organization

	Region	Number of swarm records	Number of volcanoes
1	Mediterranean	26	4
2	Africa and the Red Sea	5	1
3	Arabia and the Indian Ocean	28	1
4	New Zealand, Kermadec, Tonga, and Samoa	26	5
5	Melanesia	81	7
6	Indonesia	38	24
7	Philippines	26	6
8	Japan, Taiwan, and Marianas	138	25
9	Kurile Islands	4	4
10	Kamchatka	26	4
11	Aleutian Islands and Alaska	41	9
12	Western North America	40	5
13	Hawaiian Islands and Pacific Ocean	104	6
14	Central America	23	14
15	South America	16	6
16	West Indies	7	4
17	Iceland and Jan Mayen	8	5
18	Atlantic Ocean	2	1
19	Antarctica	2	2

Table 2A.2 List of Volcanoes in the GVESD

Volcano Name	Number	Recs.	Volcano Name	Number	Recs.
ADAGDAK	1101-112	1	ILI BOLENG	0604-22=	4
AGUNG	0604-02=	1	ILIWERUNG	0604-25=	1
AKITA-KOMAGA-TAKE	0803-23=	2	IVAN GROZNY	0900-07=	1
ALAID	0900-39=	1	IWAKI	0803-27=	1
AMBRYM	0507-04=	1	IWO-JIMA	0804-12=	1
ANAK RANAKAH	0604-071	3	IZU-TOBU	0803-01=	2
ANIAKCHAK	1102-09-	1	KARKAR	0501-03=	9
API SIAU	0607-02=	4	KELUT	0603-28=	1
ASAMA	0803-11=	10	KICK-'EM-JENNY	1600-16=	1
ASO	0802-11=	17	KILAUEA	1302-01-	95
AUGUSTINE	1103-01-	5	KIRISHIMA	0802-09=	9
BAGANA	0505-02=	13	KLIUCHEVSKOI	1000-26=	15
BANDA API	0605-09=	3	KOMAGA-TAKE	0805-02=	2
BANDAI	0803-16=	3	KOZU-SHIMA	0804-03=	1
BATUR	0604-01=	1	KRAFLA	1703-08=	6
BEERENBERG	1706-01=	1	KRAKATAU	0602-00=	2
BEZYMIANNY	1000-25=	7	KUSATSU-SHIRANE	0803-12=	11
BROMO	0603-31=	1	LAMONGAN	0603-32=	2
BULUSAN	0703-01=	11	LANGILA	0502-01=	16
CAMPI FLEGREI	0101-01=	6	LASCAR	1505-10=	1
CANLAON	0702-02=	8	LASSEN PEAK	1203-08-	1
CHICHON, EL	1401-12=	1	LIAMUIGA, MT.	1600-03=	1
CHIKURACHKI	0900-36=	1	LOIHI SEAMOUNT	1302-00-	3
COLIMA VOLCANIC COMP.	1401-04=	4	LOKON-EMPUNG	0606-10=	3
COLO [UNA UNA]	0606-01=	1	LONG ISLAND	0501-05=	1
CONCEPCION	1404-12=	1	LONG VALLEY	1203-14-	17
DECEPTION ISLAND	1900-03=	1	LONQUIMAY	1507-10=	1
DIENG VOLCANIC COMPL.	0603-20=	1	MACDONALD	1303-07-	3
DON JOAO DE CASTRO BANK	1802-07=	2	MAHAWU	0606-11=	1
DUTTON, MT.	1102-011	1	MAKIAN	0608-07=	1
EBEKO	0900-38=	1	MALINAO	0703-04=	1
EREBUS, MOUNT	1900-02=	3	MANAM	0501-02=	17
ETNA	0101-06=	18	MARAPI	0601-14=	3
FOURNAISE, PITON DE LA	0303-02=	28	MARU-YAMA	0805-061	3
FUEGO	1402-09=	1	MASAYA	1404-10=	2
FUJI	0803-03=	1	MAUNA LOA	1302-02=	6
GALUNGGUNG	0603-14=	2	MAYON	0703-03=	3
GAMALAMA	0608-06=	2	ME-AKAN	0805-07=	6
GARELOI	1101-07=	1	MEDICINE LAKE	1203-02-	1
GORELY	1000-07=	2	MEHETIA	1303-06-	1
GRIMSVOTN	1703-01=	1	MERAPI	0603-25=	5
GUAGUA PICHINCHA	1502-02=	3	MIYAKE-JIMA	0804-04=	1
HAKKODA GROUP	0803-28=	1	MOMOTOMBO	1404-09=	1
HAROHARO COMPLEX	0401-05=	1	NASU	0803-15=	5
HEKLA	1702-07=	1	NEGRA, SIERRA	1503-05=	1
HOOD, MOUNT	1202-01-	1	NII-JIMA	0804-02=	2
IJEN	0603-35=	1	NIUAFO'OU	0405-11=	1

Table 2A.2 continued. List of Volcanoes in the GVESD

Volcano Name	Number	Recs.	Volcano Name	Number	Recs.
NORIKURA	0803-06=	1	SOPUTAN	0606-03=	3
NYAMURAGIRA	0203-02=	7	SORIK MARAPI	0601-12=	3
NYOS, LAKE	0204-003	1	SOUFRIERE GUADELOUPE	1600-06=	1
OKMOK	1101-29-	1	SOUFRIERE ST. VINCENT	1600-15=	1
ON-TAKE	0803-04=	5	SPURR	1103-04-	1
OSHIMA	0804-01=	33	ST. HELENS, MT.	1201-05-	27
PACAYA	1402-11=	5	STROMBOLI	0101-04=	5
PAGAN, NORTH	0804-17=	1	SUWANOSE-JIMA	0802-03=	1
PARICUTIN	1401-06=	1	TAAL	0703-07=	3
PATATES, MORNE	1600-11=	4	TACANA	1401-13=	4
PAVLOF	1102-03-	21	TANGKUBAN PARAHU	0603-09=	3
PELEE, MONTAGNE	1600-12=	1	TARAWERA	0401-06=	1
PINATUBO, MT.	0703-083	1	TARUMAI	0805-04=	3
POPOCATEPETL	1401-09=	1	TEAHITIA	1303-03-	4
RABAUL	0502-14=	19	TECAPA	1403-08=	1
RAUNG	0603-34=	1	TELICA	1404-04=	2
REDOUBT	1103-03-	9	TOKACHI	0805-05=	9
RINCON DE LA VIEJA	1405-02=	1	TOUMA	1501-03=	1
RUAPEHU	0401-10=	22	TUPUNGATITO	1507-01=	2
RUIZ	1501-02=	10	ULAWUN	0502-12=	25
RUMBLE III	0401-13-	1	UMBOI	0501-06=	1
SAKURA-JIMA	0802-08=	13	UNNAMED SUBMARINE	0804-14*	1
SAN CRISTOBAL	1404-02=	1	UNZEN	0802-10=	6
SAN MIGUEL	1403-10=	4	USU	0805-03=	8
SANGEANG API	0604-05=	2	VENIAMINOF	1102-07-	2
SANTA MARIA	1402-03=	5	VILLARRICA	1507-12=	1
SARYCHEV PEAK	0900-24=	1	VULCANO	0101-05=	6
SEMERU	0603-30=	4	WHITE ISLAND	0401-04=	7
SHIVELUCH	1000-27=	7	YASUR	0507-10=	1
SIRUNG	0604-27=	1	YELLOWSTONE	1205-01-	1
SLAMET	0603-18=	1			

2A.3.1 Morphology, Tectonic Framework, Elevation, and Edifice Relief

The morphology or volcano type is drawn from the List of the World Active Volcanoes (Katsui and others, 1971). Table 2A.3 is a list of the morphologies and the abbreviations used in the VOLCAT table. The majority of swarm records in the GVESD occur at stratovolcanoes and shield volcanoes, with the remainder from calderas, submarine, and compound volcanoes. There are more than twice as many swarm reports from stratovolcanoes as from shield volcanoes.

Table 2A.3 Volcano Morphology

Morphology abbreviation	*Volcano morphology*	*Total number of swarm records*	*Number of swarm records with duration specified*
S	strato or composite	321	267
Sh	shield	137	130
S,Cald	strato with caldera	63	53
S,D	strato with lava dome	57	43
Cald	caldera	49	35
Cald,S	caldera with strato	33	21
S,Sh	strato on a shield	22	21
C	compound or complex	19	12
D	lava dome	17	15
Sub	submarine	17	12
S,CL	strato with crater lake	9	6
	unknown	8	7
Sh,Cald	shield with caldera	3	2
CC	cinder cone	2	2
CC,C	cinder cone in caldera	1	0
LF	lava field (flows)	1	1
S,So	strato with somma	1	1
Sh, D	shield with dome	1	1

The tectonic framework field refers to the regional tectonic setting. We define three general regimes; convergent, divergent, and hot spot. When detailed information is available, we subdivide the tectonic regimes by the type of crust involved. Table 2A.4 shows a summary of the abbreviations used in the GVESD for the tectonic framework. The majority of swarm records occur at volcanoes in convergent margins followed by oceanic hot spots and divergent margins.

Table 2A.4 Tectonic Framework

Tectonic framework abbreviation	Tectonic framework	Total number of swarm records	Number of swarm records with duration specified
C	Convergent (arc)	241	196
CM	Convergent Continental Margin	175	146
HO	Oceanic Hot Spot	133	127
CO	Convergent Intraoceanic	44	41
CM?	Uncert. Convergent Continental Margin	38	28
C?	Uncert. Convergent (arc)	29	28
DRC?	Uncert. Divergent Rift Continental	17	13
DM	Divergent Mid Ocean Ridge	12	11
CO?	Uncert. Convergent Intraoceanic	9	7
DRC	Divergent Rift Continental	8	5
HC	Continental Hot Spot	1	0

The elevation data are drawn from both the Volcanoes of the World (Simkin and others, 1981) and the Catalog of Active Volcanoes of the World IAVCEI, 1951- present. Elevations are in meters above sea level at the volcano's highest point. When more than one elevation value is given (e.g., multiple peaks within a massif) the highest value is recorded. The edifice relief or "height over the regional base" is a coarse measurement the volcano's size. Edifice relief values were extracted from List of the World Active Volcanoes (Katsui and others, 1971) for most areas and The Volcanoes of North America (Wood and Kienle, 1990) for North America.

2A.3.2 Range of Erupted Products

The range of eruptive products field is intended to give a rough idea of the silica content of the magmas erupted at each volcano. We divided this field into six categories; basalt (B), basaltic andesite (BA), andesite (A), dacite (D), rhyodacite (RD) and rhyolite (R). For example, for a volcano that has erupted basalt and dacite, the eruptive product range field is coded as B,D or 'basalt and dacite'. The silica ranges, abbreviations, and the number of cases within each field are shown in table 2A.5. Over half of the swarm records are from volcanoes with basaltic to andesitic composition. The majority of these data were extracted from Katsui and others (1971) for areas outside North America, Motyka and others (1993) for Alaska, and Wood and Kienle (1990) for the contiguous U.S. and Canada. For selected individual eruptions we recorded silica content of the erupted products. The eruption table (see below) holds these data for eruptions with well-studied swarms. The silica content data for the individual eruptions are primarily drawn from the BVE.

Table 2A.5 Erupted Products

Erupted products abbreviation	*% SiO_2*	*Lower bound*	*Upper bound*	*Erupted products*	*Total number of swarm records*	*Number of swarm records with duration specified*
B	46.5	41	52	basalt	256	220
B,BA	50	41	55	basalt to basaltic andesite	61	59
B,A	52.8	41	63	basalt to andesite	88	63
BA	53.5	52	55	basaltic andesite	1	1
B,D	55.3	41	65	basalt to dacite	0	0
BA,A	56.3	52	63	basaltic andesite to andesite	8	7
B,RD	57	41	70	basalt to rhyodacite	0	0
BA,D	58.8	52	65	basaltic andesite to dacite	0	0
A	59	55	63	andesite	199	157
B,R	59.3	41	74	basalt to rhyolite	27	19
BA,RD	61	52	70	basaltic andesite to rhyodacite	0	0
A,D	61.5	55	65	andesite to dacite	58	51
BA,R	63	52	74	basaltic andesite to rhyolite	1	1
A,RD	63.3	55	70	andesite to rhyodacite	0	0
D	64	63	65	dacite	0	0
A,R	65.5	55	74	andesite to rhyolite	2	2
D,RD	65.8	63	70	dacite to rhyodacite	0	0
RD	67.5	65	70	rhyodacite	0	0
D,R	68	63	74	dacite to rhyolite	0	0
RD,R	69.8	65	74	rhyodacite to rhyolite	0	0
R	72	70	74	rhyolite	3	3

SiO_2 values from: Cox et al., (1979), The interpretation of igneous rocks, George Allen and Unwin, London.

2A.4 SWARMCAT Organization and Parameter Description

For each volcano, one or more earthquake swarm records are linked to the volcano table's records. The swarm records are linked through the Volcanoes of the World catalog-number. Each swarm record is composed of: a header of key fields; a body of swarm, instrumental, and other geophysical parameters; a variable length section containing report excerpts; and references. Three fields are used to ensure that every earthquake swarm record is unique. These fields are called the key fields, and are the volcano catalog-number, the swarm start date, and the swarm type. Every swarm record has a unique value of these three combined fields.

2A.4.1 Swarm Dates, Durations and Uncertainties

The start date of a swarm in most cases originates directly from the BVE reports. Typically the beginning of a swarm is described as an increase in the number earthquakes reported per day (see swarm duration definition below). Gradual increases in seismicity, problems in network coverage, a high detection threshold, and the lack of a clear definition of when a swarm begins (or ends) are all problems with determining the start time and duration of a swarm. Often these difficulties lead to reports that describe the onset of a swarm in imprecise terms. In order to track these problems a field was added to capture the uncertainties in these measurements. A typical swarm report may read: "Seismicity increased in the middle of November to about 60 events per day. However, there was a decline to 5-20 per day in late December" (Bagana volcano, BVE, 1985, no. 25, p. 20). This swarm was entered into the GVESD as beginning on 85/11/15 + 5 days, with a duration of 40 + 10 days. Table 2A.6 describes the uncertainty values used in several common situations.

Table 2A.6 Reporting Uncertainties

Dates reported	*Uncertainty assigned:*
minute	0
hour	+/-0.02 day
day	+/-0.5 day
week	+/-3.5 days
month	+/-15 days

Date modifiers	*Within a month (e.g. "mid" Jan.)*	*Within a year (e.g. "mid" 1980)*
"early"	5 Jan. +/- 5 days	1 Mar. 1980 +/- 60 days
"mid"	15 Jan. +/- 5 days	1 Jul. 1980 +/- 60 days
"late"	25 Jan. +/- 5 days	1 Nov. 1980 +/- 60 days

Some reports in the BVE include vague descriptions or occurrences of seismicity that cannot be easily classified. We use one place holding record per year to incorporate this information into the GVESD. Place holder records are delimited using the start date, the uncertainty, and the key phrase fields (see below). The start date is 'year'/7/1 with an uncertainty of + 183 days for a place holding record. The key phrase field also contains the text; "place holder for 'year'..." to set these records apart. These are examples of our solutions to the problem of coding highly variable reports into quantitative form.

2A.4.2 Definition of a Swarm and Swarm Duration

Earthquake swarms are generally defined as a sequence of events closely clustered in time and space without a single outstanding shock (Mogi, 1963). Our working definition follows Mogi's

outline and also requires a significant increase in the rate of local volcanic earthquakes above the background rate. We take volcanic earthquakes to be of any type, for example A, B, (Minakami, 1960), high frequency, low frequency, short period, long period, (Koyanagi, and others, 1987), volcano tectonic, (Latter, 1981), explosion events, etc., but they must occur within an arbitrary near distance to the volcano (typically < 15 km). We do not identify a significant increase over the background rate in a strict statistical sense, but accept the experience and point of view of each reporter. In other words, if the reporter feels that an increase in seismicity is significant enough to report, then we include that report as a swarm record along with a quality modifier. We also do not consider seismic crises (peak seismicity rates within a swarm), obvious mainshock-aftershock sequences, and tremor episodes as swarms. These "non-swarm" seismic sequences are recorded in the GVESD and are delimited in a separate field (QC field explained below).

This working definition was developed through the systematic examination of over 600 swarms. One single fixed definition or algorithm might be preferable, but is not feasible due to the widely varying qualities and formats of the data. Future studies would greatly benefit from standardized reporting and the strict application of an algorithm to distinguish the starts, ends and durations of swarms.

2A.4.3 Swarm Type

We grouped volcanic earthquake swarms according to their temporal relationship to eruptive activity. The swarm types are schematically summarized in figure 2A.3. The main categories are: swarms that precede (Type I), or accompany (Type II) eruptive activity, and those not associated with eruptive activity (Type III). There are a few reported cases of eruptions occurring without a detectable increase in seismicity. These eruptions are included in the database and are identified as Type IV. Roman numerals are used throughout the discussion of swarm type, while Arabic numerals are used in the database for compactness.

Type I, or precursory swarms (46% of the GVESD records), were further divided into 4 sub-types (I a, I b, I c, and I d) according to when the swarm ends in relation to the eruptive activity. Type I a are swarms that begin and end before the eruption commences (for example, 1989 precursory swarm at Izu-Tobu). Type I b are swarms that begin before the eruption and end coincident with the start of the eruption (for example Asama, 1983). Type I c are swarms that

begin before the eruption, continue through the duration of the eruption, and end as the eruption ends (for example Oshima, 1987). Type I d swarms begin before the eruption and end after the eruption has ceased (for example Soufriere de Guadeloupe, 1976).

Type II swarms, those accompanying eruptions (15% of the GVESD records), are separated into three sub-types (II a, II b, II c). Type II a swarms begin and end with the eruption. Type II b swarms begin with the eruption and then continue after the cessation of the eruption. Type II c is reserved for swarms that occur during an extended eruption (e.g., the continuing eruption of Kilauea).

Type III swarms are not associated with eruptions (39% of the GVESD records). To separate this category from swarms of Type I a, the time period between the end of the swarm and the next eruption was measured. This quiescent duration is generally less than 10 days with no cases greater than 3 months. Using this observation 100 days is used as a cut-off to separate Type III from Type I a. Post-eruption swarms are also included in Type III category.

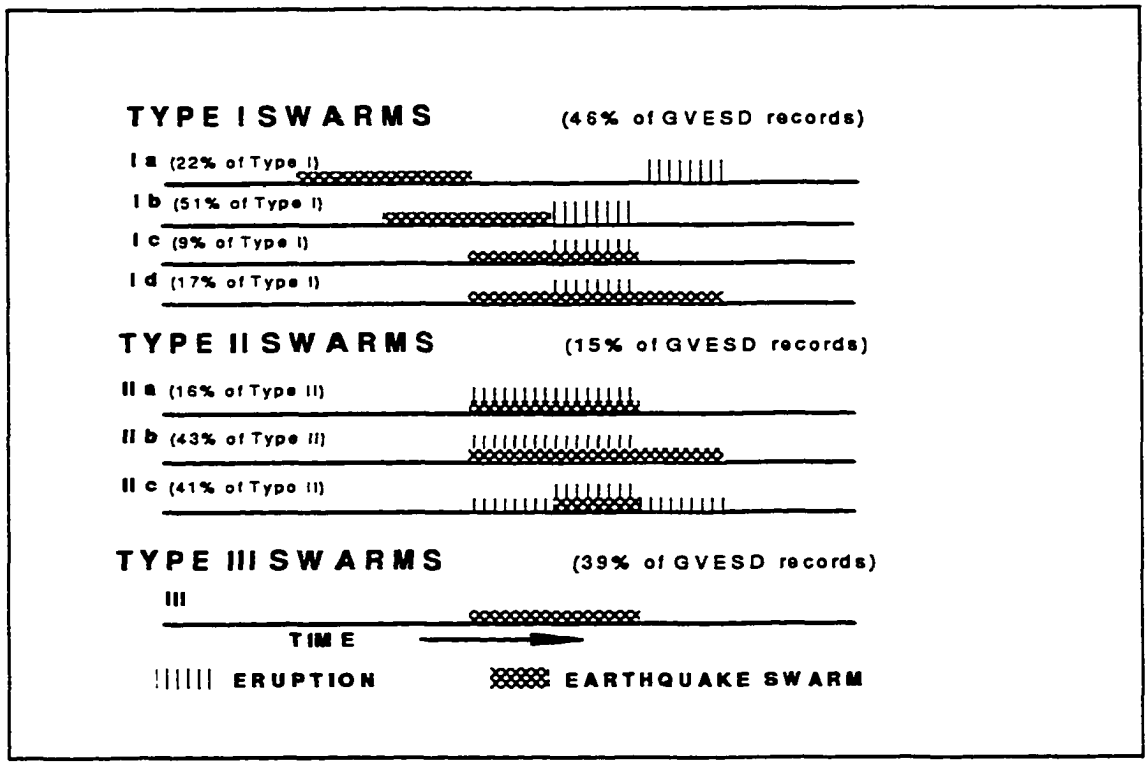

Figure 2A.3 Schematic diagram of the temporal relation between volcanic earthquake swarms and eruptive activity. The stippled boxes represent the earthquake swarms. The vertically striped boxes represent the eruptions.

2A.4.4 Event Types

In order to further describe the nature of the seismicity that makes up a swarm we added an event type(s) field. Table 2A.7 shows a list of the events types found in the GVESD. Within any swarm there maybe one or more types of seismic event recorded. The event type field attempts to reflect this complexity by listing (in the order of occurrence, if reported) all the event types that occurred during the swarm. Some swarms are defined and reported by event type. At Kilauea, for example, swarms are reported by location and event type. We separated swarms reported at this level of detail into individual swarm records. Most reports do not provide this level of detail. Therefore, most swarm records contain many different event types. Table 2A.7 lists the event types we have defined, with their abbreviations and the numbers of swarm records in which each was used.

Table 2A.7 Event Types

Event type abbreviation	*Event type*	*Number of cases*
A	A-type	24
B	B-type	82
C	C-type	6
E	explosion	16
Felt	felt earthquake	11
G	gas	2
HF	high frequency	23
LF	low frequency	36
LP	long period	49
M	mixed frequency	1
MF	medium frequecy	1
mseis	micro-seism	1
reg	regional earthquake	1
S	surface	15
SP	short period	39
SV	shallow volcanic	10
Tect	tectonic	7
t	tremor	60
tor	tornillo	2
VE	volcanic earthquake	56
VT	volcano tectonic	37

2A.4.5 Quality Grades (QC)

We assign an overall quality grade (QC) to each swarm record. The quality grade is intended to be a qualitative statement of the reliability of the report and the swarm record. We assigned quality grades of A through C to each swarm record. The first two grade levels, A and B primarily reflect the report data source. A QC grade of A is given to swarm records that are taken from the primary reviewed literature or from data to which we have primary access. We assume that swarm records derived from these sources are the most dependable. QC grades of B are assigned to swarm records extracted from reports in the BVE. This QC grade level makes up a majority of the records in the GVESD. The C grade is not a reflection of the data source, but is given to records where there is some question about whether the seismicity constitutes a swarm. Mainshock-aftershock sequences, seismic crises, and vague reports of seismic activity are given a QC grade of C. A parallel grading system is used for tremor episodes. Tremor episodes are delimited from true earthquake swarms by using a lower case QC grade (e.g., a, b, and c).

Approximately 15% (93 records) of the swarm records in the GVESD are derived from the reviewed literature or locally available data (A-QC). Over half (327 records) of the records were

drawn from the BVE (B-QC). A quarter (148 records) of the records are questionable swarms and therefore given a C-QC grade. Tremor episodes comprise about 8% (50 records) of the GVESD.

2A.4.6 Maximum Magnitude, Intensity, and Depth

The maximum magnitude field contains the magnitude of the largest shock within each swarm. Over one fourth (168 cases) of the swarm records contain the magnitude of the largest shock in the swarm. We added a magnitude scale field to qualify the type of magnitude reported (e.g., ML, mb, MJMA, etc.). A specific magnitude scale is reported with the maximum magnitude in only 6% of the swarm records.

The maximum intensity field records the felt intensity of the largest shock of the swarm. Another field holds the distance between the observer and the active vent. Intensity is reported in about 10% (67 records) of the swarm records, while the distance to the active vent is reported in only one half of these cases. We have recorded all the intensities in the GVESD using the Modified Mercalli (MM) scale. When an intensity is given in a different scale (e.g., JMA or Rossi-Forel) we assign a MM intensity to the value. Where differing intensity scales overlap, the greater MM value is used. For example, the JMA grade 1 spans MM1 to MM3, so a JMA grade 1 is given a MM3.

The depth field is a measure of the mean depth of the swarm. The depth field is supplemented with another field to express the range of depths where the earthquakes are located. The mean depth is recorded in 16% (103 records) of the swarm records. Figure 2A.4 shows the distribution of the mean depth of volcanic earthquake swarms recorded in the GVESD. Volcanic earthquakes are generally shallower than their tectonic counterparts.

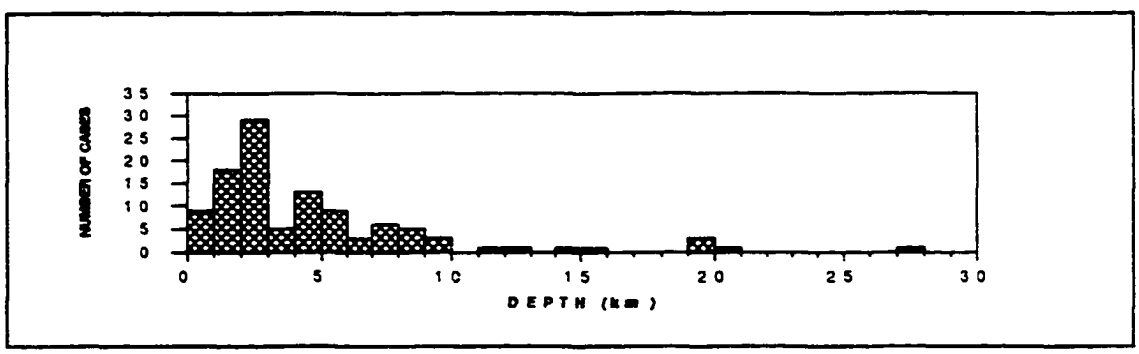

Figure 2A.4 The mean depth of volcanic earthquake swarms.

2A.4.7 Cumulative Energy, Energy Release Rate, and Repose

The cumulative energy and the energy release rate fields were included to use a standard measure for comparison with eruption parameters. In practice, the energy parameters are rarely reported (only 2% of the swarm records). This is most disappointing; with a homogenous data set the energy field could prove to be an interesting parameter to compare with eruptive activity. Energy has obvious physical relevance. The energy values and rates are reported in Joules and Joules per day, respectively.

The repose field refers to the eruption repose period. The eruption repose period is here defined as the period of time between the end of the last eruption to the beginning of the next eruption. This field is reported in 20% of the swarm records (127 cases).

2A.4.8 Earthquake Counts and Magnitude Detection Threshold

The total number of earthquakes and the number of felt earthquakes are reported in nearly one half of the GVESD records (268 records). The total number and number of felt earthquakes are recorded in the "# EQ total" and "# felt total " fields respectively. The number of reported earthquakes in a swarm is sensitive to the magnitude detection threshold of the local network. The magnitude detection threshold is recorded in a separate field. The detection threshold is reported in about a fourth of the swarm records. Where sufficient information about the network is available the detection threshold was estimated. When reported, the distance from the felt observations to the active vent is included in the comments field.

2A.4.9 Seismograph Information

The seismograph section of SWARMCAT is devoted to a summary of the seismic instrumentation at each volcano. The summary includes the type of seismometer, the distance between the nearest station and the active vent, the number of components, the natural period, and the magnification. The seismograph field indicates if the instruments are permanent or temporary stations. The distance (in kilometers) between the nearest station and the active vent is recorded in the distance to vent field. The seismograph and distance fields are commonly reported and are recorded in 84% (530 cases) of the swarm records. The type and component fields describe the type and the number of components in the instrument. We also record the natural period (in

seconds) and the magnification at the natural period when available. The natural period and the magnification fields are reported in about 60% (369 cases) of the swarm records.

2A.4.10 Previous Swarms and Other Reported Information

The previous swarms field is intended to determine whether or not there is a basis for comparison of a database swarm with other, earlier swarms. The OTHER REPORTED INFORMATION section of the SWARMCAT table provides a quick reference to other reported phenomenon. It was created to be a starting point to build or link other databases. The fields are either filled with 'Y' (yes), 'N' (no), or blank (no information reported). A 'Y' or 'N' in any of the field means some information regarding that parameter was reported. If the parameter was observed and either changed or no information on change was given, then a 'Y' is indicated. For example, a report may state "tilt measurements were conducted," this information is recorded as a 'Y' in the deformation field even though it is not clear if any tilt occurred. A 'N' or no in any field represents a negative result was reported. If, for example, a report explicitly states "no migration of earthquake hypocenters was observed" the migration field will be filled with a 'N.' The details of seismological observations are included in the comment field. For non-seismological observations details can be found in the references section of the record.

Volcanic tremor is the most commonly reported observation followed by reports on ground deformation or tilt. Table 2A.8 shows the number of positive and negative cases reported for each field. The fields are mostly self-explanatory, but a few need some further explanation. The Geothermal field refers to any temperature measurement conducted near the volcano. This includes fumaroles, crater lakes, or hot springs. As stated above, Migration refers to the migration of earthquake hypocenters. The EQ (earthquake) families field refers to earthquakes with nearly identical waveforms, also known as *multiplets*. The Rumbling field describes audible observations made at the volcano.

Table 2A.8 **Other Reported Observations**

Parameter	*number of observations*	
	yes	*no*
Tremor	340	10
Deformation	255	1
Magnetic	108	0
Geothermal	89	0
Gravity	60	0
Rumbling	47	0
Migration	42	0
EQ families	36	0
Focal mechanism	8	0

2A.4.11 References, Comment and Key Phrase fields

The references used to compile the swarm records are listed at the bottom of each record. The first reference in the list is the primary data source, unless otherwise noted. The other references of seismological interest are included with the BVE reports. The comment field is above the reference field within the swarm record. This variable length field contains text excerpted from the original reports. If the report includes pertinent figures a short note is added in the comment field. The Key phrase field is a one or two line summary of the comment field and gives the essence of the report from which the numerical data were derived.

2A.5 ERUPTCAT Organization and Parameter Description

The eruption table (ERUPTCAT) contains basic descriptive parameters for 170 eruptions. The task of systematically compiling a complete database of eruption parameters for all eruptions (occurring during the time period covered by the GVESD) is beyond the scope of this study. We selected a set of eruptions that were preceded by well-reported swarms. From these eruptions, data were collected and entered into the eruption table. The eruption parameters chosen are, the start date, the volume of erupted material, the height of the eruption plume, an estimate of the silica content of the erupted products, and the Volcanic Explosivity Index (VEI). The ERUPTCAT table is shown below as table 2A.9. The eruptions are listed in chronological order (grouped by year), beginning and ending with a few eruptions outside the time period systematically covered by the GVESD.

Table 2A.9 ERUPTCAT

Volcano		Bulletin of Volcanic Eruptions Eruption data					VOTW Eruption data				SWARMCAT Swarm data			
Number	Name	start		volume		plume SiO2	start	T	L	VEI	start	type	dur.	Mmax
0805-03=	Usu						10/7/25	6		2	10/7/22	1bq	4	Ms 5.1
0802-08=	Sakura-Jima						14/1/12	8	9	4	14/1/10	1b	2	Ms 5.2
1401-06=	Paricutin						43/2/20	9	8	4	43/1/7	1b	45	M 4.5
0802-08=	Sakura-Jima						55/10/13			3 *	55/4/20	1aq	175	
1000-25=	Bezymianny						55/10/22	9		5 *	55/10/11	1b	172	M 4.4
1000-27=	Sheveluch						64/11/12	8		4 +	64/11/2	1b	10	M 4.9
1503-05=	Negra, Sierra	79/11/13	g			14	79/11/13			3	79/11/13	1c?	2	M 4.8
1302-01-	Kilauea	80/3/11					80/3/11			0	80/3/10	1c?	1.25	M 4.2
1201-05-	St. Helens, Mount	80/5/18	g	4.0E+8		22 64	80/3/27	9	5	5 *	80/3/20	1d	59	ML 5.1
0502-12=	Ulawun	80/10/6	g			64	80/10/6	7		3	80/10/3	1b?	3	
1201-05-	St. Helens, Mount	80/7/22	g	5.0E+7		20 52	80/3/27			3 #	80/7/22	1b	0.5	M 2.0
1201-05-	St. Helens, Mount	80/10/19 1	m		1.2E+6	64	80/3/27			3 #	80/10/4	1b	11	M 2.8
1102-03-	Pavlof	80/11/8	m?			8 50	80/11/8	6		3 ^	80/11/6	1d	80	M 2.3
1201-05-	St. Helens, Mount	80/12/27 1	m		1.6E+6	63	80/3/27			1 #	80/12/24	1b	2	
0303-02=	Piton de la Fournaise	81/2/3	m		1.6E+7	48	81/2/3		7	2	81/1/21	1b	13	
1201-05-	St. Helens, Mount	81/2/5 1	m		3.6E+6	62	80/3/27			1 #	81/2/2	1b	3	
0805-04=	Tarumai	81/2/27	l	4.0E+2			81/2/27	2		0	80/11/15	1cq	240	
0101-06=	Etna	81/3/17	g		3.0E+7	0.3 48	81/3/17	5	6	1	81/3/12	1aq	6	
1201-05-	St. Helens, Mount	81/4/10 1	m		4.1E+6	62	80/3/27			1 #	81/4/5	1b	5	
0703-01=	Bulusan	81/4/27					81/4/9			3 #	81/4/20	1b	8	
0900-39=	Alaid	81/4/27				12	81/4/27	8		4 *	81/4/26	1b	6	M 3.5
0804-17=	Pagan, North	81/5/15	g	3.6E+7	4.3E+7	20 52	81/5/15	8	7	4 *	81/4/1	1b	45	M 4.0
1201-05-	St. Helens, Mount	81/6/18 1	m		4.1E+6	62	80/3/27			1 #	81/6/13	1b	5	
1502-02=	Guagua Pichincha	81/8/31	l	5.0E+3		1 64	81/8/31	4		1 ^	81/8/15	1b	15	
1201-05-	St. Helens, Mount	81/9/6	m		3.9E+6	62	80/3/27			1 #	81/8/30	1b	8	
1102-03-	Pavlof	81/9/25	m	7.5E+6		10.5	81/9/25	7	6	3	81/9/25	1d	96	M 2.3
1201-05-	St. Helens, Mount	81/10/30 1	m		3.6E+6	62	80/3/27			1 #	81/10/24	1b	7	
0203-02=	Nyamuragira	81/12/25	g			5 56	81/12/25	7	7	3	81/12/25	1b	0.13	M 1.3
1404-04=	Telica	82/2/12	m			4.3	81/11/25			2 ^	82/1/15	1cq	27	M 3.0
1201-05-	St. Helens, Mount	82/3/18	m		3.4E+6	62	80/3/27		6	3 #	82/2/24	1b	22	
1303-03-	Teahitia	82/3/25					82/3/16			0	82/3/14	1c	39	M 4.0
1401-12=	Chichon, El	82/3/28	g	5.0E+8		25 59	82/3/28	9		5 *	82/3/1	1bq	28	Md 4.0
0803-11=	Asama	82/4/26	m			0.5 59	82/4/26			2	82/1/15	1aq	15	
1302-01-	Kilauea	82/4/30	m		5.0E+5	0.05 49	82/4/30		5	0	82/4/30	1c?	0.16	
1201-05-	St. Helens, Mount	82/5/14 1	m		2.7E+6	63	80/3/27				82/5/6	1b	8	
1201-05-	St. Helens, Mount	82/8/18 1	m		4.6E+6	63	80/3/27				82/7/27	1b	21	
1302-01-	Kilauea	82/9/25	m		3.0E+6	0.07 49	82/9/25		6	1 ^	82/9/25	1aq	1.6	
1404-10=	Masaya	82/10/7	mi				65/10/10			1 ^	82/10/7	1d	1.5	M 2.3
0803-12=	Kusatsu-Shirane	82/10/26	l			0.1 59	82/10/26			1	82/10/22	1aq	1.5	
0804-12=	Iwo-Jima	82/11/28	l				82/11/28			1	82/11/25	1aq	5	
1302-01-	Kilauea	83/1/3	g		1.4E+7	49	83/1/3		7	1 ^	83/1/1	1aq	6	
1201-05-	St. Helens, Mount	83/2/2	g		1.4E+7	6 63	80/3/27		7	2 #	83/1/20	1b	13	
0101-06=	Etna	83/3/28	g	1.5E+6	1.0E+8	0.1 48	83/3/28	5	8	1	83/1/22	1b?	53	
0803-11=	Asama	83/4/8	m	1.3E+4		0.6 59	83/4/8			2	83/3/17	1aq	7	
1703-01=	Grimsvotn	83/5/28	m			3.5 49	83/5/28			2	83/5/28	1aq	0.39	M 4.0
0606-01=	Una Una	83/7/23	g			14	83/7/18			4 *	83/7/4	1c	24	M 4.6
1302-01-	Kilauea	83/7/25	m		9.0E+6	49	83/1/3			1 #	83/7/5	1b	16	
0803-12=	Kusatsu-Shirane	83/7/26	l			0.2 59	83/7/26			1	83/7/19	1aq	5	
0603-09=	Tangkuban Parahu	83/9/14					83/9/14			1	83/9/5	1bq	10	
0804-04=	Miyake-Jima	83/10/4		4.7E+6	6.0E+6		83/10/3	6	6	3	83/10/3	1b	0.06	
0502-12=	Ulawun	83/11/6	l			2 47	83/11/6			1	83/1/25	1aq	285	
1102-03-	Pavlof	83/11/14	l				83/11/14	7		3	83/11/5	1d	29	M 2.3
1302-01-	Kilauea	83/11/30	m		8.0E+6	49	83/1/3			1 #	83/11/24	1aq	1	
0303-02=	Piton de la Fournaise	83/12/4	m		8.0E+6	48	83/12/4		7	2	83/11/20	1b	14	
0803-12=	Kusatsu-Shirane	83/12/21	l			0.3 59	83/7/26			1	83/12/18	1c	2	

Table 2A.9 continued. ERUPTCAT

Volcano		Bulletin of Volcanic Eruptions Eruption data					VOTW Eruption data				SWARMCAT Swarm data			
Number	Name	start		volume	plume	SiO2	start	T	L	VEI	start	type	dur.	Mmax
1302-01-	Kilauea	84/1/20	g	1.0E+7		49	83/1/3			1 #	83/12/30	1aq	2	
1000-25=	Bezymianny	84/2/5	m		5		84/2/5	7		3 ^	84/1/15	1d	20	K 6.5
1302-01-	Kilauea	84/2/14	m	8.0E+6		49	83/1/3			1 #	84/2/5	1a	4	
1302-01-	Kilauea	84/3/3	g	1.2E+7		49	83/1/3			1 #	84/2/24	1a	7	
1302-01-	Kilauea	84/3/16	g	1.0E+7		49	83/1/3			1 #	84/3/16	1a	8	
1302-02=	Mauna Loa	84/3/25	g	2.2E+8	0.05	51	84/3/25		8	0	84/3/24	1d	120	M 4.0
1302-01-	Kilauea	84/4/18	g	2.4E+7		49	83/1/3			1 #	84/4/10	1b	10	
1302-01-	Kilauea	84/5/16	m	2.0E+6		49	83/1/3			1 #	84/5/7	1b	8	
1302-01-	Kilauea	84/6/7	m	6.0E+6		49	83/1/3			1 #	84/6/1	1a	5	
0603-25=	Merapi	84/6/15	g	8.8E+6	6	54	72/10/6			3 *	84/6/7	1b	8	
1302-01-	Kilauea	84/6/30	m	5.7E+6		49	83/1/3			1 #	84/6/17	1b	12	
1302-01-	Kilauea	84/7/28	m	9.5E+6		49	83/1/3			1 #	84/7/17	1b	11	
1302-01-	Kilauea	84/8/19	g	1.2E+7		49	83/1/3			1 #	84/8/7	1b	12	
0606-03=	Soputan	84/8/31	m		6	59	84/5/24		7	3 ^	84/8/6	1aq	19	
1302-01-	Kilauea	84/9/19	g	1.1E+7		49	83/1/3			1 #	84/9/1	1b	20	
1000-25=	Bezymianny	84/10/12	g		3.5		84/2/5	7		3 ^	84/10/12	1d	23	K 6.0
1302-01-	Kilauea	84/11/2	m	6.6E+6		49	83/1/3			1 #	84/10/2	1b	29	
1302-01-	Kilauea	84/11/20	m	8.4E+6		49	83/1/3			1 #	84/11/11	1b	9	
1302-01-	Kilauea	84/12/3	g	1.3E+7		49	83/1/3			1 #	84/11/23	1b	9	
0502-12=	Ulawun	84/12/30	l		2	47	84/12/30		5	1	84/12/24	1c	29	
1302-01-	Kilauea	85/1/3	g	1.3E+7		49	83/1/3			1 #	84/12/24	1b	11	
1706-01=	Beerenberg	85/1/6 2	m	8.0E+5 6.2E+6	1		85/1/6			2	85/1/4	1b	2	
1302-01-	Kilauea	85/2/4	g	1.4E+7		49	83/1/3			1 #	85/1/16	1b	20	
0702-02=	Canlaon	85/3/13	l		0.7		85/3/13			1	85/3/13	1bq	0.19	
1302-01-	Kilauea	85/3/13	g	1.9E+7		49	83/1/3			1 #	85/2/28	1b	14	
1302-01-	Kilauea	85/3/13	g	1.9E+7		49	83/1/3			1 #	85/3/14	1b	2	
0403-11=	Niuafo'ou	85/3/21	l	1.0E+2		54	85/3/21	2		0	85/3/21	1?	0.13	ML 2.4
1302-01-	Kilauea	85/4/21	g	1.6E+7		49	83/1/3			1 ^	85/3/27	1b	27	
0606-03=	Soputan	85/5/19	m	5.0E+6	5		85/5/19	6		2	85/3/15	1bq	65	M 5.6
0401-10=	Ruapehu	85/5/25	l				85/5/21			1	85/5/20	1d	12	ML 2.4
1302-01-	Kilauea	85/6/12	m	7.9E+6		49	83/1/3			1 #	85/5/10	1b	35	
0303-02=	Piton de la Fournaise	85/6/14	m	1.0E+6		49	85/6/14		8	1	85/5/15	1b	29	M 1.0
0805-05=	Tokachi-Dake	85/6/19	l		0.1		85/6/19			1	85/6/12	1bq	7	M 4.4
1302-01-	Kilauea	85/7/6	g	1.1E+7		49	83/1/3			1 #	85/6/21	1b	19	
1302-01-	Kilauea	85/7/26	m	7.2E+6		49	83/1/3			1 #	85/7/4	1b	13	
0604-05=	Sangeang Api	85/7/30	m	5.0E+6	6.5	47	85/7/30		7	3 *	85/4/29	1b	90	
0303-02=	Piton de la Fournaise	85/8/5	m	4.0E+6		48	85/6/14			1	85/8/5	1c	0.13	
1302-01-	Kilauea	85/9/2	g	1.2E+7		49	83/1/3			1 #	85/8/14	1b	18	
0303-02=	Piton de la Fournaise	85/9/6	g	1.7E+7		49	85/6/14			1	85/9/6	1b	0.05	
1302-01-	Kilauea	85/9/24	g	1.5E+7		49	83/1/3			1 #	85/9/10	1b	15	
1302-01-	Kilauea	85/10/21	g	1.5E+7		49	83/1/3			1 #	85/10/5	1b	16	
1302-01-	Kilauea	85/11/13	g	1.4E+7		49	83/1/3			1 #	85/10/30	1b	14	
1501-02=	Ruiz, Nevado del	85/11/13	g	4.3E+7			85/9/11	7		3 ^	84/11/13	1a	360	M 4.0
0603-09=	Tangkuban Parahu	85/11/15	l		0.2		85/11/15			1	85/4/15	1bq	210	
0502-12=	Ulawun	85/11/20	m	7.5E+6 2.0E+6	8	49	85/11/17	6	6	3 *	85/11/12	1cq	10	
0303-02=	Piton de la Fournaise	85/12/2	m	1.0E+6		49	85/6/14			1 #	85/12/2	1b	0.01	
0303-02=	Piton de la Fournaise	85/12/29	m	7.0E+6	0.15	49	85/6/14			1 #	85/12/25	1c	4	
1302-01-	Kilauea	86/1/1	g	1.2E+7		49	83/1/3			1 #	85/11/26	1a	32	
1302-01-	Kilauea	86/1/27	g	1.4E+7		49	83/1/3			1 #	86/1/19	1b	10	
1302-01-	Kilauea	86/2/22	g	1.2E+7		49	83/1/3			1 #	86/2/8	1b	16	
0303-02=	Piton de la Fournaise	86/3/19	g	2.0E+6			85/6/14			1 #	86/2/11	1a?	1.5	M 2.0
1302-01-	Kilauea	86/3/22	g	1.0E+7		49	83/1/3			1 #	86/3/7	1a	9	
1103-01-	Augustine	86/3/27	m		12	61	86/3/27	8		4 ?	86/2/10	1b	45	ML 2.1
0702-02=	Canlaon	86/3/30	l		0.7		87/3/30			1	87/3/1	1b	64	
1302-01-	Kilauea	86/4/13	g	1.2E+7		49	83/1/3			1 #	86/4/6	1b	8	

Table 2A.9 continued. ERUPTCAT

Volcano		Bulletin of Volcanic Eruptions Eruption data					VOTW Eruption data				SWARMCAT Swarm data			
Number	Name	start		volume		plume SiO2	start	T	L	VEI	start	type	dur.	Mmax
1302-01-	Kilauea	86/5/7	m		9.4E+6	49	83/1/3			1 #	86/4/27	1b	11	
1401-13=	Tacana	86/5/8	l			1	86/5/8			1	86/5/7	1b	2.5	ML 5.0
1401-13=	Tacana	86/5/8	l			1	86/5/8			1 ?	85/12/15	1a?	72	
1302-01-	Kilauea	86/6/2	m		9.8E+6	49	83/1/3			1 #	86/5/21	1b	12	
0702-02=	Canlaon	86/6/22	m	1.4E+5		4	86/6/3	5		2	86/6/14	1b	8	
1302-01-	Kilauea	86/6/26	m		8.8E+6	49	83/1/3			1 #	86/6/18	1b	8	
0601-12=	Sorik Marapi	86/7/5	l	6.7E+2		0.7	86/7/5	2		1	86/7/4	1c	8	
0203-02=	Nyamuragira	86/7/16	g	5.0E+6	6.0E+7	0.25 45	86/7/16	7	7	2	86/7/16	1b	0.54	
1302-01-	Kilauea	86/7/18	m		6.0E+6	49	83/1/3			1 #	86/7/9	1b	10	
1501-02=	Ruiz, Nevado del	86/7/20				4	85/9/11		2		86/7/20	1b	0.29	
1501-02=	Ruiz, Nevado del	86/7/20	l			4	85/9/11		2		86/7/5	1a?	5	
0603-20=	Dieng	86/8/6	l			0.3	86/8/6		1		86/4/15	1aq	45	
0303-02=	Piton de la Fournaise	86/11/12	m		3.0E+5	49	85/6/14		1	#	86/11/12	1b	0.04	
1102-03-	Pavlof	86/11/16					86/4/16		6	3 ^	86/4/7	1d	16	M 2
0804-01=	O-Shima	86/11/21	g	2.5E+7	2.2E+7	16 55	86/11/15	7	7	3 ^	86/11/21	1c	9	M 6
0604-22=	Ili Boleng	86/11/24	m			1	86/5/28			1	86/11/14	1b	10	
0303-02=	Piton de la Fournaise	86/11/26	m		3.0E+5	48	85/6/14			1 #	86/11/17	1aq	9	M 3
1000-26=	Klyuchevskoy	86/11/27					86/11/27		7	3 ^	87/12/27	1d?	10	Ks 9
0303-02=	Piton de la Fournaise	86/12/18		2.0E+6	m	48.9	85/6/14			1 #	86/12/2	1b	6	
0303-02=	Piton de la Fournaise	86/12/30				48.9	85/6/14			1 #	86/12/29	1b	1.5	M 2.0
0303-02=	Piton de la Fournaise	87/1/6	m		1.1E+6	49	85/6/14			1 #	87/1/6	1b	1.3	Md 1.0
1000-26=	Klyuchevskoy	87/2/23	l			53	86/11/27		7	3 ^	87/2/20	1c	14	
1501-02=	Ruiz, Nevado del	87/6/9	l				85/9/11			2 ?	87/5/21	1a	1.5	M 2.0
0303-02=	Piton de la Fournaise	87/6/13					85/6/14		8	1	87/6/8	1a	4	M 2.7
0303-02=	Piton de la Fournaise	87/7/19	m		1.0E+6	49	85/6/14			1 #	87/7/11	1b	8	
1501-02=	Ruiz, Nevado del	87/8/10	l				85/9/11	7		3 ^	87/7/31	1a	1.5	
0401-10=	Ruapehu	87/8/24	l				87/8/24			1	87/8/18	1b	6	ML 2.0
0604-22=	Ili Boleng	87/10/2	l			0.3	87/10/2			1	87/6/20	1a	5	
0303-02=	Piton de la Fournaise	87/11/6	m		1.6E+6	49	85/6/14			1	87/11/3	1b	3	
0804-01=	O-Shima	87/11/16				4.3	87/11/16	4		3 ^	87/9/15	1c	64	
0303-02=	Piton de la Fournaise	87/11/30	g		1.0E+7	49	85/6/14			1 #	87/11/29	1b	1.5	
0203-02=	Nyamuragira	87/12/30	m		3.0E+6	45	87/12/30	6	6	1	87/11/1	1b	30	
0604-071	Anak Ranakah	88/1/3	l			1.5	87/12/28	7	6	3 *	87/12/30	1b	5	
0805-07=	Me-Akan	88/1/5					88/1/5			1	87/9/9	1a	105	
1000-26=	Klyuchevskoy	88/1/20	g		3.4E+7	47	86/11/27			2	88/1/19	1b	12	
0303-02=	Piton de la Fournaise	88/2/7	m		8.0E+6	49	85/6/14			1 #	88/2/4	1b	3	
0608-06=	Gamalama	88/2/12	l			2	88/2/12			2	88/1/5	1bq	28	
0703-01=	Bulusan	88/2/20	m	3.2E+4		1.5	88/2/20	4		2	88/1/20	1b	30	
0605-09=	Banda Api	88/5/9	m	3.2E+4	6.0E+6	3.5	88/5/9		6	3 ?	88/4/20	1b	18	M 3.7
0702-02=	Canlaon	88/6/21	l			1	88/6/21			1	88/5/6	1b	45	
0608-07=	Kie Besi	88/7/29	g			10	88/7/29			3	88/7/20	1b	9	
0303-02=	Piton de la Fournaise	88/12/14	m		8.0E+6	48	85/6/14			1	88/12/14	1b	0.16	
1507-10=	Lonquimay	88/12/27	m			5.5 58	88/12/25	8	8	3 ^	88/12/7	1b	18	M 4.6
0502-12=	Ulawun	89/1/1				2 47	89/1/1			2	88/10/5	1c	66	
1000-26=	Klyuchevskoy	89/1/1				0.2 47	86/11/27			2	89/1/1	1c	16	
0900-24=	Serychev Peak	89/1/13					89/1/13			1 ?	89/1/5	1b	7	
1402-11=	Pacaya, Volcan de	89/3/7				3	65/7/4			3 ^	89/2/25	1b	10	
0803-01=	Izu-Tobu	89/7/13				71	89/7/13	5		1	89/6/30	1aq	11	M 5.5
1000-26=	Klyuchevskoy	89/7/30				3 47	86/11/27			2 ?	89/7/22	1bq	8	
0101-06=	Etna	89/9/11				47	89/9/11		7	2	89/8/17	1aq	9	
1103-03-	Redoubt	89/12/14 3	m	4.4E+5		10 61	89/12/14			2 #	89/12/13	1b	0.95	ML 2.0
1103-03-	Redoubt	90/1/2 3	g	2.5E+7		12 61	89/12/14		7	3 #	89/12/26	1b	7	
0603-28=	Kelut	90/2/10	m			12	90/2/10	8		4	89/11/15	1a	90	Md 2.0
1103-03-	Redoubt	90/2/15 3	m	5.6E+6		10 61	89/12/14		7	2 #	90/2/12	1b	3.42	
1103-03-	Redoubt	90/3/14 3	m	1.2E+6		12 61	89/12/14		7	2 #	90/3/13	1b	1.42	

Table 2A.9 continued. ERUPTCAT

Volcano		Bulletin of Volcanic Eruptions Eruption data					VOTW Eruption data				SWARMCAT Swarm data			
Number	Name	start		volume	plume	SiO2	start	T	L	VEI	start	type	dur.	Mmax
1103-03-	Redoubt	90/3/23	3	m 3.8E+5	10	61	89/12/14		7	2 #	90/3/22	1b	1.42	
1103-03-	Redoubt	90/3/29	3	m 1.1E+6		61	89/12/14		7	1 #	90/3/28	1b	1.17	
1103-03-	Redoubt	90/4/6	3	m 5.2E+5	9	61	89/12/14		7	2 #	90/4/6	1b	0.54	
1103-03-	Redoubt	90/4/14	3	m 8.5E+5	10	61	89/12/14		7	2 #	90/4/15	1b	0.13	ML 1.7
0802-10=	Unzen	90/11/17		l	0.3		90/11/17	6	8	1	89/11/21	1a?	3	M 3.7
0703-083	Pinatubo	91/6/12		g 3.0E+9	40		91/4/2	10		6 *	91/4/2	1b	70	ML 4.3
1103-05-	Spurr		4	5.0E+7	14.5	57	92/6/27	7		4 ^	91/8/15	1bq	180	ML 1.7
1401-09=	Popocatepetl			m 1.4E+6	1		94/12/21			2	94/10/15	1b	60	M 2.9

1 Swanson, D. A. and R. T. Holcomb (1989)
2 BVE No. 26 (1986)
3 Scott and McGimsey (1994)
4 Alaska Volcano Observatory staff (1993)
Symbols are explained in the text.

2A.5.1 Data Sources

The ERUPTCAT table is composed of three sections. The first section is eruption data drawn from the Bulletin of Volcanic Eruptions (BVE). The second section is eruption data drawn from Volcanoes of the World second edition (VOTW). The third section is the associated swarm data preceding each eruption drawn from the SWARMCAT table. The BVE section of the table includes the eruption start date, erupted volume, plume height, and silica content. The VOTW section also includes the start date, tephra and lava volumes, and adds the VEI for each eruption. The third section shows the precursory swarm parameters including the swarm start date, type, duration, and the magnitude of the largest earthquake preceding the eruption.

Both the BVE and VOTW data are listed because the two data sources differ in some respects. The BVE section describes all of the eruptions that were preceded by the well-reported swarms. In the VOTW directory, in many cases, these eruptions have been grouped as an eruptive phase of a longer eruptive sequence. For example, all the eruptions at Mount St. Helens between 1980 and 1986 are considered as one eruptive sequence in the VOTW directory. The BVE describes these as individual phases. All of the data listed in the BVE section are drawn from the BVE covering that year, unless an italic numeral (e.g., 1) is listed following the start date. The italic numeral points to a reference used to complete or supplement data for that eruption or eruptive phase.

2A.5.2 Erupted Volume, Plume Height, Silica Content, and the VEI

The BVE classifies the size or intensity of an eruption into three categories: Little (l), medium (m), and great (g) according to the bulk volume of erupted material. The BVE uses the following correlation between them:

(l) $<1x10^4 m^3$, (m) $1x10^4$ to $1x10^7 m^3$, (g) $>1x10^7 m^3$.

This field gives an estimate of the size of the eruption when no estimate of the erupted volume is available. This one letter size code is recorded in the first column of the volume field. The next two columns of volume field are the bulk tephra and lava volumes in cubic meters. If a range of values are reported the average is recorded.

The plume field records the maximum height in kilometers of the eruption cloud above the crater. The SiO_2 field records the silica content of the main erupted product. The silica content values are taken directly from the BVE reports. In many cases, silica values are explicitly stated while others are derived from reported rock names.

The VOTW section of the ERUPTCAT table is directly extracted from the Smithsonian Institution's Global Volcanism Program eruption data file. The start date, tephra and lava volume, and the VEI are listed. The following field descriptions are from the Global Volcanism Program eruption data file.

The eruptive volume is broken into two fields, tephra (T) and lava (L). The volume is an order of magnitude value in cubic meters (e.g., 8 = >10 to the 8th power cubic meters = >100,000,000 m^3 = >0.1 km^3, 9 = >1 km^3, etc.). The tephra volume is a bulk volume, not dense rock equivalent.

The VEI is a 0-8 scale of explosive magnitude. An asterisk (*) follows the maximum VEI of an eruption for which additional VEI values have been assigned for specific phases. We have added a "pound sign" (#) to these specific phases where we have estimated the VEI. A "plus" (+) following VEIs greater than 4 identifies eruptions in the upper third of that VEI range. A "^" accompanies those eruptions early in a region's historical record that have been upgraded by 1 VEI unit, as explained in *Volcanoes of the World* and Newhall & Self (1982).

The parameters of the third section of the ERUPTCAT table are described in the SWARMCAT organization and parameter description section of this report.

2A.6 Improvements and Future Work

In designing this project we hoped to cast a wide net over seismological phenomena occurring at volcanoes. We found that the net had many holes; only very few parameters are frequently reported in the literature. Filling in the blanks of this current version of the database would be highly desirable. We believe that much of this data exists, but was never published. The next step is to contact the individual reporters and begin collecting this primary data.

The database would be improved by the addition of new high quality records. The number and quality of case studies on volcanic earthquake swarms have been steadily improving as more volcanoes are becoming monitored. The addition of the most recent swarms (occurring after 1989) will be given priority over the cases studied before 1979.

Along with the addition of more records, each record could be expanded to included summary figures such as; seismicity rate, time-depth, time-magnitude, earthquake location, and example seismograms. The database software that we are currently using does support fields that contain digital images. Future versions of the GVESD will incorporate these figures.

Future work with the GVESD will explore more fully the relationship between swarm parameters (such as the duration, M_{max}, and event types) and specific eruption parameters such as the Volcanic Explosivity Index, chemistry of the erupted products, eruption repose, volcano edifice height, etc. We are developing a generic volcanic earthquake swarm model, which will provide a conceptual framework to interpret sequences or swarms of volcanic earthquakes which involve several different types of events. The GVESD will provide the data to explore the succession of particular event types within swarms and their durations.

2A.7 Acknowledgments

We thank J. Lahr and C. Nye for providing helpful comments and suggestions, which improved this report. We also thank L. Siebert for providing an advance of copy of the second edition of Volcanoes of the World. This work was supported by the Alaska Volcano Observatory under the US Geological Survey Volcano Hazards and Geothermal Studies Program, and by additional funds from the State of Alaska.

2A.8 *References*

Alaska Volcano Observatory staff, 1993, Mt. Spurr's 1992 eruptions: Eos (Transactions of American Geophysical Union), v. 74, p. 217 and 221-222.

Bulletin of Volcanic Eruptions No.26, 1986.

Cox, K.G., Bell, J. D., and Pankhust, 1979, The interpretation of igneous rocks, George Allen and Unwin, London, 450 p.

Katsui, Y., (Ed.), 1971, List of active volcanoes (with map): Special issue of Bulletin of Volcanic Eruptions, 160 p.

Koyanagi, R. Y., Chouet, B., and Aki, K., 1987, The origin of volcanic tremor in Hawaii: Part 1, Data from the Hawaiian Volcano Observatory 1969-1985, in Volcanism in Hawaii v. 2, eds. Decker, R. W., Wright, T. L., and Stauffer, P. H., U.S. Geological Survey Professional Paper 1350, p. 1221-1258.

Latter, J. H., 1981, Volcanic earthquakes, and their relationship to eruptions at Ruapehu and Ngauruhoe volcanoes: Journal of Volcanological and Geothermal Research, v. 9, p. 293-309.

Minakami, T., 1960, Fundamental research for predicting volcanic eruptions (part 1): Earthquakes and crustal deformations originating from volcanic activities: Bulletin of the Earthquake Research Institute, v. 38, p. 497-544.

Mogi, K., 1963, Some discussions on aftershocks, foreshocks, and earthquake swarms--The fracture of a semi-infinite body caused by an inner stress origin and its relation to the earthquake phenomena, 3: Bulletin of the Earthquake Research Institute, v. 41, p. 615-658.

Motyka, R. J., Liss, S. A., Nye C. J., and Moorman, M. A., 1993, Geothermal resources of the Aleutian Arc: Alaska Division of Geological and Geophysical Surveys Professional Report 114, 17 p.

Scott, W., and McGimsey G., 1994, Character, mass distribution and origin of tephra-fall deposits of the 1980-1990 eruptions of Redoubt Volcano, south-central Alaska: Journal of Volcanological and Geothermal Research, v. 62, p. 251-273.

Simkin, T., Siebert, L., McClelland, L., Bridge, D., Newhall, C., and Latter, J. H., 1981, Volcanoes of the World, Hutchinson Ross Pub. Co., Stroudsburg, PA, 232 p.

Simkin, T., and Siebert, L., 1994, Volcanoes of the World second edition, Geoscience Press, Tucson, Arizona, 349 p.

Swanson, D. A., and Holcomb, R. T., 1989, Regularities in growth of the Mount St. Helens dacite dome, 1980-1986: in Silicic lava domes, IAVCEI proceedings in volcanology v. 2 lava flows and domes, (Fink, Ed.), Springer-Verlag, Heidelberg, p. 1-24.

Wood, C.A., and Kienle, J., 1990, Volcanoes of North America: United States and Canada, Cambridge University Press, 354 p.

Chapter 3

The Duration-Amplitude Distribution of Volcanic Tremor[3]

Section 1.01 Abstract

The amplitude distribution or frequency-size scaling of volcanic tremor was examined at 8 volcanoes and 1 geothermal area. The hypothesis that the frequency-size distribution may be approximated by an exponential function was tested. The exponential model, implying a scale-bound source process, is found to be a better fit to the data then a power-law (scale invariant) model. The exponential model gives a satisfactory description of tremor associated with a range of volcanic activity, including tremor associated with magmatic and phreatic eruptions, shallow and deep source regions, and geothermal sources. The frequency-size distribution of tremor is determined by measuring the duration of tremor at given amplitudes. We used the exponential model described by: $d(D_R) = d_t e^{-\lambda D_R}$ where d is the duration of tremor greater than or equal to a particular amplitude D_R, d_t is the total duration of tremor, and the inverse of λ is the characteristic or mean amplitude of the distribution. λ^{-1} takes on values of 0.003-7.7 cm^2. Our results show that the characteristic amplitude for eruptive tremor is greater than non-eruptive tremor; that for deep tremor is greater than shallow tremor; and that for tremor associated with magmatic eruptions is greater than for tremor associated with phreatic eruptions. We suggest that the characteristic amplitude of the duration-amplitude distribution is useful parameter to discriminate the type of activity associated with the tremor. The exponential scaling of tremor provides evidence that tremor is not composed of a series of low-frequency events closely spaced in time. Further, the exponential scaling requires the source to be scale bound. We propose that exponential scaling of tremor amplitude is due to fixed source geometry driven by a variable excess pressures. This implies that the characteristic amplitude of the duration-amplitude distribution is proportional to a geometric dimension of the source. The exponential scaling of tremor demonstrates that tremor source processes are fundamentally different from those for earthquakes.

[3] In preparation for submission to *Journal of Geophysical Research*

Section 1.02 Introduction

Most phenomena in nature show systematic relationships between their numbers and their size. Thus, the measurement and modeling of the frequency-size distribution provides a simple means to begin to understand the source processes underlying a phenomenon. This understanding may provide important physical constraints on theoretical source models. For instance, in earthquakes studies, the frequency-size distribution is well described by a power law [*e.g. Ishimoto and Ida*, 1939; *Gutenberg and Richter*, 1954]. This observation has lead to several insights into the earthquake source process, for example, stress drop is relatively constant and independent of earthquake size [*Aki*, 1972; *Kanamori and Anderson*, 1975]. Additional physical implications can be derived from an examination of variations in the frequency-size distribution (i.e. variations in b-value). Some of these include; the stress drop involved during rupture [*Wyss*, 1972], the applied stress [*Scholz*, 1968], and the temperature [*Warren and Latham*, 1970] and heterogeneity of the medium [*Mogi*, 1962]. Work with bathymetric data by *Jordan and Smith* [1987] has shown instead that an exponential relation, rather than a power, governs the frequency-size distribution of seamount heights, which has implications for the magma source depths beneath oceanic crust. In this study we wish to find an analogous relationship for volcanic tremor and explore its implications.

We investigate the frequency-size or scaling relationships between the duration of volcanic tremor and its amplitude at eight volcanoes including: Kilauea (Hawaii), Mt. Spurr (Alaska), Karkar, Ulawun (Papua New Guinea), Pavlof (Alaska), Fuego (Guatemala), Arenal (Costa Rica), and, Redoubt (Alaska). The tremor from these volcanoes is associated with a range of different

volcanic phenomena. A case from a geothermal area, Old Faithful Geyser (Yellowstone National Park), and a swarm of long-period earthquakes from Redoubt volcano are also studied for comparison. The amplitude scaling of volcanic tremor has received very little attention in the literature, in stark contrast to the amplitude scaling of earthquakes or "b-value," which is the second most widely studied parameter in seismology [*Bath* 1983].

Aki and Koyanagi [1981] were the first to propose an exponential distribution for the frequency-size distribution of tremor. They found that for deep (≥30 km) tremor at Kilaeua an exponential law applies rather than a power law, and they postulated that there is a unique length scale involved in the source process of volcanic tremor, such as the average size of the conduits. *McNutt* [1992] expanded this work by comparing data from Kilauea with Pavlof. In this paper we extend these results to several other volcanoes and examine the implications for the source processes.

This paper is divided into five sections. The first section discusses two common distributions, the exponential and the power-law, which describe many frequency-size distributions in nature. The second section outlines the methodology we used to measure the frequency-size distribution of volcanic tremor. The third section describes measurements made at eight volcanoes and one geothermal area. A brief description of the accompanying volcanic activity is given for each case study. The fourth section investigates the hypothesis that volcanic tremor is composed of a series of low-frequency events closely spaced in time. The last section summarizes these measurements and explores the physical and hazard implications.

Section 1.03 Frequency-size distributions

Power-law and exponential distributions are among the most commonly used distributions to describe frequency-size relations in geology and geophysics. They also provide a good contrast between a scale invariant and a scale bound distributions. The power-law is the only distribution that does not include a characteristic scale length [*e.g. Turcotte*, 1992]. While, the exponential distribution is one of several distributions, such as the gamma and Weibull, which are bounded about a mean or characteristic size. We chose the exponential distribution for further examination because it is perhaps the simplest; can be described by a single-parameter; and provides a good starting point in which to compare scale invariant and scale bound processes.

A power-law describes source processes for which no characteristic scale is involved, or, in other words, the source processes are self-similar. For example, the frequency-size distribution for earthquakes [*e.g. Ishimoto and Ida*, 1939; *Gutenberg and Richter*, 1954], faults [*e.g. Okubo and Aki*, 1987], rock fragments (e.g. volcanic ash and pumice) [*Hartman*, 1969], and volcanic eruptions [*Simkin*, 1993] are all adequately described with a power-law model. In contrast, however, the exponential distribution describes phenomenon where the source process is scale-bounded. For example, fault blocks [*Korvin*, 1989], volcano spacing [*Vogt*, 1974], and seamount heights [*Smith and Jordan*, 1987] are well described with an exponential distributions.

The mean of an exponential distribution completely describes the distribution and can have implications for source processes. The mean of the exponential distribution is also referred to as the characteristic size. For fault blocks and volcano spacing, the characteristic size or length is essentially equal to the thickness of the lithosphere [*Korvin*, 1989; *Vogt*, 1974]. Similarly, the characteristic length associated with contraction-crack polygons has been a related to the elastic

properties and thickness of the contracting layer [e.g. *Neal et al.*, 1968]. Seamount height studies have shown that the characteristic length is consistent with the depth of a magma source at the base of the oceanic crust [*Smith and Jordan*, 1987].

Recently, power-law scaling has received a great deal of attention because of its broad application to geological data, and to chaos theory [e.g. *Korvin*, 1989; *Turcotte*, 1992]. Several authors have applied a power-law scaling to describe the frequency-magnitude relation for low-frequency, long-period, or b-type volcanic events, hereafter referred to as low-frequency events [*e.g. Minakami*, 1960; *Shimozuru and Kagiyama*, 1989]. Hence, if volcanic tremor is the superposition of low-frequency events [e.g. *Fehler*, 1983] then the frequency-size distribution for tremor should also exhibit power-law scaling [*Nishimura*, 1995]. We test this hypothesis at several different volcanoes for which we have high quality data on the durations of tremor for different amplitudes and by using synthetic data. If, on the other hand, low-frequency events are produced by geometrically bounded structure such as the average size of cracks or conduits, an exponential distribution may be a more appropriate distribution to describe the frequency-size relation. This should be evident from comparing plots of duration versus log amplitude to plots of log duration versus log amplitude.

Section 1.04 Methodology

The determination of the frequency-size distribution, for discrete events, requires only the counting of events of a particular size and then plotting their numbers verse their size. Volcanic tremor, a continuous signal, requires a different approach. In order to determine the frequency of occurrence or event count for tremor we use the tremor duration as an analog. The tremor duration at particular amplitude or greater is then measured. An example measurement is shown

in Figure 3.1 for tremor associated with the December 27, 1996 eruption of Pavlof volcano. Three techniques were used to measure tremor durations; the first was by simply using a scale (ruler) and directly measuring the duration from an existing figure; the second was the processing of digital Real-Time Seismic Measurement (RSAM) data [*Endo and Murray*, 1991]; and the third was the automatic calculation of amplitudes and durations in near-real-time using the Iceworm seismic acquisition system [*Lindquist et al., 1997*]. When sufficient accessory information was available tremor amplitudes are reported as reduced displacements (D_R). Reduced displacement for volcanic tremor is a normalized amplitude metric, analogous to the magnitude scale for earthquakes. The D_R accounts for the instrument magnification, distance to the source, and the type of waves composing the tremor. The definition of D_R and the details of these calculations are given in Appendix 3A. Using this normalized standard allows comparison of tremor amplitudes at many volcanoes.

Numerous plots of tremor amplitude verses time exist in the literature. The frequency-size distribution can be easily determined by measuring durations from these figures using a scale. Figure 3.1 shows a duration of 46 hours measured for tremor amplitude greater than or equal to a reduced displacement of 5 cm^2. This duration is then plotted against amplitude to examine the form of the frequency-size distribution. This technique allows a broad spectrum of tremor from several volcanoes to be analyzed, however, this technique is labor intensive and quite time consuming.

When primary or derivative amplitude data (e.g. RSAM data) are available, these data sources were used instead. The frequency-size distribution can be directly measured using RSAM data of tremor episodes. RSAM data are one-minute averages of the absolute value of signal amplitude [*Endo and Murray*, 1991] and the final recorded output is a 10 minute average of the one-minute averages (*J. Power, pers. comm.*, 1995). Tremor durations are measured by producing

a histogram of the RSAM values and tallying the number of occurrences greater than a specific amplitude. The number of occurrences is then proportional to the duration because each occurrence represents the same duration: 10 minutes of signal. This algorithm does an excellent job of quickly determining the durations and allows one or more tremor episodes to be analyzed together or separately. This technique gives, within measurement errors, the same results as the hand measurements from a figure using a scale. Unfortunately, the RSAM data are not "true" peak-to-peak amplitudes of the signal. Using a method given in Appendix 3A reduced displacements may be estimated from RSAM data. Other drawbacks of using the RSAM data are the indiscriminate inclusion of non-tremor signals such as teleseisms, regional earthquakes, microseisms, wind noise, and seismometer calibration pulses. The data must be carefully screened for these types of signals before amplitude-duration measurements can be made.

Near-real time tremor duration-amplitude measurements were made using the Iceworm data acquisition system during the 1996 eruption of Pavlof volcano [*Lindquist et al., 1997*]. The amplitude of the tremor is measured in the frequency domain, to minimize non-volcanic signals such as wind noise and microseisms. Spectra are calculated for 10-second windows with 50% overlap and then averaged over 15-minutes. The maximum spectral amplitude is taken between 0.8-10.0 Hz, which essentially acts as a bandpass filter to minimize energy from microseisms and wind noise. The spectral amplitude is then converted to an RMS ground displacement using Parseval's identity and accounting for the instrument response. The reduced displacement is then calculated by incorporating the station-vent distance to correct for geometrical spreading. Results from this technique are comparable to the above methods. However, during periods of high noise, the measured amplitudes are somewhat lower than those measured on a helicorder or by RSAM. The details on this overestimation are given in Appendix 3B.

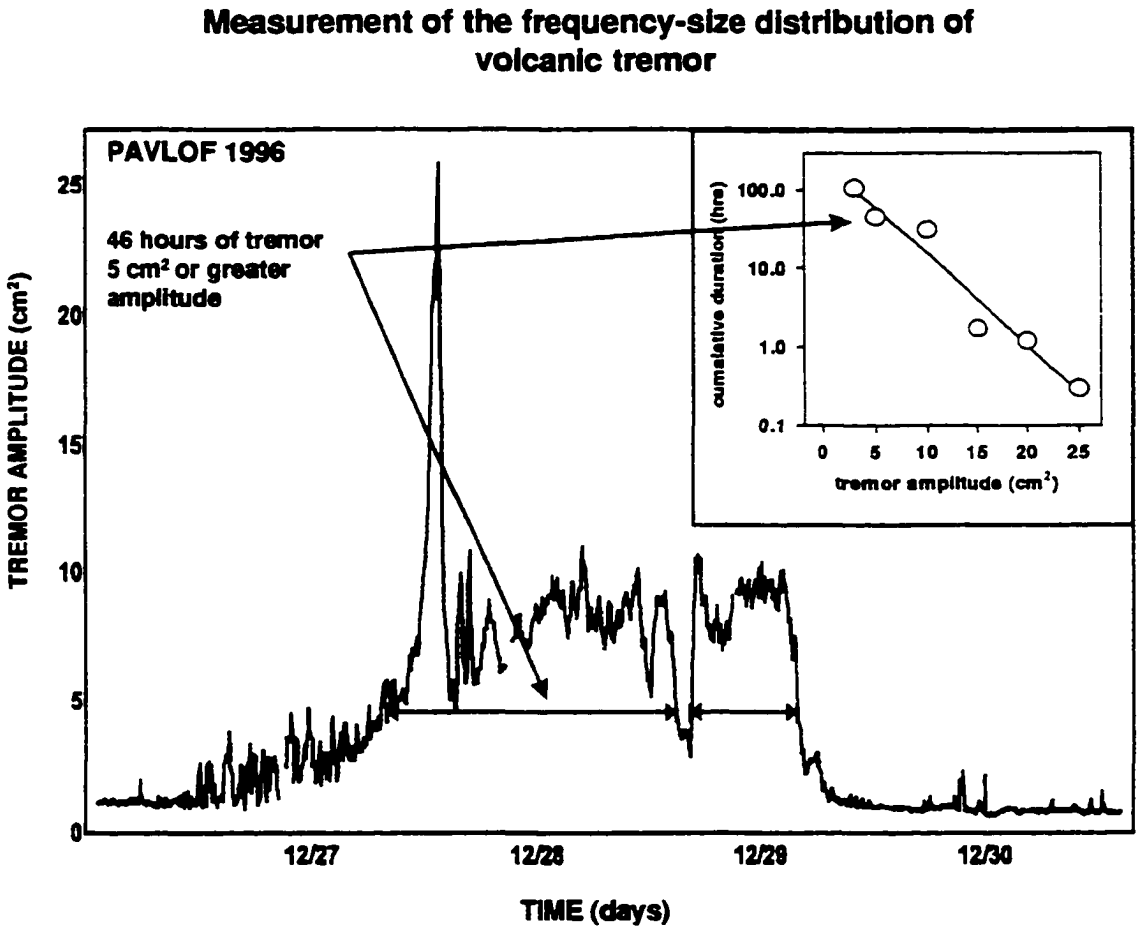

Figure 3.1 Measurement of the frequency-size or duration-amplitude distribution for volcanic tremor. Since tremor is a continuous signal, the duration is taken as the frequency of occurrence and the size is measured as the amplitude. An example of the duration-amplitude measurement for tremor recorded at Pavlof volcano between December 26th and 30th is shown. The inset shows the duration-amplitude distribution for this time period with a fit to an exponential scaling model.

We fitted power-law and exponential models to the duration-amplitude distributions, after the amplitude and duration measurements were made. Figure 3.2 shows a comparison of these models for non-eruptive tremor recorded at Mt. Spurr volcano. Figure 3.2a shows a plot of log tremor duration versus amplitude. The line is a weighted-least-squares fit corresponding to an exponential distribution of the form

$$d(D_R) = d_t e^{-\lambda D_R} \tag{3.1}$$

where D_R, is the tremor amplitude, d is the total duration of tremor with amplitudes greater than or equal to D_R, d_t is the total duration of tremor during of the period studied, and λ is the slope of the line or scaling parameter. The inverse of the scaling parameter, λ^{-1}, can be thought of as the characteristic or mean amplitude of the distribution. Figure 3.2b shows a plot of log tremor duration versus log amplitude. The line is a weighted-least-squares fit to a power-law distribution in the form

$$d(D_R) = d_t (D_R)^{-\gamma} \tag{3.2}$$

where γ is the is the slope of the line, similar to the "b-value" for earthquakes. The parameter γ also can be related to the fractal dimension of the amplitudes.

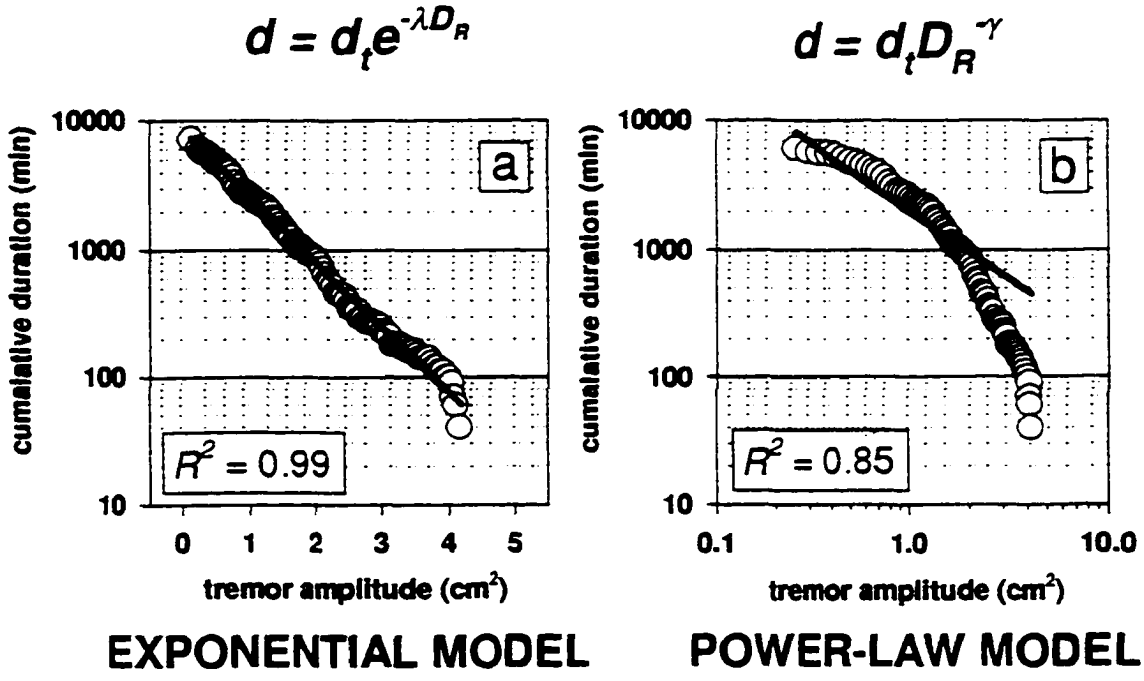

Figure 3.2 Comparison between an exponential and a power-law scaling model for the duration-amplitude distribution of volcanic tremor. The lines shown through the data are weighted-least-squares fits to exponential and power-law models. These data are from a non-eruptive tremor sequence recorded at Mt Spurr volcano.

Visual inspection of Figure 3.2 immediately shows that the exponential model is a better fit than the power-law model. Two methods are employed to establish a formal goodness-of-fit between these models and the data. The first test is a comparison of the correlation coefficients (R^2) for both models. The correlation coefficient is a measure of variability about the modeled distribution and the higher the value the better the fit. Correlation coefficients of 0.99 and 0.85 are calculated for the exponential and power-law models, respectively. In other words, the exponential model accounts for 99% of the variability in the distribution. For the Mt. Spurr case and all other cases studied, the exponential model is found to have higher correlation coefficients, and therefore, considered superior to the power-law model (Table 3.1).

A second formal method, the chi-square test (X^2), is also used is to test the goodness-of-fit for both models. The hypothesis tested is; the duration sample was randomly drawn from either an exponential or a power-law distribution. These hypotheses can be rejected if the X^2 statistic is greater than a critical value. The X^2 statistic is defined by

$$X^2 = \sum_{i=1}^{n} \frac{(O_i - E_i)^2}{E_i} \qquad (3.3)$$

where n is the number of sample classes, O_i is the observed frequency, E_i the expected frequency as calculated by the power-law or exponential models. The critical value ($X^2_{\nu,p}$) is found in tables and depends on the number of degrees of freedom (ν) and the confidence level (p) at which the test is performed. The degrees of freedom are defined by the number of observations minus one ($n - 1$) minus the number of parameters being estimated (one parameter for the both exponential and power-law models; e.g. Mt. Spurr case $\nu = (97\text{-}1)\text{-}1 = 95$). For the Mt Spurr case, the X^2 statistic for the exponential and power-law models, 690 and 81442 respectively, are both less than the critical value of $X^2_{95,0.975} = 1.3 \times 10^5$. Therefore, we are unable to formally reject either model

at the 97.5% confidence level. However, the X^2 statistic for the power-law model is substantially greater than the X^2 statistic for the exponential model, showing that the exponential model is a superior fit. Both the R^2 and the X^2 statistics are summarized for all the case studies in Table 3.1. For all the cases studied, the exponential model has higher correlation coefficients (R^2) and lower X^2 statistics than the power-law model. In four of the twelve cases we are able to formally reject the power-law model at the 97.5% confidence level. The failure to reject the power-law model in the other cases with the X^2 test may be due to 1) sensitivity to the classes or bins with low probability density chosen for these tests, or, 2) the small sample sizes.

Table 3.1 Goodness-of-fit as measured by the correlation coefficient R^2 and the X^2 statistic for the power-law and the exponential models.

Case	R^2 correlation coefficient		X^2 statistic				
	model		model*				critical
	power law	exponential	power law		exponential		value**
Spurr 1992 eruptive	0.73	0.99	5085	A	112	A	20816
Spurr 1992 non-erupt.	0.85	0.99	81442	A	690	A	1.3E+05
Kilauea shallow	0.79	0.98	134	A	9.1	A	307
Kilauea deep	0.70	0.99	336	A	1.3	A	1067
Karkar 1978-1979	0.59	0.97	4.4E+05	R	626	A	11566
Ulawun 1978	0.84	0.98	68	A	9.3	A	471
Pavlof 1973-1986	0.84	0.96	302	A	32	A	1395
Pavlof 1996	0.86	0.94	219	R	31	A	148
Arenal 1993	0.90	0.95	318	A	221	A	4057
Fuego 1973	0.83	0.99	8843	R	74	A	6699
Redoubt 1989	0.88	0.95	1.8	A	0.7	A	60
Old Faithful 1972	0.95	0.99	2464	R	33	A	1945

* The X^2 statistic is given for each case along with an "A" or "R" symbolizing whether or not the model can be rejected (R) or accepted (A) under the chi-square test at the 97.5% confidence level.

** If the X^2 statistic is greater than the critical value the tested distribution can be rejected at the 97.5% confidence level.

Section 1.05 Case studies

The duration-amplitude distributions of ten episodes of tremor at eight volcanoes are examined in the following section. These case studies were chosen to given a broad sample of tremor associated with a suite of different volcanological processes. At Mt. Spurr we compare eruptive and non-eruptive tremor. At Kilauea we examine shallow (< 2km) tremor associated with the 1983 eruptions of Pu'u O'o, and deep tremor (≥30 km) recorded between 1962-1979. In Papua New Guinea, Karkar and Ulawun give a comparison between tremor associated with phreatic and magmatic eruptions. Four other cases from Fuego, Arenal, and Pavlof are shown to further generalize these observations. Finally, two "non-tremor" cases are presented for comparison; a long-period swarm of earthquakes at Redoubt and geothermal "seismic noise" at Old Faithful Geyser. Details on how the durations and amplitudes were measured are presented for each case along with a summary of the volcanic activity occurring during the observations.

3B.1 Crater Peak, Mt. Spurr Alaska

Volcanic tremor preceded the first eruption of Crater Peak, a satellite cone of Mt. Spurr, on June 27, 1992, accompanied the June 27, August 18, and September 16-17 eruptions, and followed the September 17 eruption [*McNutt et al.*, 1995]. The tremor sequences between September 16 and October 10 are chosen for study because they include the last eruption as well as several episodes of continuous tremor not associated with an eruption. Five seismic stations were recording RSAM data during this period. Here, we examine RSAM data from one station, CKN, because it had the best signal-to-noise ratio of the available stations. The other stations all

showed similar results. Station CKN is 6.3 km south-southeast from the eruptive vent Crater Peak.

Tremor durations and normalized amplitudes were estimated from the RSAM data (details are given in Appendix 3A). Two periods were studied in detail; 24 hours surrounding the September 16-17th eruption, and a six-day period (October 2-7th) including several episodes of non-eruptive tremor.

The September 16-17th eruption lasted about 3.5 hours and sent an ash plume to an elevation of 14 km above sea level. Several pyroclastic flows were generated and some entrained snow to become lahars. The erupted volume of tephra was estimated to be 20 x 10^6 m^3 DRE [*Neal et al.*, 1995]. The duration-amplitude distribution for the tremor associated with this eruption is shown in Figure 3.3 with a weighted-least-squares fit to the exponential model. The individual measurements are shown as open circles. The correlation coefficients for the power-law and exponential models are 0.73 and 0.99, respectively (Table 3.1). This shows that the exponential model is a superior to the power-law in modeling the duration-amplitude distribution. The inverse of the slope or characteristic amplitude is 5.6 cm^2 (Table 3.2). These parameters are summarized in Table 3.2 for Spurr and all other cases for which information was available to calculate normalized amplitudes.

Inspection of the lowest amplitudes of the eruptive tremor distribution shows a departure in slope. The slope is much steeper than the eruptive tremor distribution and is similar to the non-eruptive tremor distribution. These points at the lowest amplitudes represent a break in scaling and probably represent a second tremor-generating process occurring at the lowest amplitudes. The eruption tremor lasted for only 3.5 hours of the full 24 hours analyzed. Therefore, we may not have completely isolated the eruption tremor from a secondary source. The result is a mixture

of these two distributions. These points at the lowest amplitudes have negligible effect on either the correlation coefficients or the calculation of the characteristic amplitude.

Tremor continued for one week following the September 17th eruption and ceased on September 25th [*McNutt et al.*, 1995]. The tremor resumed on October 1st. The tremor sequence showed significant temporal variations, including patterns similar to those that have preceded eruptions at Mt Spurr and elsewhere. Tremor starting on October 1st increased nearly exponentially on October 2nd, after which is stopped rather abruptly. On October 3rd a series of five tremor episodes occurred, each about 1.5 hours long. This signal resembled banded tremor. On October 4th, tremor returned and the amplitude again increased nearly exponentially. When this tremor declined in amplitude on October 5th, another series of episodes occurred, each about 2 hours long, similar to those on October 3rd, but followed by a gradual decline. The duration-amplitude measurements for October 2-7th are shown in Figure 3.3. The individual measurements are shown as open squares.

The data in Figure 3.3 are fit well by weighted-least-squares regression to an exponential model. The correlation coefficients are 0.85 and 0.99 for the power-law and exponential models, respectively (Table 3.1), again demonstrating a better fit with the exponential model. Inspection of the highest amplitudes of the non-eruptive tremor distribution shows a departure in slope. The slope is much steeper than the majority of the distribution. These points at the highest amplitudes represent a break in scaling and may denote an upper bound for non-eruptive tremor. There is a significant difference in the slope between the eruptive and non-eruptive tremor. The characteristic amplitude for the non-eruptive tremor is 0.8 cm^2 (Table 3.2). This is the smallest characteristic amplitude for any true volcanic tremor in this study.

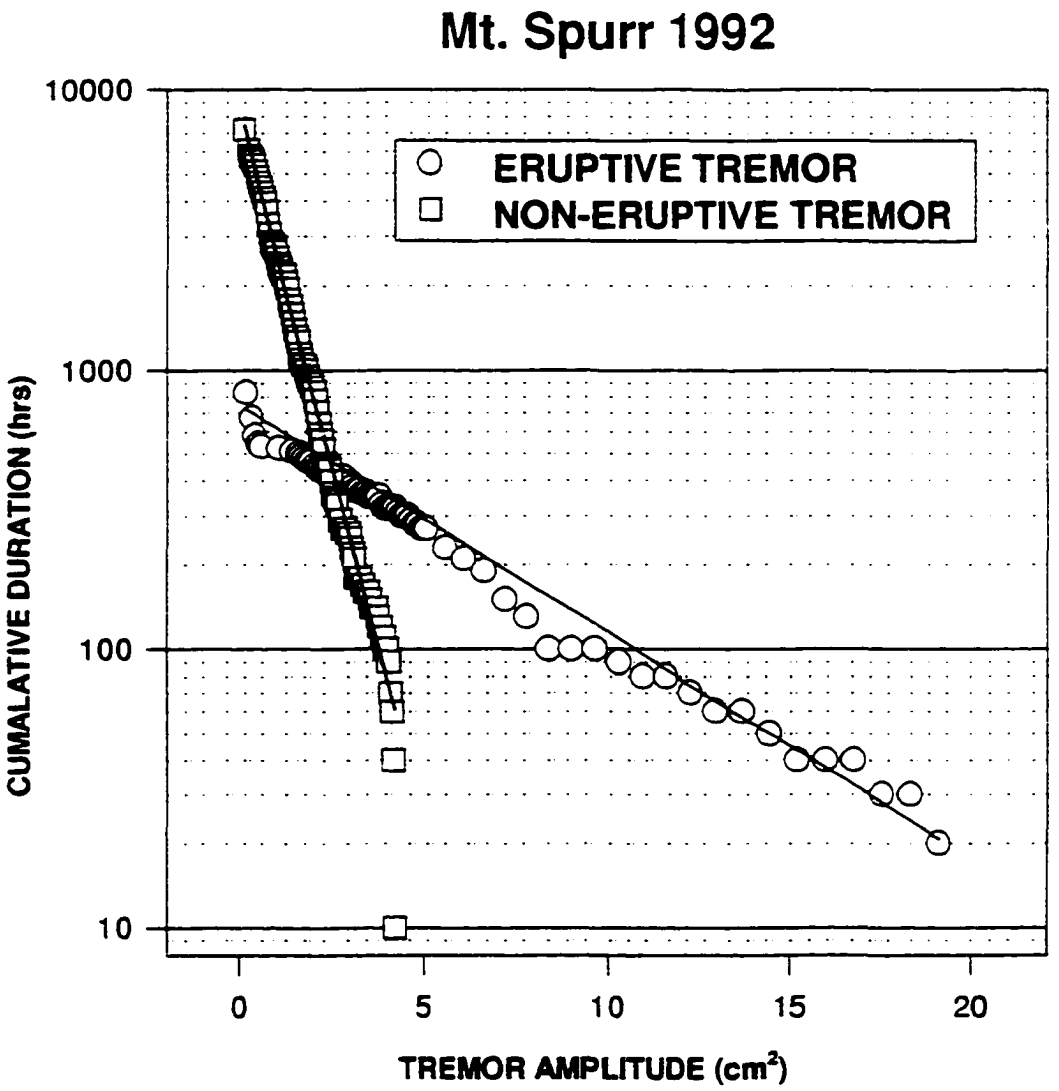

Figure 3.3 Tremor duration-amplitude distribution for Mt. Spurr. Two periods are shown: tremor associated with the eruption of September 16-17, 1992 (open circles) and tremor occurring between October 2-7, 1992 (open squares). Both distributions are well modeled with an exponential distribution. Note the difference in slope between the eruptive and non-eruptive tremor.

Table 3.2 Slope of the duration-amplitude distribution curve (λ) and characteristic or mean amplitude (λ^{-1}), determined using a weighted-least-squares regression.

Case	max amp (cm^2)	λ (cm^{-2})	λ^{-1} (cm^2)	Associated Volcanic Activity
Kilauea 1962-1979 deep	64	0.13	7.7	quiescence and varied activity at the surface
Spurr 1992 eruptive	19	0.18	5.6	sub-Plinian eruption
Pavlof 1973-1986	18	0.19	5.3	lava fountianing; Strombolian explosions
Pavlof Dec. 1996	25	0.22	4.5	lava fountianing; Strombolian explosions
Kilauea 1983 shallow	9	0.44	2.3	fissure eruption; lava fountaining
Redoubt 1989	2.5	0.74	1.4	precursory LF earthquake swarm
Spurr 1992 non-eruptive	4	1.18	0.8	post-eruption tremor
Old Faithful 1972	0.03	340	0.003	geysering; hydrothermal boiling

3C.1 Kilauea, Hawaii

Tremor from shallow (< 2 km) and deep (≥30 km) source regions are examined at Kilauea volcano, Hawaii. Data for the shallow tremor duration-amplitude distribution is drawn from measurements of the January 2-11, 1983 eruption of Pu'u O'o (episode 1) [*Koyanagi et al.*, 1989]. The Pu'u O'o eruption began as a fissure eruption with linear lava fountains several hundred meters long, on a 1 km-long segment of the East Rift Zone. The total volume erupted during this episode was estimated to be 4.0 x 10^6 m^3 at an average rate of 1.1 x 10^6 m^3/hour [*Wolfe et al.*, 1989]. The duration and amplitude measurements were made using a scale on published histograms of tremor amplitude at station MPR, approximately 6 km from the tremor source [*Koyanagi et al.*, 1989]. The amplitudes were normalized to reduced displacement using a

surface-wave formulation [*Felher*, 1983] (using the following parameters: predominant tremor frequency = 3 Hz; wave speed = 2 km/s; source-receiver distance = 6 km). The duration-amplitude distribution is shown in Figure 3.4. Individual measurements are shown as open circles and the line is a weighted-least-squares fit to the exponential model. The correlation coefficients for the power-law and exponential models are 0.79 and 0.98, respectively (Table 3.1). The characteristic amplitude is 2.3 cm^2 (Table 3.2).

Amplitude-duration measurements for the deep (≥30 km) tremor at Kilauea were drawn directly from *Aki and Koyanagi* [1981, table 5]. Deep tremor was distinguished from shallow tremor by its spatial amplitude distribution. The deep tremor shows uniform amplitudes at many stations over a large area and the frequencies were usually 3 to 5 Hz. Some of the deep tremor has been located at depths of 30-50 km. Duration-amplitude measurements cover an 18-year period between 1962 and 1979. These data are plotted along with the shallow tremor in Figure 3.4. This period included several episodes of quiescence and varied eruptive activity at the surface. During this period approximately 570 x 10^6 m^3 of lava was erupted at the surface. As noted by *Aki and Koyanagi* [1981], the duration-amplitude is well fit by an exponential distribution. The correlation coefficients are 0.70 and 0.99 for the power-law and exponential models, respectively (Table 3.1). The characteristic amplitude for the deep tremor is 7.7 cm^2, which is somewhat larger than the shallow tremor (5.3 cm^2, Table 3.2).

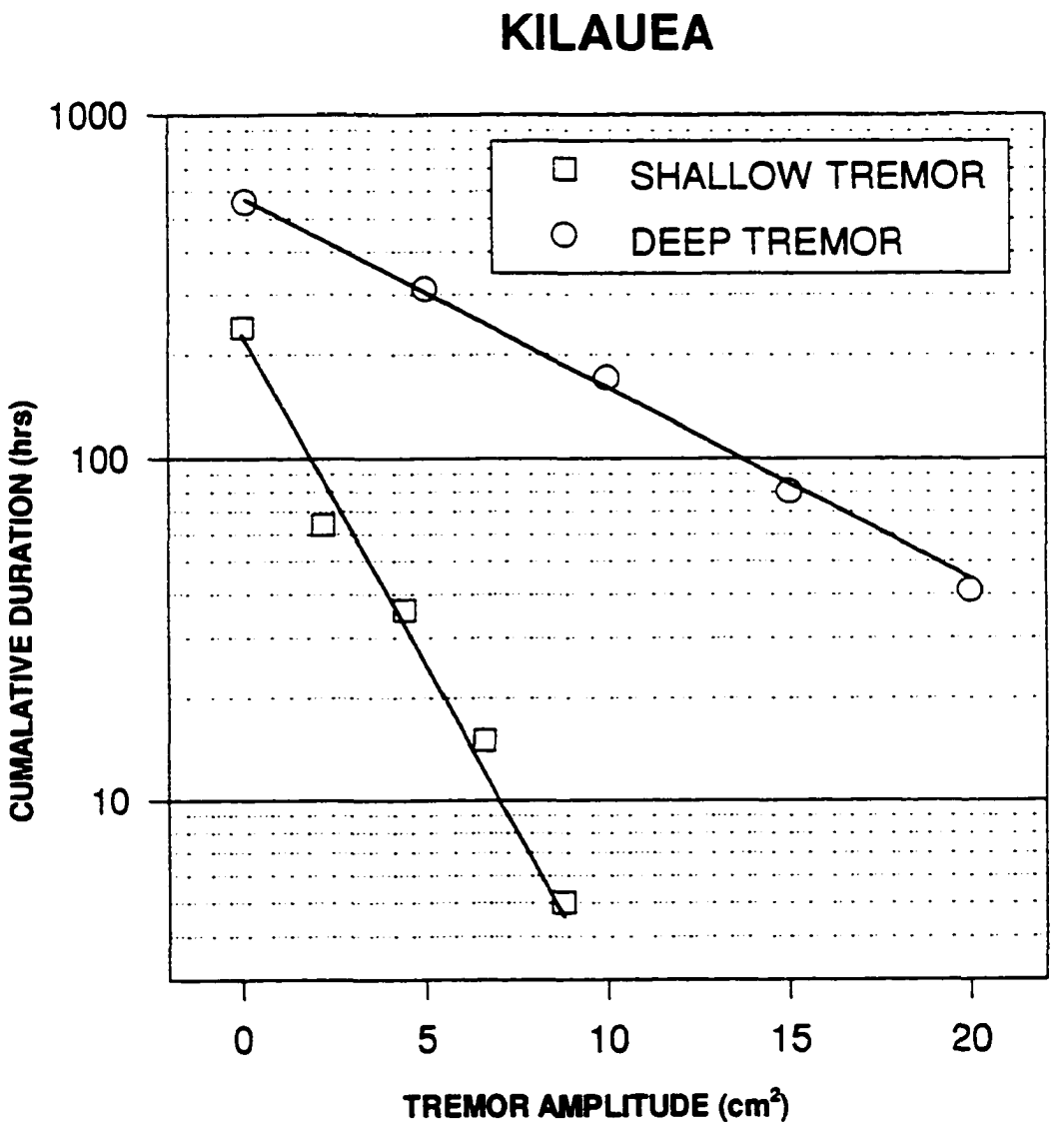

Figure 3.4 Duration-amplitude distribution for shallow (open squares) and deep (open circles) tremor at Kilauea volcano. The shallow tremor was recorded during the first episode the Pu'u O'o eruption in 1983. The deep tremor was recorded between 1962-1979. Note the difference in the slope, or characteristic amplitude, for the shallow and deep tremor.

3C.2 Karkar and Ulawun, Papua New Guinea

Tremor amplitude-duration measurements for Karkar volcano, Papua New Guinea, were made for a six-month long tremor sequence that preceded a series of phreatic eruptions in 1979. Using a scale, the amplitude-duration measurements were made from figure given in *McKee et al.*, [1981a, figure 4] showing tremor amplitudes recorded from July to December 1978, at a seismic station approximately 12 km from the eruptive vent. The tremor during this period showed intervals of stronger and weaker tremor giving the seismograms a characteristic banded appearance. The banded tremor was most noticeable for the period between July and early October 1978 and during the eruptions. Resistivity and self-potential electrical surveys provided evidence for the existence of 100-200 m-deep body of hot aquifer, which is believed to be the focus of the phreatic explosions. No unambiguous juvenile material was detected in the ejecta produced by the 1978-79 explosions [*McKee et al.*, 1981a].

The amplitude-duration measurement data are shown as open squares in Figure 3.5. An exponential model is fit through the data by a weighted-least-squares regression. The correlation coefficients for the power-law and exponential models are 0.59 and 0.97, respectively, again showing that the exponential model is a superior fit (Table 3.1).

Tremor amplitude-duration measurements for Ulawun volcano, Papua New Guinea, were made for a nine-day long tremor episode that accompanied a week-long magmatic eruption in 1979. The eruption consisted of, first, ash ejection from the summit crater, second, expulsion of pyroclastic flows from a new fissure, and, finally, fountaining and flow of lava from a new fissure low on the flank. Tremor was recorded on a seismic station approximately 10 km northwest from the volcano's summit and 15 km from the site of the flank eruption. Tremor amplitudes reached a

maximum the day before the formation of the fissure high on the southeastern flank. These eruptions produced an estimated 20 x 10^6 m^3 of tephra and 7.2-9.0 x 10^6 m^3 of lava [*McKee et al.*, 1981b].

Using a scale, the amplitude-duration measurements were made from figure given in *McKee et al.* [1981b, figure 3] and are shown in Figure 3.5. The individual duration-amplitude measurements are shown as open circles and the line is a weighted-least-squares fit to the exponential model. The correlation coefficients for the power-law and exponential models are 0.84 and 0.98, respectively (Table 3.1).

Unfortunately, absolute amplitude units were not available for the Karkar and Ulawun tremor data. Nonetheless, Figure 3.5 shows a clear difference in the slopes or characteristic amplitudes for the Karkar and Ulawun duration-amplitude distributions. The characteristic amplitude for tremor associated with the magmatic eruptions is greater than for the tremor associated with the phreatic explosions.

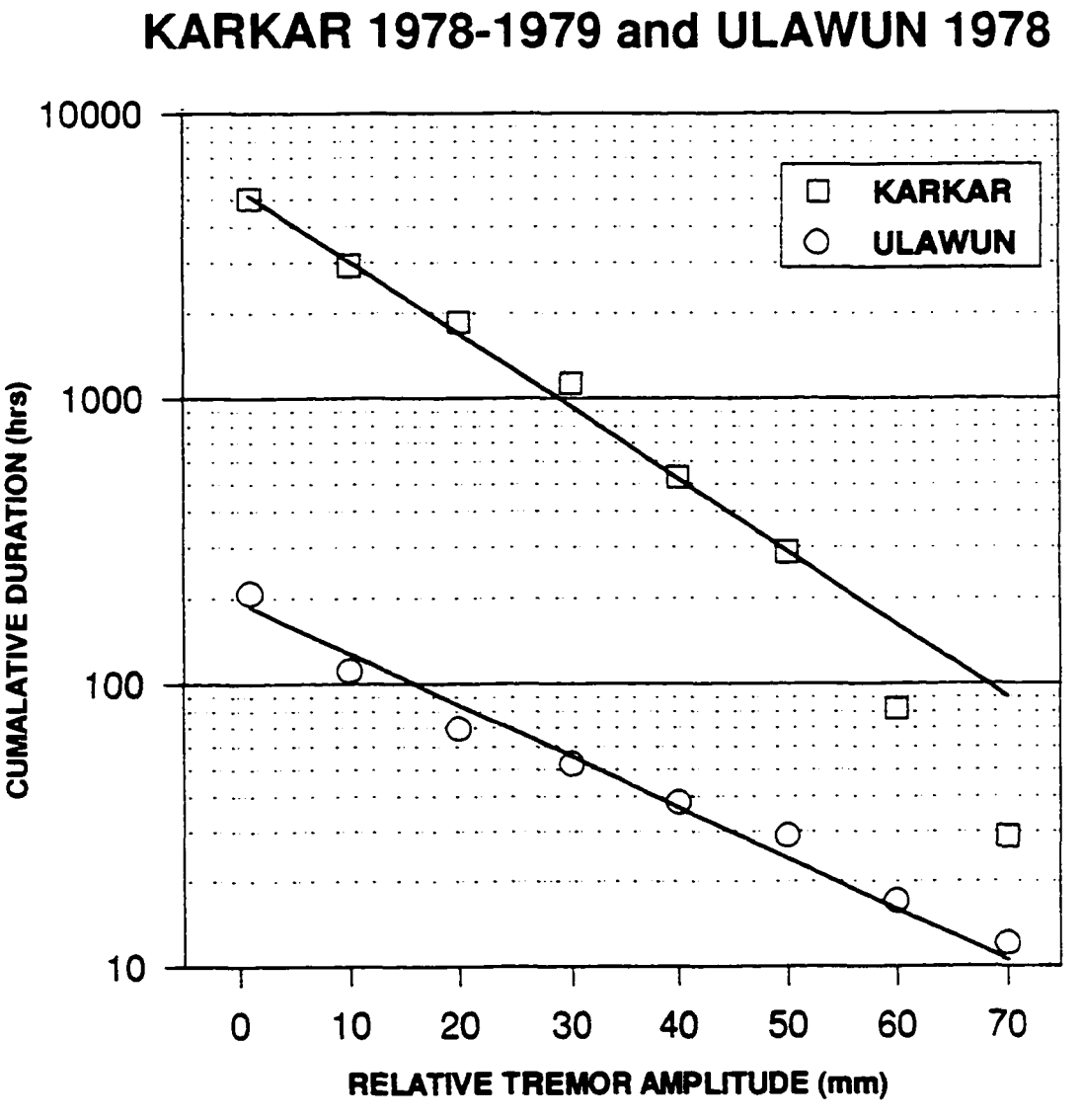

Figure 3.5 Duration-amplitude distribution for tremor associated with the phreatic explosions at Karkar in 1978-1979 (open squares) and the magmatic eruption at Ulawun in 1978 (open circles). Note the difference in slopes between tremor associated with a series of phreatic explosions and a magmatic eruption.

3C.3 Pavlof, Alaska

The data presented for Pavlof are gathered from two data sets. The first data set is from tremor accompanying several eruptions that occurred between 1973-1986 [*McNutt*, 1987]. The eruptions primarily consisted of lava fountaining and Strombolian explosions. The second data set is from the tremor sequence that accompanied the last eruptive episode of the 1996 eruption (Figure 3.1). For the 1973-1986 data set, amplitudes and durations were scaled off helicorder records from a seismic station 8.5 km from the eruptive vent. The resulting duration-amplitude distribution is plotted in Figure 3.6a. An exponential model was fit to all the data except the point representing the lowest amplitudes (shown as a filled circle). This point represents a break in the scaling, and, like the Spurr case, probably represents a second tremor-generating process occurring at low amplitudes. A weighted-least-squares regression, through only the open circles, yields a characteristic amplitude of 5.3 cm^2. A comparison of the correlation coefficients (R^2 = 0.84 for the power-law and R^2 = 0.96 for the exponential) again shows the exponential model as a superior fit over the power-law model (Table 3.1).

The second Pavlof data set was collected during the last episode of the 1996 eruption. The 1996 eruptions were, in general, very similar to the eruptions of the last 23 years and consisted primarily of lava fountaining and Strombolian explosions. Durations and amplitudes were measured for this eruption in near-real time using the Iceworm seismic data acquisition system [*Lindquist et al.*, 1997]. The results are shown in Figure 3.6b. As for the other cases, the correlation coefficients show that the exponential model (R^2 = 0.94) fit the data better than the power-law (R^2 = 0.86; Table 3.1). The characteristic amplitude for the 1996 eruptions is 4.5 cm^2. This is very similar to the characteristic amplitude of 5.3 cm^2 for tremor recorded over the last 23

years (Table 3.2). The duration-amplitude distribution was changed very little even though the structure of the vent was modified somewhat during the 1986 eruption [*McNutt, et al.*, 1991].

3C.4 Fuego, Guatemala and Arenal, Costa Rica

To further generalize the result that tremor is adequately described by an exponential model we present data from Fuego volcano in Guatemala and Arenal volcano in Costa Rica. Figure 3.6c-d shows these distributions with their fits to the exponential model.

The tremor analyzed at Fuego was recorded following a VEI 2 explosive eruption during which an estimated 1x 10^6 m^3 of tephra was erupted. Data were recorded on a helicorder from station FGO, 6 km southeast of the vent [*Yuan et al.*, 1984]. The dominate tremor frequency was 1 Hz. The correlation coefficients for the power-law and exponential models at Fuego are 0.83 and 0.99, respectively (Table 3.1).

Tremor amplitudes and durations at Arenal were measured directly from helicorder records. Four days of tremor were examined and amplitudes were measured once per minute. The tremor was associated with the continuous effusion of a block andesite lava flow, punctuated with periodic Strombolian explosions. A comparison of the correlation coefficients for the fits of the exponential and power-law models show again that the duration-amplitude distribution is well described with the exponential model (Table 3.1).

The scaling properties of acoustic records of degassing sounds were also examined at Arenal. A discussion of the measurements and results is given in Appendix 3C.

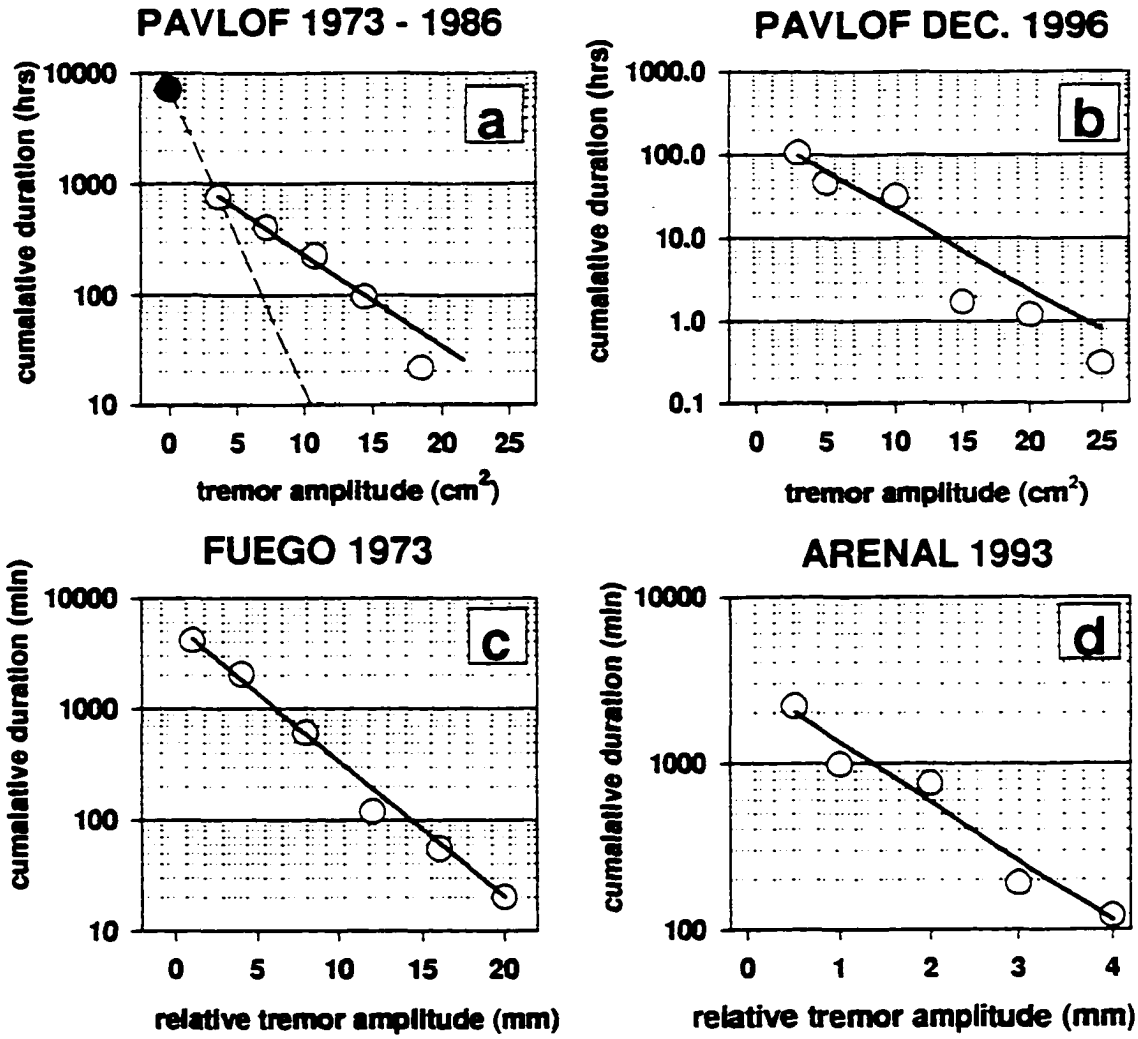

Figure 3.6 Duration-amplitude distribution for Pavlof 1973-1986 (a), Pavlof, December 1996 (b), Fuego (c), and Arenal (d) volcanoes. The distributions for Pavlof 1973-1986 (a) and for 1996 (b) show very similar slopes or characteristic amplitudes. The solid circle point (a) was excluded from the regression. This break in scaling suggests a mixture of more than one process generating the tremor. Duration-amplitude distributions are shown from Fuego (c) and Arenal (d) to further generalize the result that tremor is adequately described by an exponential model.

3C.5 Old Faithful Geyser, Yellowstone National Park Wyoming

The seismicity at geysers has been used as an analog for volcanic seismicity [*Kieffer*, 1984; *Kedar et al.*, 1996]. Old Faithful geyser provides an isolated source of geothermal noise and an excellent data set to examine the duration-amplitude distribution. The same method of measuring tremor durations and amplitudes was applied to 8 hours of "geothermal noise" recorded on a small aperture array with an average distance of 50 m from Old Faithful geyser, Yellowstone National Park. Using a scale, duration-amplitude measurements were made from amplitude data published by *Iyer and Hitchcock* [1974, figure 7]. The duration-amplitude distribution is shown in Figure 3.7a with a fit to the exponential model. As with the tremor, the geyser noise also is better fit with an exponential model ($R^2 = 0.99$) rather than a power-law model ($R^2 = 0.95$; Table 3.1). The characteristic amplitude is 0.003 cm^2, which is smaller than all the volcanic cases and hence is the smallest of all the cases studied (Table 3.2).

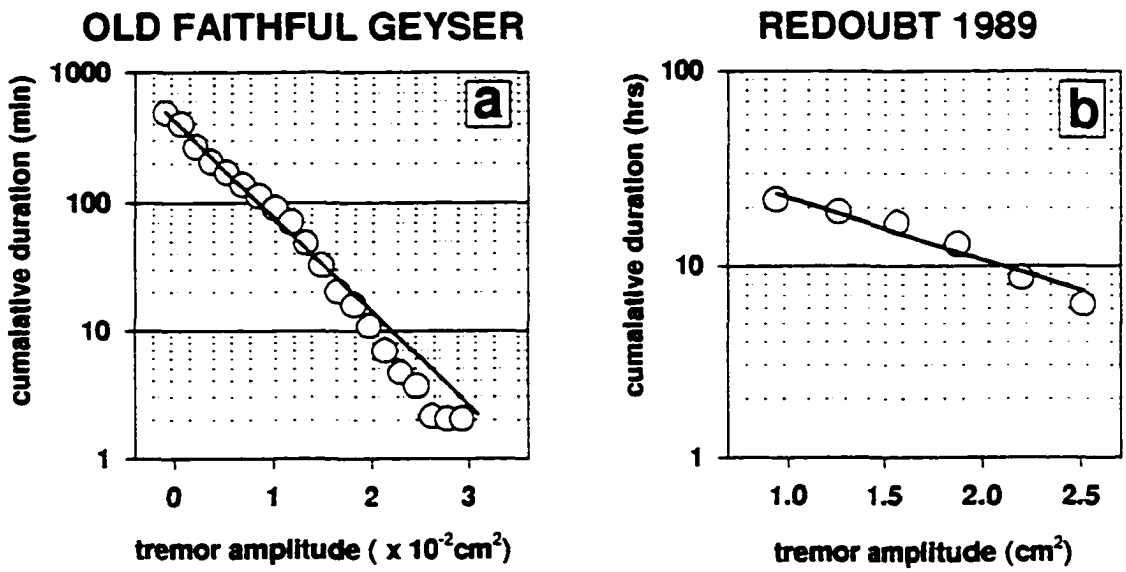

Figure 3.7 Duration-amplitude distributions for (a) seismic noise recorded in 1972 near Old Faithful Geyser, Yellowstone National Park and (b) the December 13-14th, 1989 low-frequency swarm at Redoubt.

3C.6 Redoubt, Alaska

A Redoubt, we examine the duration-amplitude distribution for a non-tremor sequence. Durations and amplitudes were measured from RSAM data collected during the 24-hour swarm of low-frequency events preceding the December 15th, 1989 eruption of Redoubt volcano. This swarm initially consisted of large (M>1.0) long-period events, which occurred more frequently in time over the next 19 hours until they coalesced into high amplitude tremor. The average amplitudes then began to decline at the time of the transition between individual events and continuous tremor [*Power et al.*, 1994]. The magnitude distribution for the located low-frequency events of the swarm were uniformly distributed from the detection threshold to M 1.4 and does not fit the Gutenberg-Richter distribution [*Lahr et al.*, 1994]. The swarm culminated in a phreato-magmatic eruption with a volume of 1.0-3.3 x 10^5 m^3 DRE and sent a plume to greater than 10 km above sea level [*Scott and McGimsey*, 1994].

The duration-amplitude distribution is shown in Figure 3.7b with a fit to the exponential model. As with the tremor, the low-frequency swarm is better fit with an exponential model (R^2 = 0.95) rather than a power-law model (R^2 = 0.88; Table 3.1). The characteristic amplitude is 1.4 cm^2, which is smaller than all eruptive tremor studied but greater than the non-eruptive tremor and the geothermal noise at Old Faithful (Table 3.2).

Section 1.06 Is volcanic tremor a series of low-frequency events closely spaced in time?

Using the general result of this study, exponential scaling of the duration-amplitude distribution of tremor, we now test an accessory hypothesis; tremor is composed of a series of low-frequency events closely spaced in time [e.g. *Fehler*, 1983]. This hypothesis comes from the observation that low-frequency events sometimes occur with an increasing rate until they grade into continuous tremor. Continuous tremor has also been observed to decay in episodic bursts of low-frequency events [e.g. *Koyanagi et al.*, 1987]. Further, the spectral features of tremor and low-frequency events are very similar [e.g. *Fehler*, 1983]. The frequency-size statistics for some sequences of low-frequency events have been shown to exhibit power-law scaling [*e.g. Minakami*, 1960; *Shimozuru and Kagiyama*, 1989; *Nishimura*, 1995]. Hence, if volcanic tremor is the superposition of many low-frequency events it should also exhibit power-law scaling [*Nishimura*, 1995]. Two approaches are used to test this hypothesis. First, the duration-amplitude distribution is examined using a series of synthetic low-frequency earthquakes, and second, using an analytical examination of a low-frequency earthquake amplitude envelope function.

A synthetic time series grossly resembling volcanic tremor may be created by summing many low-frequency events closely spaced in time. The low-frequency events are approximated by

$$\dot{u}_i(t) = \begin{cases} 0 & t < t_{i0} \\ A_i e^{\left(i\omega - \frac{(t-t_{i0})}{\tau}\right)} & t \geq t_{i0} \end{cases} \qquad (3.4)$$

where A_i is the amplitude of the i^{th} event, ω is the event frequency (e.g. $\omega = 2\pi * 3$ Hz), τ is a decay constant ($\tau = 0.9$ s), and t_{i0} is the time of the event onset. The events were randomly

arranged in time, using a Poisson distribution for the inter-event spacing. We drew low-frequency earthquake amplitudes (A_i) from two distributions, a power-law and a normal population. For the power-law distribution, a range of scaling parameters or "b-values" were tested from 0.5 to 5, and, for the normal population, several mean amplitudes and standard deviations were tested.

Figure 3.8 shows a typical example of the synthetic time series (Figure 3.8a), the frequency-magnitude distribution for low-frequency events (Figure 3.8b), and the resulting duration-amplitude distribution (Figure 3.8c). A power law distribution was obtained with a relatively high b-value (2.2) which is commonly observed for low-frequency events near volcanoes [e.g. *Endo et al.*, 1981]. The average amplitude is plotted superimposed on the synthetic time series (Figure 3.8a). The durations and amplitudes are then measured and displayed in Figure 3.8c. The plot of log duration versus log amplitude (Figure 3.8c) shows a linear relationship corresponding to power-law scaling for the duration-amplitude distribution. Similar results are obtained when the input parameters were varied (e.g.: b-value, inter-event spacing, and decay constant).

Low-frequency events at some volcanoes have been observed to occur only in a narrow band of magnitudes [e.g. Redoubt and Pinatubo, *Lahr et al.*, 1994; *Ramos et al.*, 1996]. For this reason, runs were conducted using the normally distributed amplitudes for the low-frequency events. The resulting tremor duration-amplitude distribution were irregular and neither the power law nor the exponential model fit these distributions.

The results from these synthetic time series tests show that exponential duration-amplitude scaling cannot be reproduced through the superposition of many low-frequency events closely spaced in time.

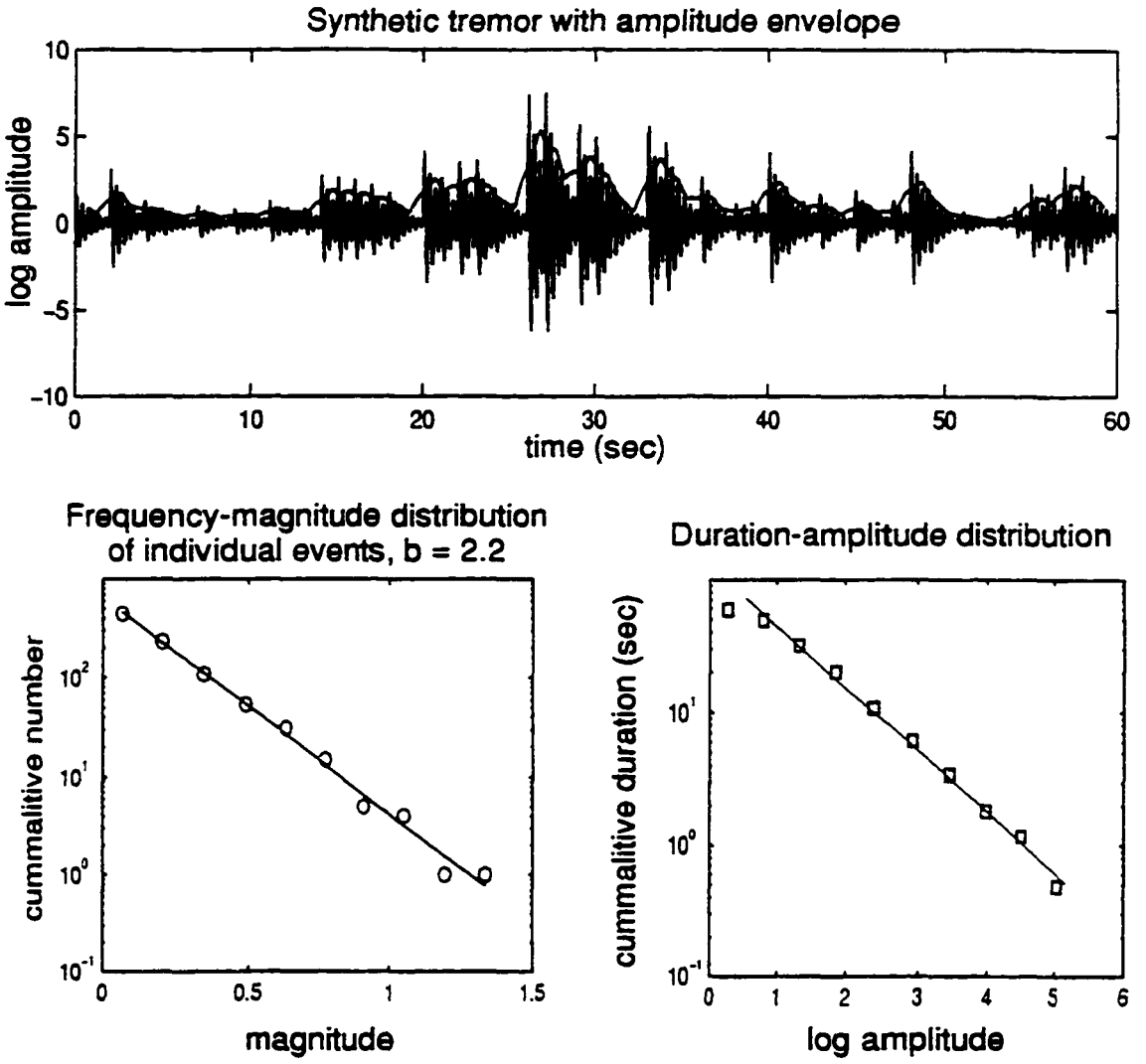

Figure 3.8 A) Typical synthetic tremor created by summing a series of low-frequency events closely spaced in time. The black line shows a sliding average of absolute value of the synthetic tremor. B) The frequency-magnitude distribution of the individual low-frequency events (b-value = 2.2) composing the synthetic tremor. C) The duration-amplitude distribution calculated for the synthetic tremor. The linear relation, on this log-log plot, suggests power-law-scaling.

We now show that the exponential scaling duration-amplitude distribution is not simply an artifact of our measurement technique on an exponentially decaying waveform such as the coda of a low-frequency earthquake. This demonstration also bears on the argument that tremor is a superposition of many low-frequency events.

The amplitude envelope of a low-frequency earthquake can be approximated by a simplified version of Equation 3.4

$$A(t) = A_0 e^{-\alpha t} \tag{3.5}$$

where A is the amplitude at time t, A_0 is the maximum amplitude to the earthquake, and α is a constant related to the attenuation. The duration-amplitude measurements similar to those made on tremor can be made on the envelope function by solving Equation 3.4 as a function of A, as given below

$$t(A) = \frac{1}{\alpha}\ln(\frac{A_0}{A}). \tag{3.6}$$

In this case the duration of the signal at a given amplitude is $t(A)$ and the duration-amplitude distribution is formed by plotting this function. An inspection of the curve plotting log duration ($t(A)$) versus amplitude shows a non-linear relation and therefore is not a candidate to produce the exponentially scaled duration-amplitude distribution. This test also suggests that the exponential duration-amplitude scaling cannot be reproduced through the superposition of many low-frequency events closely spaced in time.

Section 1.07 Discussion

The above case studies show clearly that an exponential scaling model, not a power-law, provides an adequate description of the frequency-size (duration-amplitude) distribution for volcanic tremor. The exponential model differs from the power-law model primarily in that the exponential model requires the source process to be scale bound, not scale invariant. In other words, the amplitude variations of tremor are distributed about a constant characteristic amplitude. We suggest that the physical significance of the characteristic amplitude is that it is related to some constant feature of the tremor source. Two basic classes of features providing a scaling bound on the amplitude of tremor are considered: 1) fixed source geometry with variable excess pressures, or 2) constant excess pressure and variable source geometries. The following discussion will attempt to determine which of these processes is most important or most applicable.

Field observations of exhumed dikes provide evidence for a fixed geometric dimension associated with the tremor source. *Chouet et al.* [1987] noted that dike widths have a fixed average value for a given area. For example, the average width is 4 m for Iceland, 1.8 m for Scotland, 6 m at the Columbia river [*Williams and McBirney*, 1979], and 0.5 m at Kilauea [*Swanson et al.*, 1976]. Field observations have also shown that repeated eruptions can occur through the same vent and show very little or no modification of the vent [e.g. Pavlof *McNutt et al.*, 1991; and Mt. Spurr *Miller et al.*, 1995]. These fixed dimensions may provide a geometrical scaling constraint or bound on the tremor source. For many cases, the dominant period of shallow tremor appears fixed, independent of its amplitude, suggesting that the source size does not change, but the force (e.g. excess pressure) that drives the tremor source does [*Fehler*, 1983; *Chouet et al.*, 1987].

For deep tremor at Kilauea, *Aki and Koyanagi* [1981] observed a positive correlation between tremor period and amplitude. They interpret this observation as a constant excess pressure that drives a crack, generating tremor, and is independent of the source size. The variations in amplitude are interpreted to be due to a distribution of crack sizes. A similar correlation between tremor period and amplitude has been observed for shallow tremor at Arenal volcano, Costa Rica [*Benoit and McNutt*, 1997; Chapter 4, this thesis, figure 4.9]. *Benoit and McNutt* describe the tremor source at Arenal as a vertically oriented 200-600 m long resonator and that is likely to be a gas-charged, magma-filled conduit. A source mechanism similar to Kilauea may be occurring at Arenal, that is, a constant excess pressure is driving the tremor source and the source dimension (length) is changing. Alternatively, variable excess pressures may excite a relatively constant length resonator.

To discriminate between these possibilities we examine both of these models in more detail. At Arenal, tremor frequencies systematically increase up to 75% within minutes after a vigorous expulsion of ash and gas. Either shortening or an increase of the acoustic velocity of the resonator can explain this effect. A change of 75% in period requires 50-150 m shortening, corresponding to an 8000-24000 m^3 decrease in volume of the resonator (these values assume a cylindrical conduit with a radius of 5 m and acoustic velocity of 2 km/s; see chapter 4 of this thesis). This shortening can be accomplished by reducing the distance between bubble nucleation depth and the magma surface. Explosions decapitating the top of the magma column or shoaling the bubble nucleation depth are two possible shortening mechanisms. The decapitation of the top of the magma column can be discounted as a possible mechanism because; the explosions expel a rather small volume of material, which is not sufficient to cause the 75% change in volume and hence the observed change in frequency.

Shoaling the bubble nucleation depth is the remaining mechanism to decrease the length of the resonator. The pressure in the conduit and the initial volatile concentration are the primary control on the bubble nucleation depth. Over the time scale of minutes we expect the initial volatile concentrations to remain constant, leaving the pressure within the conduit as the primary factor. This pressure is comprised of four component pressures; the weight of the overlying magma or magma-static head, any pressure from below driving magma through the conduit, the pressure required to balance the surface tension of the liquid-gas interface, and the pressure required for a bubble to expand against a viscous fluid [*Williams and McBirney*, 1979]. Of these pressures, the magma-static head is the most likely to significantly change during an explosion. A portion of the magma column is removed during an explosion, lowering the magma-static head throughout the conduit. This effect should deepen, not shoal, the bubble nucleation front. This would result in a longer resonator and progressively low frequencies, not the observed higher frequencies. For these reasons, length changes seem unlikely; however, changes in the acoustic velocity of a resonator can be accomplished rather easily. For example, a velocity change corresponding to a 75% change in tremor frequencies can result from a 5 parts-per-thousand decrease in the gas fraction within the magma. Therefore, the Arenal case supports the hypothesis that the size (e.g. length) of the tremor source is constant and the force driving it is varying.

As the Arenal case demonstrates, the walls of a conduit or dike may not be the only boundaries restricting the source size. Near the surface, the physical properties of the magma column change dramatically. Surfaces, such as the bubble nucleation front or the fragmentation surface, provide strong acoustic reflectors, which may bound the vertical scale lengths involved in the tremor source region. These surfaces may vary in both time and depth, but within a restricted range as determined by the properties of the magma (e.g. the initial volatile concentration and the magma-static head).

The maximum excess pressures allowable may have an upper bound constrained by the available potential energy stored in the magma. We assume that the excess pressures are caused by the explosive exsolution of volatiles from a supersaturated magma. The maximum size of the explosion is constrained by the initial volatile concentration within the magma. Therefore, each parcel of magma carries a finite amount of energy and under a constant replenishment rate, the tremor amplitudes produced may be restricted. Unfortunately, this argument is greatly complicated by variations in the rate of replenishment of fresh magma. Parameters such as the initial volatile concentration and magma flux rate are most certainly coupled and their interactions may be very complicated and difficult to predict.

The tensile strength of the wall rock may also give an upper bound to the size of the tremor. If pressures exceed the strength of the surrounding rock, then brittle fracture may dominate the source process. At this point the scaling character of the tremor should change dramatically, perhaps exhibited by a change in slope of the duration-amplitude distribution. Such a break in scaling at large amplitudes was not observed for the cases examined for this study. All of the cases are from relatively small eruptions and the strength of the wall rock may not have been exceeded. To observe this effect, tremor associated with a large eruption must be recorded on-scale in the near field. To our knowledge, on-scale continuous recording of eruption tremor from a very large eruption (VEI $\geq$ 4) does not yet exist. Future studies will benefit from the installation of modern high-dynamic-range broadband seismic instrumentation near explosive volcanoes.

In summary, our data supports the hypothesis that exponential scaling of tremor amplitudes is caused by a fixed source geometry driven with variable excess pressures. This implies that the inverse of the duration-amplitude distribution or the characteristic amplitude (λ^{-1}) is proportional

to a geometric dimension of the source, such as the distance between the bubble nucleation front and the magma surface, or the average length dimension of cracks or conduits.

Characteristic amplitudes were calculated for case studies with the appropriate instrumental information. These varied from 7.7 cm^2 to 3 x 10^{-3} cm^2 (Table 3.2). The greatest characteristic amplitude was recorded for deep tremor at Kilauea and the smallest was measured for geothermal noise at Old Faithful. The two smallest characteristic amplitudes are observed in association with hydrothermal activity. The seismic signals produced from Old Faithful are unambiguously associated with the boiling of groundwater within a conduit 22-175 m long [*Kieffer*, 1984]. The October 1992 Spurr non-eruptive tremor episodes exhibited banding, which is interpreted as a cyclic interaction between a heat source (magma) and water [e.g. *McKee et al.*, 1981a; *Kieffer*, 1984; *McNutt*, 1992]. Furthermore, the volcano was emitting large quantities of steam, but no ash, at this time, providing additional evidence for the hydrothermal origin of the tremor. The December 1989 low-frequency swarm at Redoubt also had relatively small characteristic amplitude. There was a phreatic component to the following eruption. This swarm has been interpreted to be caused by the interaction of groundwater with magmatic gases, steam and water driving a fixed crack (280-380 x 140-190 x 0.05-0.20 m) at a stationary point throughout the swarm [*Chouet et al.*, 1994]. We suggest that, in general, tremor of hydrothermal origin will have smaller characteristic amplitudes than tremor of magmatic origin. Two main factors lead to this outcome, smaller source dimensions (cracks and conduits within a hydrothermal system) and the intrinsically limited ability of hydrothermal boiling to generate strong tremor [*Leet*, 1988].

The characteristic amplitudes for shallow tremor at Kilauea, eruptive tremor at Spurr and both Pavlof cases are similar. These characteristic amplitudes are 4.5 - 5.6 cm^2 for volcanic activity that spans; fissure eruptions, lava fountaining and sub-Plinian eruptions (Table 3.2). It seems quite remarkable that such a wide variety of activities would exhibit similar characteristic

tremor amplitudes. It is possible that similar source sizes exist for all of these cases. Perhaps, the distance between the bubble nucleation front and the magma's surface are similar for each of these cases. The characteristic amplitudes for deep tremor at Kilauea (7.7 cm^2) is somewhat greater than the shallow eruptive tremor studied. This difference suggests either that different processes are generating the tremor, or that the average source dimension is larger for the deep tremor.

Spurr eruption tremor (Figure 3.3) and Pavlof (Figure 3.6a) both show breaks in the scaling at low amplitudes, corresponding to distinct characteristic scale lengths. In each of these cases the lowest amplitude tremor show a greater slope or smaller characteristic amplitude. We suggest that low amplitude tremor that is generated through hydrothermal processes contributes to these distributions, and that at greater amplitudes tremor is associated with magmatic processes. *Leet* [1988] suggested a similar explanation for the maximum amplitude of tremor associated with the August 7 and October 16-18, 1980, eruptions of Mount St. Helens. Unfortunately, absolute amplitude units were not available for the Karkar and Ulawun tremor data. Nonetheless, clear differences exist in the slopes of the tremor plots from Karkar and Ulawun (Figure 3.5). The characteristic amplitude for tremor associated with the magmatic eruptions is greater than the tremor associated with the phreatic explosions. Thus, all three cases show the same polarity; greater characteristic amplitudes for magmatic processes. The non-eruptive tremor at Mt. Spurr shows a break in scaling at ~4 cm^2, above which tremor durations decrease rapidly (Figures 3.2a and 3.3). We suggest, that this scaling change represents an upper amplitude bound for tremor generated through hydrothermal processes.

Exploiting these differences in the characteristic amplitudes could provide a useful method for the remote monitoring of volcanoes. Real-time measurement and monitoring of this parameter may provide a simple discriminant between eruptive and non-eruptive or

hydrothermally generated tremor. This could be especially important at remotely monitored volcanoes where visual or other observations are difficult to conduct.

Section 1.08 Conclusions

In conclusion, we have shown that the frequency-size or duration-amplitude distribution of volcanic tremor is well described by an exponential function, not a power-law as noted for earthquakes. This observation holds for eight different volcanoes and is associated with a range of different volcanic phenomena. This type of amplitude scaling suggests that the tremor generating process is scale bound. We propose that exponential scaling of tremor amplitude is caused by a fixed source geometry driven by variable excess pressures. This implies that the inverse of the duration-amplitude distribution, or the characteristic amplitude (λ^{-1}), is proportional to a geometric dimension of the source. There are variations in the characteristic or mean amplitude for tremor associated with different types of volcanic activity. The strongest differences appear to be between tremor associated with magmatic and phreatic activity. This difference may provide a useful monitoring discriminant between tremor associated with magmatic and phreatic eruptions.

The exponential scaling of tremor demonstrates that tremor source processes are fundamentally different from those of earthquakes. Finally, we have provided a fundamental observational constraint which future theoretical tremor source models reconcile.

Section 1.09 Acknowledgements

We thank R. Hansen for his comments, which have improved this manuscript. This work was supported by the Alaska Volcano Observatory under the U.S. Geological Survey Volcano Hazards and Geothermal Studies Program, and by additional funds from the State of Alaska.

Section 1.10 References

Aki, K., Earthquake mechanism, *Tectonophys.*, 13, 423-446, 1972.

Aki, K., and R. Y. Koyanagi, Deep volcanic tremor and magma ascent mechanism under Kilauea, Hawaii. *J. Geophys. Res.*, 86, 7095-7109, 1981.

Bath, M., Earthquake magnitude - recent research and current trends. *Earth Sci. Rev.*, 17, 315-398, 1981.

Benoit, J. P. and S. R. McNutt, New constraints on source processes of volcanic tremor at Arenal volcano, Costa Rica, using broadband seismic data, *Geophy. Res. Lett.*, 24, 449-452, 1997.

Chouet, B., R. Y. Koyanagi, and K. Aki, Origin of volcanic tremor in Hawaii; part II theory and discussion, *in*: Volcanism in Hawaii, Decker, R. W., T. L. Wright, and P. H. Stauffer eds., US Geol. Survey Prof. Paper 1350, 1259-1280, 1987.

Chouet, B. A., R. A. Page, C. D. Stephens, J. C. Lahr, and J. A. Power, Precursory swarms of long-period events at Redoubt Volcano (1989-1990), Alaska: Their origin and use as a forecasting tool, *J. Volcanol. Geotherm. Res.*, 62, 95-135, 1994.

Endo, E. T., S. D. Malone, L. L. Noson, and C. S. Weaver, Locations, magnitudes, and statistics of the March 20-May 18 earthquake sequence, *in*: The 1980 eruptions of Mount St. Helens, Washington, Lipman, P. W., and D. R. Mullineaux eds., US Geol. Survey Prof. Paper 1250, 93-107, 1981.

Endo, E. T, and T. Murray, Real-time Seismic Amplitude Measurement (RSAM): a volcano monitoring and prediction tool, *Bull. Volcanol.*, 53, 533-545, 1991.

Fehler, M., Observations of volcanic tremor at Mount St. Helens volcano, *J. Geophy. Res.*, 88, 3476-3484, 1983.

Gutenberg, B., and C. F. Richter, Magnitude and energy of earthquakes, *Ann. Geof.* 9, 1-15, 1954.

Hartmann, W. K., Terrestrial, lunar, and interplanetary rock fragmentation, *Icarus*, 10, 201-213, 1969.

Ishimoto, M. and K. Ida, Observations sur les seismes enregistres par le microsismographe construit dernierement (in Japanese with French abstract), *Bull. Earthq. Res. Inst.*, Univ. Tokyo, 17, 443-478, 1939.

Iyer, H. M. and T. Hitchcock, Seismic noise in Yellowstone National Park, *Geophys.*, 39, 389-400, 1974.

Kanamori, H., and D. L. Anderson, Theoretical basis for some empirical relations in seismology, *Bull. Seis. Soc. Amer.* 65, 1073-1095, 1975.

Kedar, S., B. Sturtevant, and H. Kanamori, The origin of harmonic tremor at Old Faithful geyser, *Nature*, 379, 708-711, 1996.

Kieffer, S. W., Seismicity at Old Faithful Geyser: An isolated source of geothermal noise and possible analogue of volcanic seismicity, *J. Volc. Geotherm. Res.* 22, 59-95, 1984.

Korvin, G. Fractured but not fractal: fragmentation of the Gulf of Suez basement, *PAGEOPH*, 131, 289-305, 1989.

Koyanagi, R. Y, Chouet, B., and K. Aki, Origin of volcanic tremor in Hawaii, Part I, data from the Hawaiian Volcano Observatory 1969-1985, *in*: Volcanism in Hawaii, Decker, R. W., T. L. Wright, and P. H. Stauffer, eds., US Geol. Survey Prof. Paper 1350, 1221-1257, 1987.

Koyanagi, R. Y., Tanigawa, W. R., and J. S. Nakata, Seismicity associated with the eruption, *in*: The eruption of Pu'u O'o eruption of Kilauea volcano, Hawaii: Episodes 1 through 20, January 3, 1983, through June 8, 1984, Wolfe, E. W., ed., US Geol. Survey Prof. Paper 1463, 183-235, 1989.

Lahr, J. C., B. A. Chouet, C. D. Stephens, J. A. Power, and R. A. Page, Earthquake classification, location, and error analysis in a volcanic environment: implications for the magmatic system of the 1989-1990 eruptions at Redoubt volcano, Alaska, *J. Volc. Geotherm. Res.*, 62, 137-151, 1994.

Leet, R. C., Saturated and subcooled hydrothermal boiling in groundwater flow channels as a source of harmonic tremor, *J. Geophy. Res.*, 93, 4835-4849, 1988.

Lindquist, K. G., J. P. Benoit, and R. A. Hansen, Near-real-time monitoring on a network of seismic stations with IceWorm: Automatic alarms for and spectral signals of the 1996 eruptions of Pavlof Volcano (abs.), *Seis. Res. Lett.*, 68, 332, 1997.

McKee, C. O., D. A. Wallace, R. A. Almond, and B. Talai, Fatal hydro-eruption of Karkar volcano in 1979: Development of a maar-like crater, *in*: Cooke-Ravian Vol. of Volcanological Papers, Johnson, R. W., ed., Geol. Survey of Papua New Guinea Memoir, 10, 63-84, 1981a.

McKee, C. O., R. A. Almond, R. J. S. Cooke, and B. Talai, Basaltic pyroclastic avalanches and flank effusion from Ulawun volcano in 1978, *in*: Cooke-Ravian Vol. of Volcanological Papers,. Johnson, R. W, ed., Geol. Survey of Papua New Guinea Memoir, 10, 153-165, 1981b.

McNutt, S. R., Observations and analysis of B-type earthquakes, explosions, and volcanic tremor at Pavlof Volcano, Alaska. *Bull. Seis. Soc. Amer.*, 76, 153-175, 1986.

McNutt, S. R., Volcanic tremor at Pavlof volcano, Alaska, October 1973-April 1986. *PAGEOPH*, 125, 153-175, 1987.

McNutt, S. R., T. P. Miller, J. J. Taber, Geological and seismological evidence of the increased explosivity during the 1986 eruptions of Pavlof volcano, Alaska, *Bull. Volc.* 53, 86-98, 1991.

McNutt, S. R., Volcanic Tremor, *in:* Encyclopedia of Earth System Science, 4, Academic Press, 4, 417-425, 1992.

McNutt, S. R., and G. Tytgat, Volcanic tremor during eruptions (abs.), *Eos, trans. AGU*, 75, 715, 1994.

McNutt, S. R., G. Tytgat, and J. Power, Preliminary analyses of volcanic tremor associated with the 1992 eruptions of Crater Peak, Mt. Spurr, Alaska, *in:* The 1992 eruptions of Crater Peak Vent, Mt. Spurr volcano, Alaska, Keith, T. E. C., ed., US Geol. Survey Bull. 2139, 161-178, 1995.

Miller, T. P., C. A. Neal, and R. B. Waitt, Pyroclastic flows of the 1992 Crater Peak eruptions: Distribution and origin, *in*: The 1992 eruptions of Crater Peak Vent, Mt. Spurr volcano, Alaska, Keith, T. E. C., ed., US Geol. Survey Bull. 2139, 81-87, 1995.

Minakami, T., Fundamental research for predicting volcanic eruptions (part 1): earthquakes and crustal deformations originating from volcanic activities. *Bull. Earthq. Res. Inst.*, 38, 497-544, 1960.

Mogi, K., Magnitude-frequency relation for elastic shocks accompanying fractures of various materials and some related problems in earthquakes. *Bull. Earthq. Res. Inst.*, 40, 831-853, 1962.

Neal, C. A., R. G. McGimsey, C. A. Gardner, M. L. Harbin, and C. J. Nye, Tephra-fall deposits from the 1992 eruptions of Crater Peak, Mount Spurr volcano, Alaska: A preliminary report on distribution, stratigraphy, and composition, *in*: The 1992 eruptions of Crater Peak Vent, Mt. Spurr volcano, Alaska, Keith, T. E. C., ed., US Geol. Survey Bull. 2139, 65-80, 1995.

Neal, J. T., A. M. Langer, and P. F. Kerr, Giant desiccation polygons of Great Basin playas, *Geol. Soc. Am. Bull.*, 79, 69-70, 1968.

Nishimura, T., Estimation of Ishimoto-Ida's m-value for seismic sources included in volcanic tremor, *Bull. Volcanol. Soc. Japan*, 40, 53-57, 1995.

Okubo, P. G. and K. Aki, Fractal geometry in the San Andreas fault system, *J. Geophys. Res.* 92, 345-355, 1987.

Power, J. A., J. C. Lahr, R. A. Page, B. A. Chouet, C. D. Stephens, D. H. Harlow, T. L. Murray, and J. N. Davies, Seismic evolution of the 1989-1990 eruption of Redoubt volcano, Alaska, *J. Volc. Geotherm. Res.*, 62, 153-182, 1994.

Ramos, E. G., E. P. Laguerta, and M. W. Hamburger, Seismicity and magmatic resurgence at Mount Pinatubo in 1992, *in*: Fire and mud eruptions and lahars of Mount Pinatubo, Philippines, Newhall, C. G., and R. S. Punongbayan eds., Philippines Inst. Volc. Seis., Quezon City and Univ. Washington Press, Seattle, 387-408, 1996.

Scholz, C.H., The frequency-magnitude relation of microfracturing in rock and its relation to earthquakes, *Bull. Seis. Soc. Amer.*, 58, 399-415, 1968.

Scott, W. E. and W. G. McGimsey, Character, mass, distribution, and origin of tephra-fall deposits of the 1989-1990 eruption of Redoubt volcano, south-central Alaska, *J. Volc. Geotherm. Res.*, 62, 251-272, 1994.

Shimozuru, D. and T. Kagiyama, Some significant features of pre-eruption volcanic earthquakes, *in*: Volcanic hazards, IAVCEI proc. 1, Latter, J. H., ed., Springer-Verlag, Berlin, 504-512, 1989.

Simkin, T., Terrestrial volcanism in space and time, *Ann. Rev. Earth. Planet. Sci.*, 21, 427-452, 1993.

Smith, D. K, and T. H. Jordan, The size distribution of Pacific seamounts, *Geophys. Res. Lett.* 14, 1119-1122, 1987.

Swanson, D. A., W. A. Duffield, and R. S. Fiske, Displacement of the south flank of Kilauea volcano: the result of forceful intrusion of magma into the rift zones, US Geol. Survey Prof. Paper 963, 1-39, 1976.

Turcotte, D. L., *Fractals and chaos in geology and geophysics*, Cambridge Univ. Press, 221 p., 1992.

Vogt, P. R. Volcano-spacing, fractures, and thickness of the lithosphere, *Earth Planet. Sci. Lett.*, 21, 235-252, 1974.

Warren, N. W., and G. V. Latham, An experimental study of thermally induced microfracturing and its relation to volcanic seismicity, *J. Geophys Res.*, 75, 4455-4464, 1970.

Welch, P. D., The use of fast Fourier transform for the estimation of power spectra: A method based on time averaging over short, modified periodograms, *IEEE Trans. on Audio and Electroacoustics*, AU-15, 70-73, 1967.

Williams, H., and A. R. McBirney, *Volcanology*, Freeman and Cooper, San Francisco, 397 p., 1979.

Wolfe, E. D., C. A. Neal, N, G. Banks, and T. J. Duggan, Geologic observations and chronology of the eruptive events, *in*: The eruption of Pu'u O'o eruption of Kilauea volcano, Hawaii: Episodes 1 through 20, January 3, 1983, through June 8, 1984, Wolfe, E. W., ed., US Geol. Survey Prof. Paper 1463, 1-98, 1989.

Wyss, M., Towards a physical understanding of the earthquake frequency distribution. *Geophys. J. Roy. Astr. Soc.*, 31, 341-359, 1973.

Yuan, A. T. E., S. R. McNutt, and D. H. Harlow, Seismicity and eruptive activity at Fuego volcano, Guatemala: February 1975-January 1977, *J. Volc. Geotherm. Res.*, 21, 277-296, 1984.

Appendix 3A

3B.1 Definition of reduced displacement

The reduced displacement is the root-mean-square (RMS) ground displacement corrected for geometrical spreading. It has units of distance*amplitude or cm^2, and is thus a measure of the intensity or strength of the tremor source that can be used to compare intensities of tremor sources at different volcanoes. The normalizing factors depend on the types of seismic waves, body or surface waves, which are predominantly carrying the energy.

The body wave reduced displacement is defined as [*Aki and Koyanagi*, 1981]:

$$D_R = \frac{A}{2\sqrt{2}} \cdot \frac{r}{M} \qquad (3A.1)$$

The surface wave reduced displacement is defined as [*Fehler*, 1983]:

$$D_R = \frac{A}{2\sqrt{2}} \cdot \frac{\sqrt{r\lambda}}{M} \qquad (3A.2)$$

where A is the peak-to-peak ground displacement, r is the distance between source and receiver, M is the instrument magnification, and λ is the wavelength.

3B.2 Calculation of reduced displacement from RSAM data

RSAM data are reported in digital counts. These values represent the average ground velocity detected by the seismometer at that station per unit time [*Endo and Murray*, 1991]. Endo and Murray state that the average ground velocity has no simple relationship to commonly measured earthquake parameters such as magnitude, seismic energy and seismic moment. For

continuous seismic signals such as volcanic tremor, the reduced displacement offers a standardized measure.

With a few assumptions, we developed a method to convert RSAM counts to average reduced displacement. If the frequency and amplitude of the signal are relatively constant, the signal can be approximated by a sine wave. We now show that the peak-to-peak amplitude of a sine wave is π times the average of the absolute value or the RSAM value in counts.

The average of the absolute value of a sine wave in discrete form can be written as:

$$c_{RSAM} = \frac{1}{N}\sum_{i=0}^{N}\left|A \cdot \sin(\omega t)\right| \qquad (3A.3)$$

where c_{RSAM} are RSAM counts, A is the amplitude, ω the frequency, t the time, and N the number of samples.

To convert to a continuous integrable function, multiply by Δt_i on top and bottom.

$$c_{RSAM} = \frac{1}{N}\sum_{i=0}^{N}\frac{\left|A \cdot \sin(\omega t)\right| \cdot \Delta t_i}{\Delta t_i} \qquad (3A.4)$$

Because the absolute value of the signal is taken, only one-half wavelength is considered. Therefore the limits of integration will be from 0 to T/2.

$$c_{RSAM} = \frac{\int_0^{\frac{T}{2}} A \cdot \sin(\omega t) \cdot dt}{\frac{T}{2}} \qquad (3A.5)$$

$$c_{RSAM} = \frac{2A}{T}\int_0^{\frac{T}{2}} \sin(\omega t)dt \qquad (3A.6)$$

$$c_{RSAM} = \frac{2A}{T} \cdot \frac{2}{\omega} = \frac{2A}{\pi} \qquad (3A.7)$$

To find the peak-to-peak amplitude (2A)

$$2A = \pi \cdot c_{RSAM} \qquad (3A.8)$$

This method was applied to the Mt. Spurr eruption tremor on 17 September 1992. The results vary from $D_R = 3$ cm^2 at station SPU to $D_R = 34$ cm^2 at station CKN. The four station average for the 17 September eruption is 15 cm^2 which is within a factor of two of the reduced displacement of 25 cm^2 calculated directly from the seismograms [*McNutt and Tytgat*, 1994].

Appendix 3B

3B.1 Overestimation of RMS ground displacement using helicorders or RSAM data

Traditionally the measurement of amplitudes of volcanic tremor has been done using helicorders or through a derivative product such as RSAM. Measurements from these types of records may lead to significant errors in the estimation of the RMS amplitude. Possible sources of measurement error lay in the difficulty to measure signal amplitudes contaminated by noise and the non-stationarity of the signal frequency. During times of high noise, for example, when an Aleutian winter storm passes over the network, tremor amplitudes may be overestimated.

Figure 3B1 shows synthetic waveforms to illustrate this point. Volcanic tremor is grossly approximated as a sine wave with a constant frequency of 2 Hz and amplitude = 15 units (Figure 3B1 frame A). Environmental noise, such as microseisms and wind noise, is simulated by adding two distributions of random numbers (Figure 3B1, frame B). Wind noise is imitated with zero-mean uniformly distributed random numbers or "white noise" with zero-to-peak amplitudes of 0-5 units. Microseisms were mimicked by the addition of random numbers in the frequency domain with a frequency dependent amplitude distribution. The sum of the simulated tremor and noise is shown in Figure 3B1, frame C. Zero-to-peak amplitudes measured by visual inspection of the synthetic signal (Figure 3B1, frame C) are on the order of 20 units, a 33% overestimate of tremor amplitude.

By measuring the amplitude in the frequency domain the errors caused by the addition of non-volcanic signals can be reduced. Frame D of Figure 3B1 shows an amplitude spectrum normalized so that a unit sinusoid in the time domain corresponds to unit amplitude in the frequency domain. The peak for the 2 Hz synthetic tremor is clearly visible and the amplitude of the peak is 15.6 units, a 4% overestimate of the true amplitude.

The amplitude variance in the estimated spectrum can be further reduced by using the Welch method [*Welch*, 1967], which windows the time series into many segments and averages the resulting spectra. This method was applied to the amplitude measurements during the 1996 eruptions at Pavlof volcano (see Figure 3.1 of this chapter).

Measurement of volcanic tremor amplitudes in the frequency domain also reduces the uncertainty due to time varying frequency content. The dominant frequency of volcanic tremor has been observed to change dramatically [e.g. *McNutt et al., 1994; Chapter 4 of this thesis*]. This directly impacts the surface wave formulation of reduced displacement, which is dependent on the wavelength.

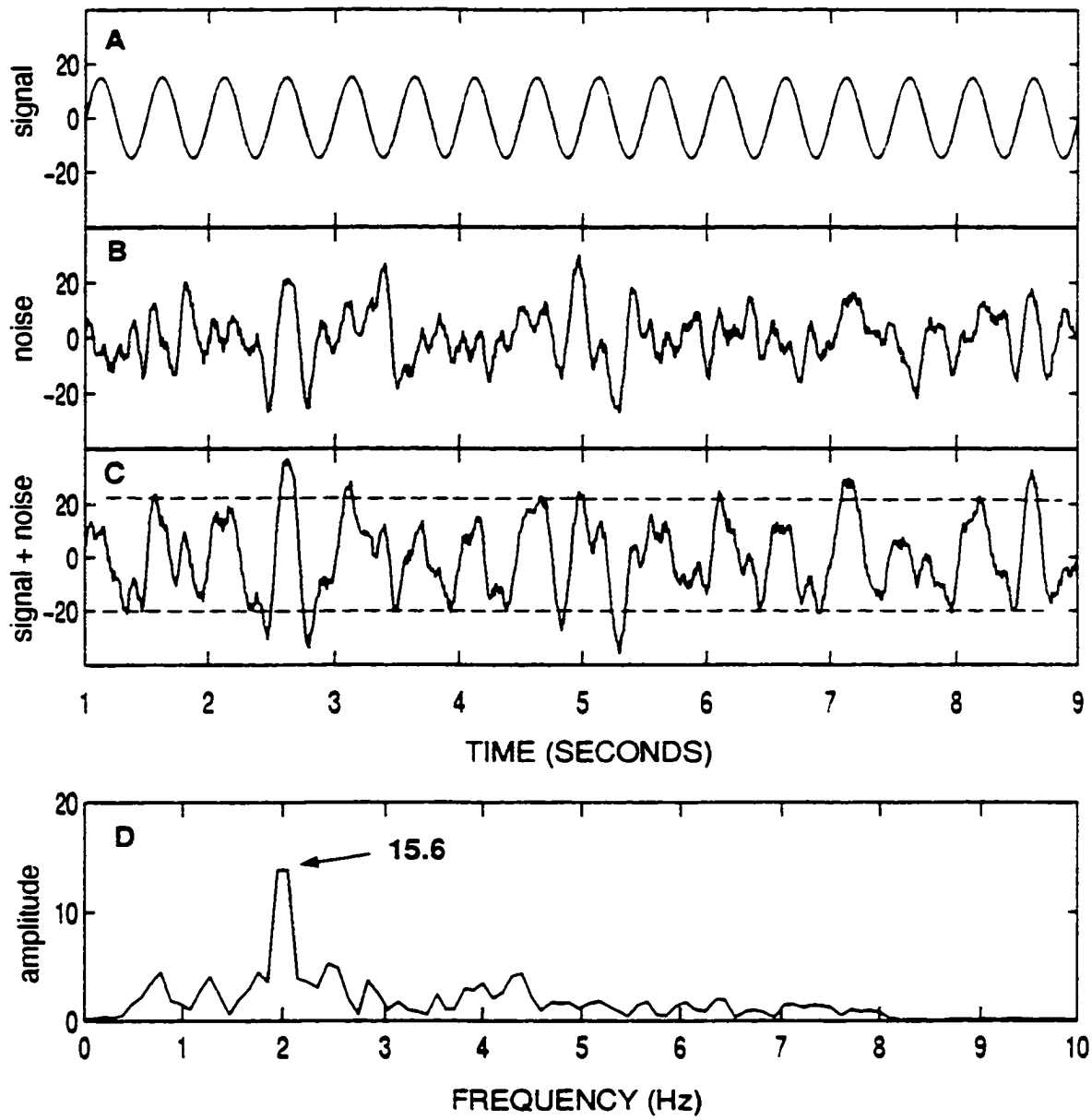

Figure 3B.1 Amplitude measurements for synthetic tremor. A) Synthetic tremor grossly approximated by 15sin(2*2πt). B) Synthetic noise approximated by the sum of white noise (wind) and frequency dependent noise (microseisms). C) The sum of the synthetic tremor and noise with a visual estimate of the peak amplitude, shown as a dashed line. D) Normalized amplitude spectrum shows a strong peak at 2 Hz with amplitude = 15.6 units.

Appendix 3C

3C.1 The duration-amplitude scaling of acoustic signals at Arenal volcano

The purpose of this appendix is to summarize duration-amplitude scaling measurements of acoustic signals produced by degassing events at Arenal volcano. These degassing events are locally known as "chugs" (see Chapter 4 for a further description and discussion of these events). Stephen McNutt made these acoustic measurements at the summit of Arenal volcano on January 17, 1982.

3C.2 Data

These acoustic signals were recorded on a Sanyo Model M1540A portable cassette recorder with a long period damping circuit (T~= 20 seconds). The frequency response of the system is unknown, but it probably is flat between 20-20,000 Hz. A one-hour recording was made approximately 50 m from the active vent. Over 2000 chugs were recorded. Three larger blasts (small Strombolian explosions) ejected red-hot pyroclastics to a distance of ~70 m from the vent. During this period lava was being issued at a rate of approximately 2×10^{-2} $m^3 s^{-1}$ (Wadge, pers. comm., 1982).

3C.3 Duration-Amplitude Measurements

The acoustic data were played back on a Siemens chart recorder at a speed on 9 mm s^{-1} and a signal-to-noise ratio of 20 dB. Using a scale, the peak-to-peak amplitudes of all the readable signals were measured to the nearest millimeter. The event durations and the intervals between the events were measured to the nearest 0.1 seconds.

Figure 3C.1 shows the duration-amplitude distribution for the chug events and fits to both the exponential and the power-law models. The models were fitted to these data using a weighted-least-squares regression. The correlation coefficients are 0.88 and 0.65, for the exponential and power-law models, respectively. Using the chi-squared statistic, we are able to reject the power-law model at the 97.5% confidence level. However, the same test is unable to reject the exponential model. The exponential model fits these data better than the power-law, but there is structure in the residual between the modeled distribution and the data. In addition, the correlation coefficient for the exponential model ($R^2 = 0.88$) is lower than any of the tremor episodes studied. This suggests that the exponential model may not be appropriate for the duration-amplitude distribution of these acoustic data. The exponential model fit to the duration-amplitude distribution can be substantially improved by plotting the squared amplitudes (proportional to energy). Figure 3C.1C shows this distribution and a weighted-least-squares fit to the data. The correlation coefficient becomes 0.98 when the amplitudes are squared.

We anticipated that the chugs would show similar scaling to the tremor at Arenal because both are presumably related to the same process or suite of processes. Instead, we found that by squaring the amplitudes we are now modeling a new distribution, which may be thought of as the "duration-energy" distribution. The full implications of this new scaling are beyond the scope of the present work. However, it must be noted that the distribution is clearly not a power law, the demonstration of which was the original intent of the investigation. The acoustic recording of degassing events at other volcanoes should be examined to determine if exponential scaling of squared amplitudes (duration-energy) is a general result for these types of signals.

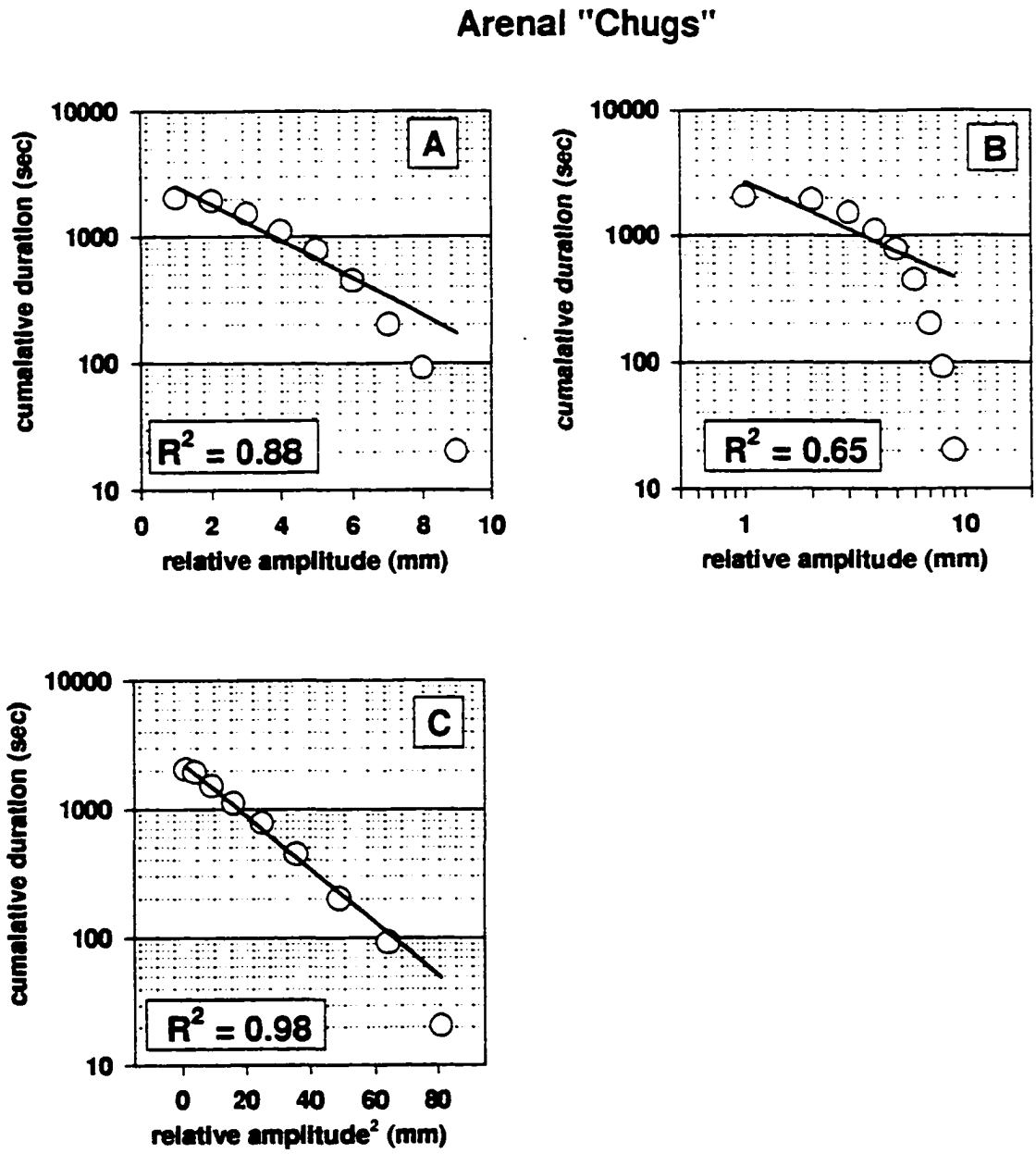

Figure 3C.1 Comparison of the exponential (A) and power-law (B) models for the duration-amplitude distributions for acoustic records of "chugs" at Arenal volcano. Frame C shows an exponential fit to the "duration-energy" distribution.

Chapter 4

New Constraints on Source Processes of Volcanic Tremor at Arenal Volcano, Costa Rica, Using Broadband Seismic Data[4]

4.0 Abstract

Broadband seismic data recorded 2.3 km from the active vent of Arenal Volcano, Costa Rica, provide new constraints on tremor source processes. Arenal's tremor contains as many as seven harmonics, whose frequencies vary temporally by up to 75 percent, from initial values of 1.9 Hz for the first peak immediately following explosive eruptions to 3.2-3.5 Hz several minutes later. The tremor amplitude shows an inverse correlation with its frequency. Wave speeds are estimated using the arrival of the ground-coupled airwave following an explosion. Minimum values of V_p and V_s are estimated at 2.0 and 1.2 km/s, respectively, for the shallow part of the volcanic structure. Large amplitude transverse waves that travel at speeds of about 800 m/s are observed following explosions. These waves show normal dispersion and are inferred to be surface waves. We infer that the source is a shallow, 200-660 m-long, vertically oriented 1-D resonator with matched boundary conditions, radiating seismic energy from a displacement antinode. We infer that the resonator is a gas-charged magma with variable bubble concentration within the conduit and also changes as a function of time, thereby changing the acoustic velocity and the boundary conditions. Polarization analyses of the tremor show that particle motion azimuths abruptly rotate, which may be explained by a decrease of the incidence angle. We suggest that energy is radiated predominantly from a displacement antinode that is changing position with time. P waves in the magma conduit will couple very efficiently into S waves in the surrounding medium when there is virtually no impedance contrast between the two media for these two types of waves. The tremor at Arenal is similar to tremor at least nine other volcanoes.

[4]Chapter 4 is an expanded version of: New constraints on source processes of volcanic tremor at Arenal volcano, Costa Rica, using broadband seismic data, by J. P.Benoit and S. R. McNutt, published in: *Geophysical Research Letters* 24, 449-452, 1997.

4.1 Introduction

Volcanic tremor is a very common but poorly understood type of seismic signal produced by active volcanoes. Tremor has been documented at 160 volcanoes [*McNutt*, 1994], and a variety of source models have been proposed [*Julian*, 1994, *Gordeev*, 1993, and *Chouet et al.*, 1994 provide recent reviews]. Worldwide observations suggest that there are probably several source mechanisms.

We operated a broadband three-component seismometer (Guralp CMG-40T) at two sites 2.3 and 2.8 km from Arenal Volcano, Costa Rica (10N27.8', 84W42.3', elevation 1633m a.s.l. and 1100m above the surrounding area), for two weeks in April 1994 (Figure 4.1). During this deployment we recorded high quality tremor data as well as other events characterized as whooshes, chugs and explosions (Figure 4.2), complemented with visual and audio observations (W. Melson, writ. comm., 1994). Whooshes are small eruptions that sound like a jet plane, accompanied by emergent seismic events with durations 2-20 seconds. Whooshes are often accompanied by small ash plumes. Chugs are series of small events that sound like a steam locomotive with pulses 0.5-1.5 seconds apart accompanied by gas only. When chugs are audible at a distance of 2.8 km, strong volcanic tremor is usually recorded. Explosions are impulsive seismic events with an audible acoustic wave and audible fallback of ejected material. A commonly observed temporal sequence is an explosion followed by a whoosh, then by loud chugs and strong tremor, then by weaker tremor [*Melson*, 1989]. A visit to the crater by S. McNutt in 1983 showed that chugs are venting gas along the crater edge continuously, but with variable amplitudes. All these events occur at crater C near the summit (Figure 4.1) from which

lava flows are also emitted. Each of these eruptive phenomena is accompanied by a characteristic seismic signal (Figure 4.2).

Arenal has had almost continuous effusion of lava since September 1968, following a series of powerful explosions in July 1968 [*Melson and Saenz*, 1973]. There has been a permanent lava pool at the summit since 1974. The volcano produces basaltic-andesite lavas with 54-56 % SiO_2 that initially contained an estimated 2-4 wt % H_2O [*Reagan et al.*, 1987; *Melson*, 1985]. Eruption rates have varied from 53 x 10^6 m^3 per year to the present rate of about 9 x 10^6 m^3 per year [*Reagan et al.*, 1987]. Several seismic studies have been carried out at Arenal including; *Alvarado and Barquero* [1987] and *Morales et al.* [1988] investigated relations between the seismicity and the type of eruptive activity; *Barboza and Melson* [1990] examined correlations between seismic signals and eruption sounds; *Barquero et al.* [1992] detected increases in seismicity before several explosive phases; *Metaxian et al.* [1996] recorded digital seismic data from a small network of stations for one month and estimated the minimum Vp = 1.3 km/s of the shallow part of the volcanic structure; and *Hagerty et al.* [1996] were the first to record data from a network of 5 broadband stations.

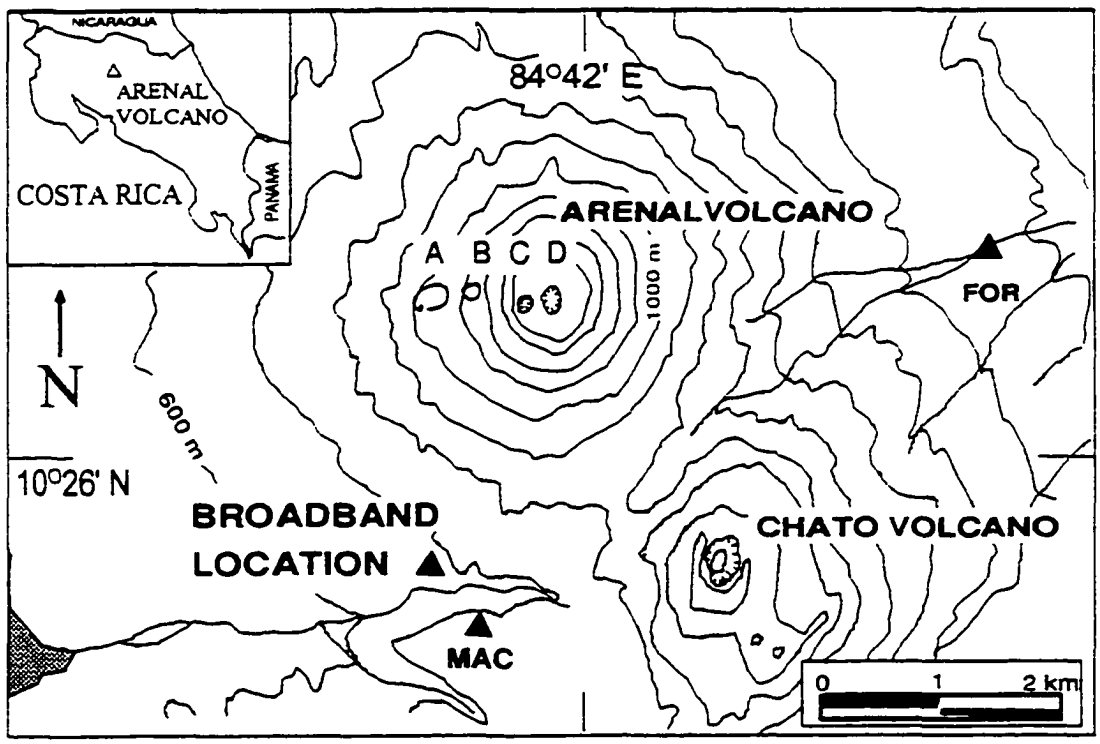

Figure 4.1 Map of Arenal Volcano, Costa Rica. The currently active crater is Crater C. The temporary broadband deployment was 2.3 km south-southeast of Crater C. The permanent seismometer (MAC) is located 2.8 km south of Crater C. Modified from *Barquero* [1992].

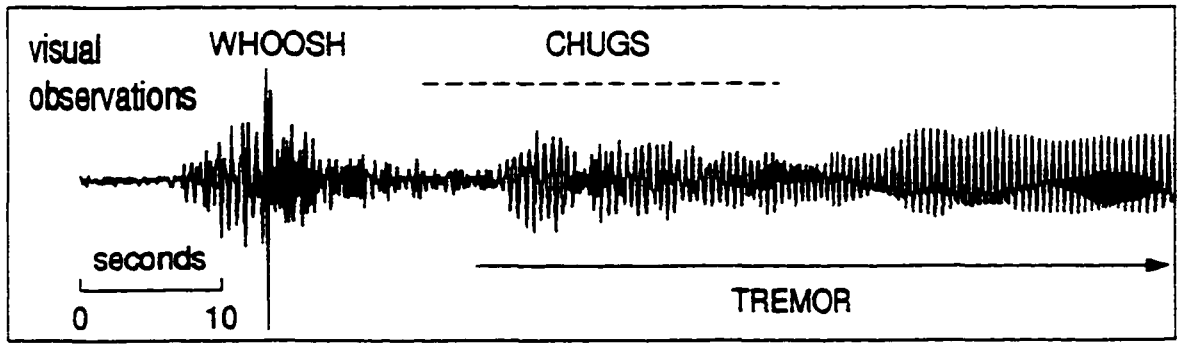

Figure 4.2 An example seismogram (radial component) of a small eruption (whoosh) followed by rhythmic degassing (chugs). Visual and audio observations show this eruption ejecting ash to ~500 m above the crater and the following chugs were audible at 2.8 km for ~25 s. Harmonic tremor begins during the chugs and continues for several minutes.

4.2 Analyses and Results

We first analyzed spectra to determine how tremor frequencies changed as a function of time, and to illuminate source versus path effects. We found that tremor frequencies varied by as much as 75 % within minutes; a clear source effect. Second, polarization analyses were conducted to discriminate wave types and to determine the wave azimuths and incidence angles. We found that waves come from at least two different regions.

Velocity spectrograms were produced using a standard method of averaging periodograms. Figure 4.3 shows a typical example of the broadband seismic data. Three small eruptions (whooshes), each ejecting ash to ~500 m above the crater, occurred during this 50-minute interval. Each whoosh lasted 10 - 20 seconds and was followed by a series of rhythmic gas emissions, or chugs, audible at a distance of 2.8 km for approximately 30 seconds and continuously near the vent. Note the close association between strong tremor and these two gas release processes. We found that the whoosh is expressed as a relatively broadband seismic signal with energy from 0.5 to 7 Hz. The seismic signals associated with the chugs and the following tremor are dominated by narrow spectral peaks at regular intervals (1.9, 3.8, 5.7, 7.6, ... Hz). Tremor stops abruptly when the frequency of the first peak reaches about 3.2-3.5 Hz (e.g. "A" in Figure 4.3). The strongest tremor occurs immediately following whooshes and chugs. The tremor amplitude shows a systematic decrease as frequencies increase. The temporal sequence of a whoosh followed by loud chugs and strong tremor is repeated many times (e.g. Figure 4.3).

To obtain information about wave velocities, we examined 3-component data for several explosions. An example is shown in Figure 4.4. The explosions are assumed to be, to first order, point sources originating at shallow depths near the summit of the volcano. The first waves

observed are weak, with particle motions longitudinal to the vent, and are inferred to be P waves. Larger amplitude waves are next observed showing particle motions transverse to the vent and are inferred to be S waves. The estimated P- and S-wave velocity is 2.0 and 1.2km/s, respectively, using the arrival of the acoustic wave to fix the origin time. The largest amplitude waves with elliptical particle motion appear shortly after the S waves and travel at 800 m/s. These waves show normal dispersion and are inferred to be surface waves (Figure 4.5). The group velocities were measure on the transverse component of the seismogram. A theoretical dispersion curve was calculated using a single layer over a half-space model for the volcanic structure (the method and source code are given in Appendix 4A). We used a trial-and-error method to determine the best fitting structure to the observed group velocities. The best model was a layer 190 m thick with an S-wave velocity of 650 m/s and a density of 2.0 gm/cm^3 overlying a half-space with S-wave velocity of 750 m/s and a density of 2.5 gm/cm^3. Both the S waves and surface waves may be produced by P waves impinging upon a low-velocity layer or layers near the source. This effect has recently been observed at Old Faithful geyser by *Kedar et al.* [1996].

The polarization azimuth and incidence angles of the tremor waves were estimated using the covariance method described by *Montalbetti and Kanasewich* [1970]. The analyses were conducted by windowing each spectral peak in time and frequency. The covariance matrix is formed over the three orthogonal components of the seismogram and then diagonalized. The direction of the largest eigenvector is taken to be the polarization direction of the particle motion. The polarization direction is then decomposed into azimuth and incidence angles. The rectilinearity is a normalized ratio of the largest eigenvector and the intermediate eigenvector. Linearly and circularly polarized waves are represented by a rectilinearity of 1 and 0, respectively. Typical sample windows were 1 to 2 seconds in time and 3 Hz in frequency.

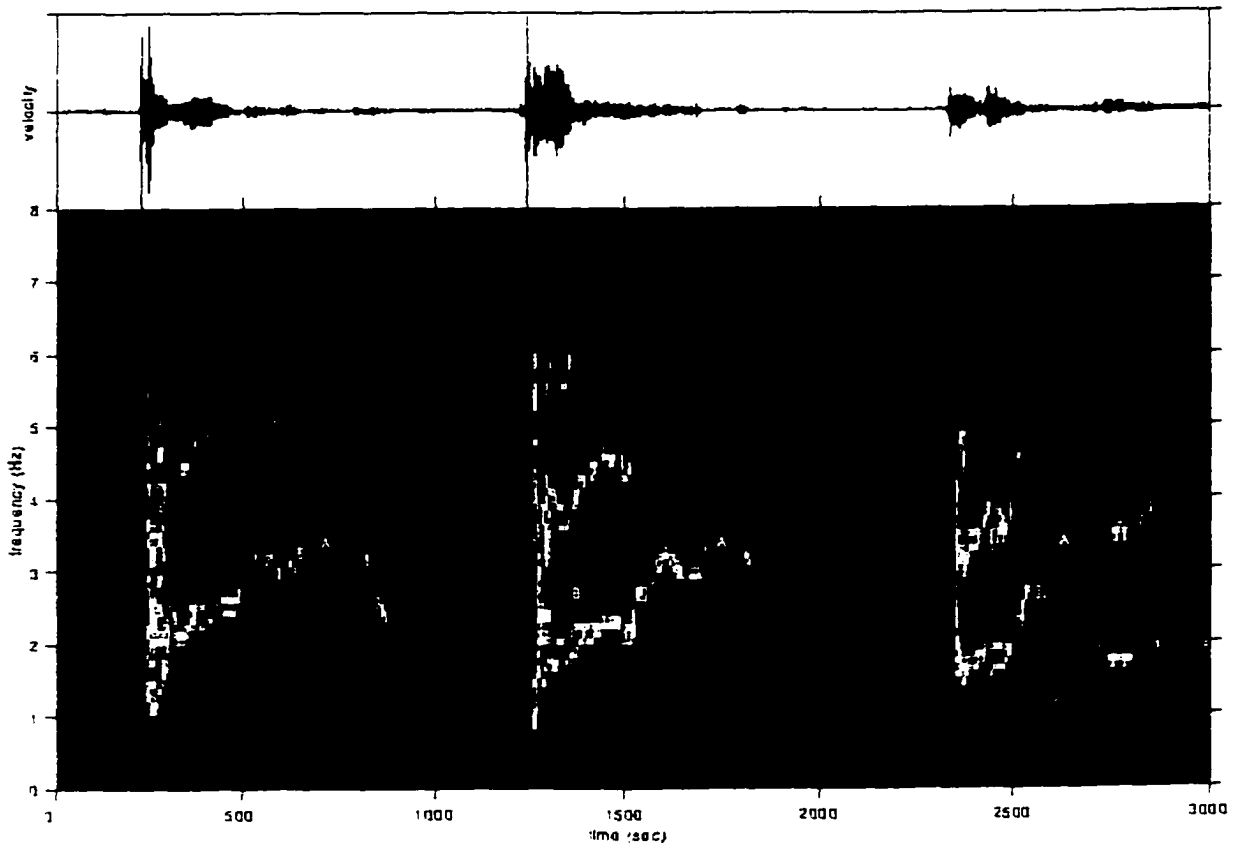

Figure 4.3 Velocity seismogram and spectrogram (radial component), beginning at 01:05 UT, April 25, 1994, showing three small eruptions. The beginning of the second event is shown in detail in Figure 4.2. The spectra of the volcanic tremor are dominated by narrow peaks spaced regularly in frequency, each of which changes frequency systematically with time. The tremor stops abruptly when the frequency of the first peak reaches ~3.2 Hz (see point "A"). The spectrogram is constructed by stacking 10 second FFT spectra with 50% overlap.

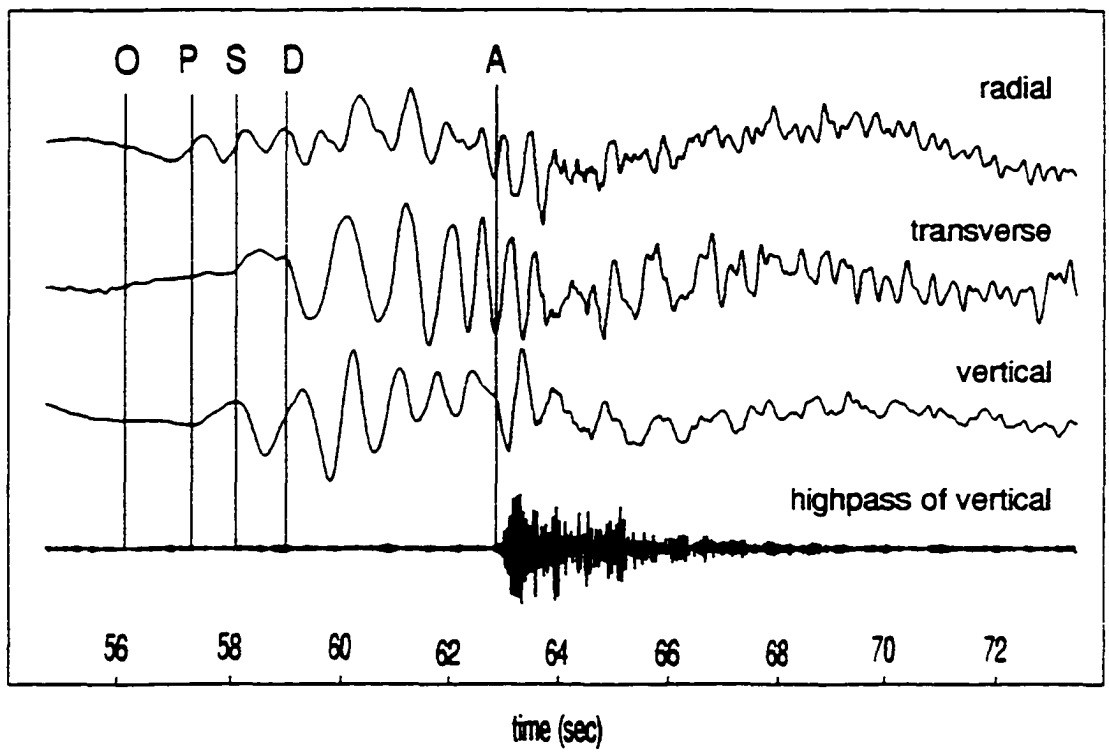

Figure 4.4 Example displacement seismogram of a small explosion recorded on the broadband instrument. All three components and a 15 Hz highpass filter of the vertical trace are shown. Assuming the explosion source is very shallow within the conduit and using the station-crater distance, the sound speed in air (330 m/s), and the ground-coupled airwave arrival (A) the origin (O) time is calculated. The inferred P, S, and strong transverse waves (P, S, and D) are labeled at the top of the figure. Using this origin time the phase velocities for the P, S, and D are 2.0, 1.2, and 0.8 km/s, respectively.

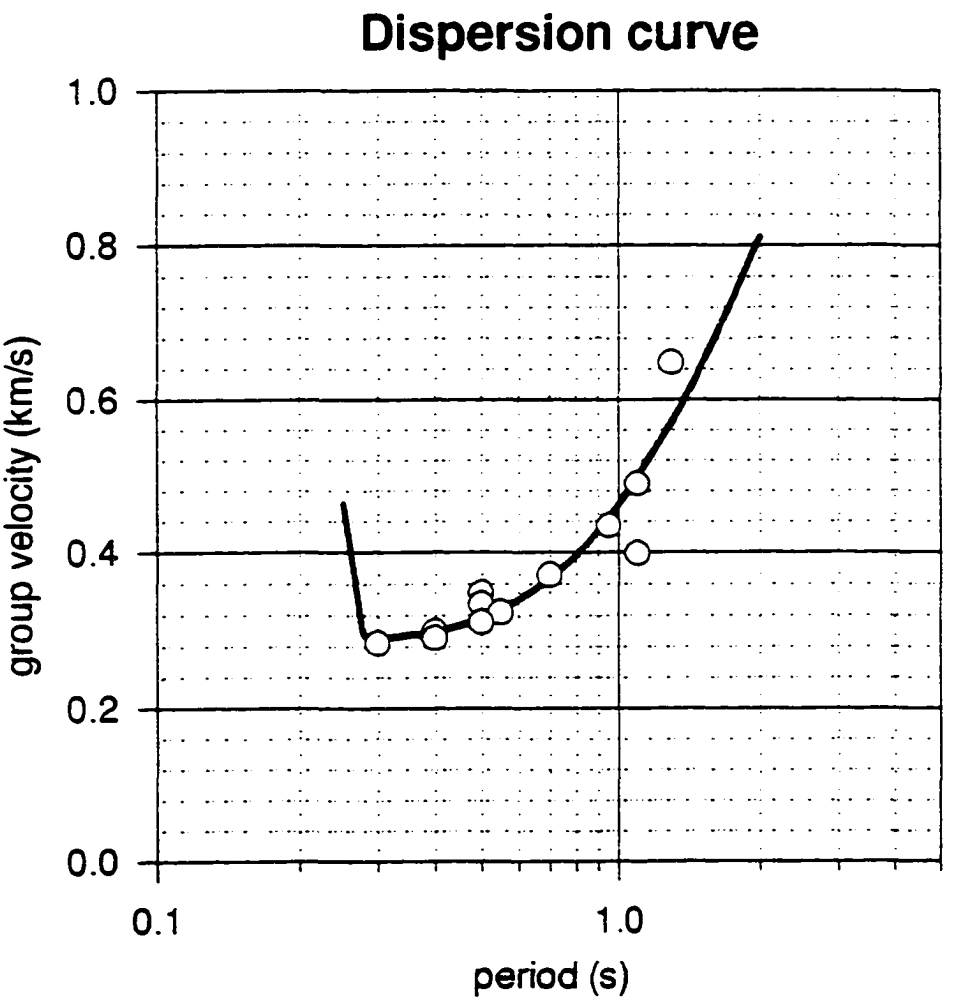

Figure 4.5 Dispersion curve for the large amplitude transverse waves (inferred surface waves) shown in Figure 4.4. Phase velocities were calculated using the origin time determined from the ground-coupled airwave. The line is a theoretical Love wave dispersion curve for a layer over a half-space. The layer thickness is 190 m with a S-wave velocity of 650 m/s and a density of 2.0 gm/cm^3. The parameters for the half-space are a S-wave velocity of 750 m/s and a density of 2.5 gm/cm^3.

We chose the first spectral peak for detailed analysis (Figure 4.6). This peak (1.9-3.2Hz) contains the longest wavelengths (~800m) and is therefore least susceptible to path effects. This peak was linearly polarized and the polarization angle was stable for up to 90 seconds. The tremor episodes began with linearly polarized particle motion (N40W azimuth; grazing incidence; "A" in Figure 4.7). Then, after 90 seconds the particle motion azimuth of the first spectral peak rapidly rotated clockwise 105° to N65E. The transition occurred within 12 seconds ("C" in Figure 4.7). At the same time the apparent incidence angle steepened suggesting that the source had deepened (Figure 4.7). This shows that either the source wave type is changing, that waves began to follow two different paths, or that there are two spatially distinct sources. The frequency content did not change significantly during this transition, suggesting that the overall source dimensions had not changed. Figure 4.8 shows the horizontal particle motions for three 1 second windows around this transition. Figure 4.8 also shows theoretical particle motions for a plane shear wave, propagating at N34E azimuth, incident at three angles that span the critical angle of ~36° [after *Nuttli*, 1961]. The dramatic change in the surface particle motion shown in Figure 4.7 and Figure 4.8 can be explained by an S-wave source that becomes deeper with time. If a spherical wave front is used the same behavior is observed but the critical angle is smaller [*Booth and Crampin*, 1985].

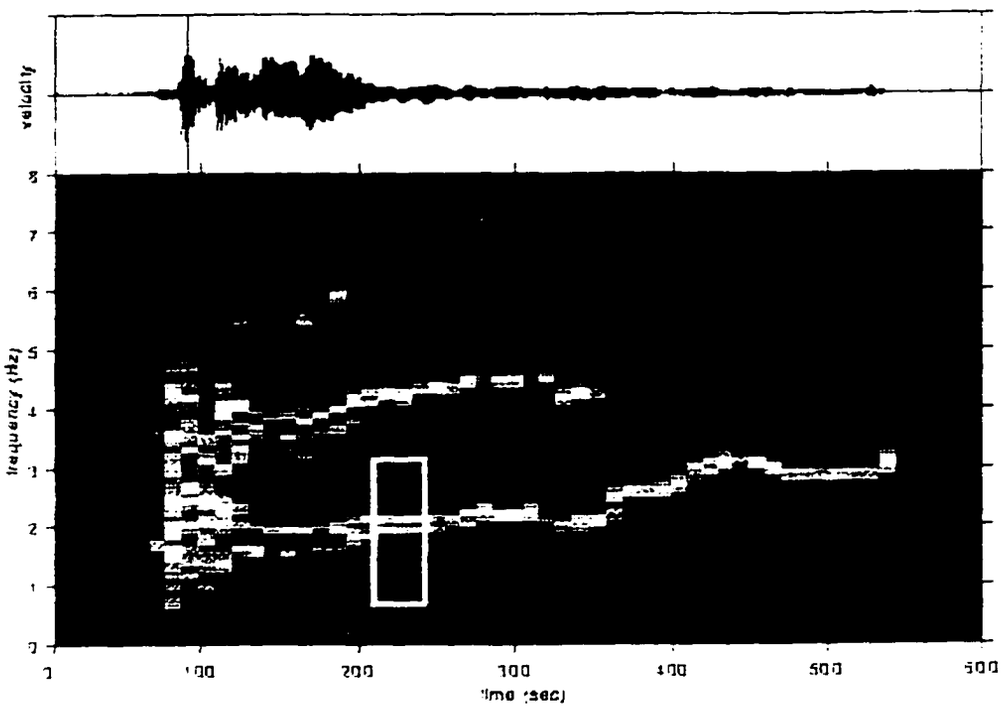

Figure 4.6 An example window (white rectangle) in time and frequency used in polarization analysis plotted on an enlarged view of the second eruptive event shown in Figure 4.3.

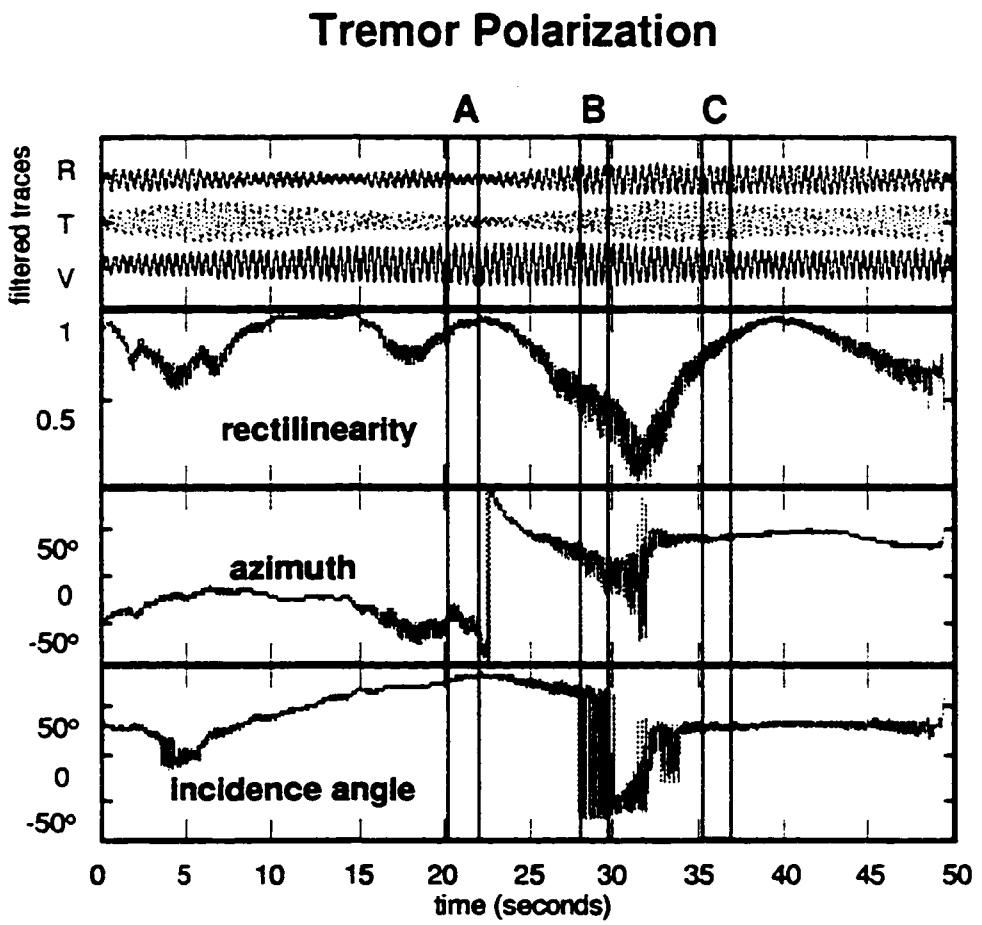

Figure 4.7 Polarization analysis showing a dramatic rotation in the tremor particle motions. The top frame shows three-component bandpass filtered (0.5-3.0 Hz) displacement seismograms. The next frames show the polarization parameters; rectilineary, azimuth, and incidence angle. These parameters are calculated at 0.01 second intervals using a 2 second-long sliding window.

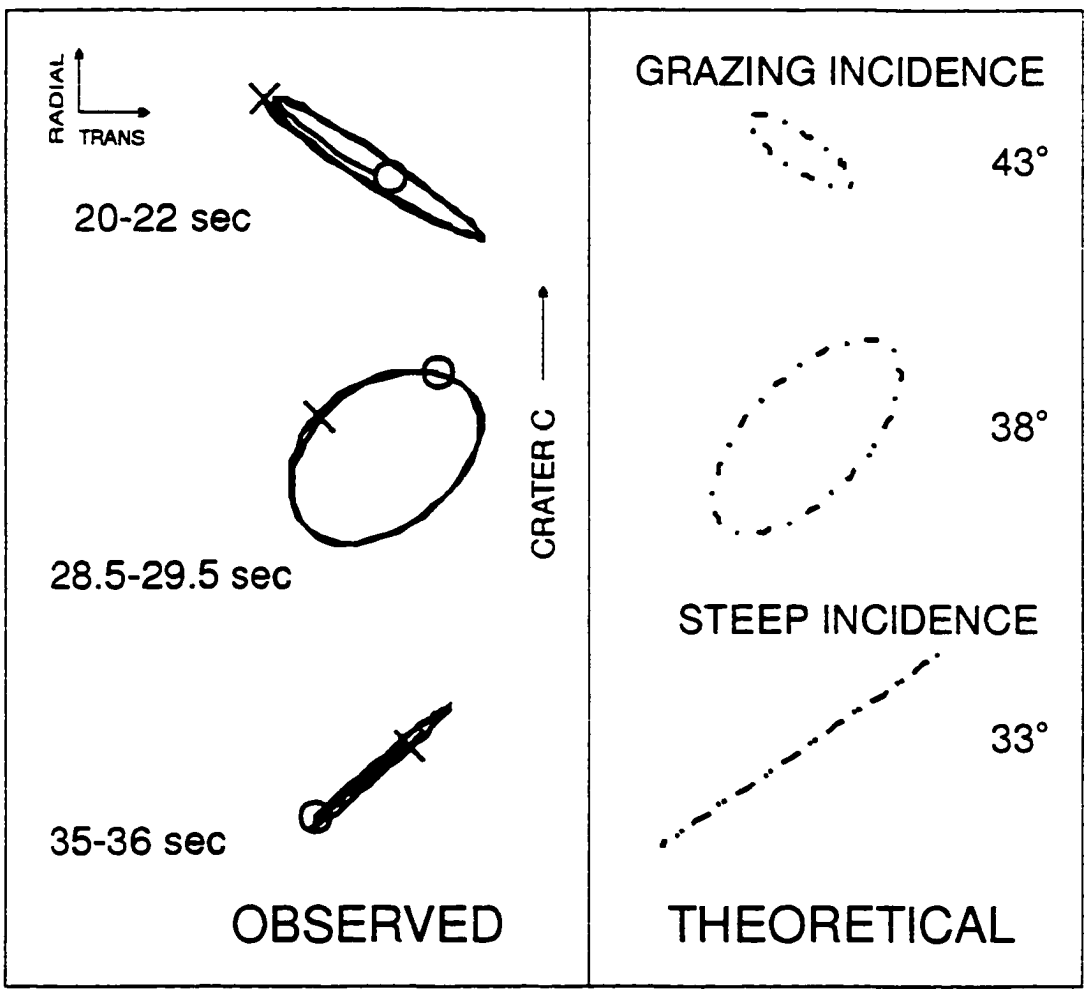

Figure 4.8 Observed and theoretical particle motions in the horizontal plane. The left column shows a 12 second sequence (0.5-3 Hz bandpass) taken from the second tremor episode ("B") in Figure 4.3. An "x" marks the beginning and an "o" the end of each one-second trace. The particle motion azimuth abruptly rotates clockwise 105°. The right column shows theoretical particle motions on a horizontal free surface due to a shear wave (polarization angle $\varepsilon = 20°$, Poisson's ratio = 0.25) incident at three angles (measured from the vertical). The observed tremor particle motions may be explained by an apparent steepening of the incidence angle.

4.3 Discussion and Conclusions

The tremor at Arenal is a uniform, regular signal with spectra showing as many as seven evenly spaced peaks, with the inter-peak frequency spacing the same as the zero-to-first-peak spacing. This type of spectral pattern has been attributed to both source and path effects. The non-stationarity of the signal with time points strongly towards source effects. Several source models may be employed to explain these observation; including the non-linear excitation due to unsteady flow [*Julian*, 1994] and the resonance of a fluid-filled cavity with various geometries [e.g. *McNutt*, 1986; *Chouet et al.*, 1994].

The unsteady-flow model [*Julian*, 1994] and the stationary crack model [*Aki and Koyanagi*, 1981] both predict systematic variations between the tremor amplitude and frequency. Figure 4.9 shows a clear inverse correlation between the tremor frequency and amplitude: as the frequency of a particular spectral peak increases, the amplitude decreases. This effect may also be due to frequency dependent attenuation and therefore not due solely to a source effect. The unsteady-flow model also predicts bifurcations in the spectral peaks as the frequencies increase, but no clear bifurcations were observed in the spectra.

We prefer the resonance of a fluid-filled cavity model, because such signals have been produced naturally at hydroelectric dams by resonance in the outflow tunnels, e.g. as Tarbela dam, Pakistan; [*McNutt*, 1986], and have also been produced in the laboratory [*Leet*, 1988]. Furthermore the resonator model provides a spatially extended source. Using the lowest frequency observed, 1.9 Hz (Figure 4.3), and the highest laboratory value for velocity of P waves in andesite melt, 2.5 km/s [*Murase and McBirney*, 1973], yields a maximum length of 658m. The resonator is certainly shorter than this because it contains gas bubbles, which lower the acoustic

velocity. If we use the value of 800 m/s, measured for the strong transverse waves in the wall rock, then the length would be 212 m. At 800 m/s we infer that the impedance contrast between the fluid and the wall rock is at a minimum, creating the most efficient generation and transmission of S waves from the interface.

We suggest that the source fluid is gas-charged magma for several reasons. First, incandescent lava is being emitted continuously from the same vent area that produces the whooshes and chugs. Second, the tremor is quite strong, of order 20 cm^2 reduced displacement. Tremor that has been observed in hydrothermal systems is weaker, <5 cm^2 [*McNutt*, 1992], and theoretical modeling of energy available from bubble collapse in water shows values of <10 cm^2 [*Leet*, 1988]. Third, a gas cavity or bubbly water column would have poor coupling with the wall rock because of the high impedance contrast between the fluid column and the wall rock.

We do not see evidence of 2-D modes as noted by *Chouet et al.* [1994] for rectangular cracks, although our instrument may be too far away to record high frequencies from such modes. Data recorded by us at five different sites 2-7 km from Arenal all show the same regular tremor with the same frequencies. Due to the lack of a second set of modes we choose a 1-D model. The matched boundary conditions, which are suggested by the spectra, may consist of two configurations, "open-open" or "closed-closed." The "open-open" system has pressure nodes and displacement anti-nodes at each end whereas for the "closed-closed" system the pressure and displacement nodes are switched. These boundaries or impedance discontinuities are controlled by either geometric or velocity contrasts within the conduit. Geometric boundaries may consist of the open vent on top and a flaring of the conduit diameter at the bottom, corresponding to an "open-open" system. Velocity-controlled boundaries may consist of a very slow, gas-bubble-rich layer overlain by relatively cool, fast, crust at the top of the conduit, and the bubble nucleation front at the bottom, corresponding to a "closed-closed" system (Figure 4.10).

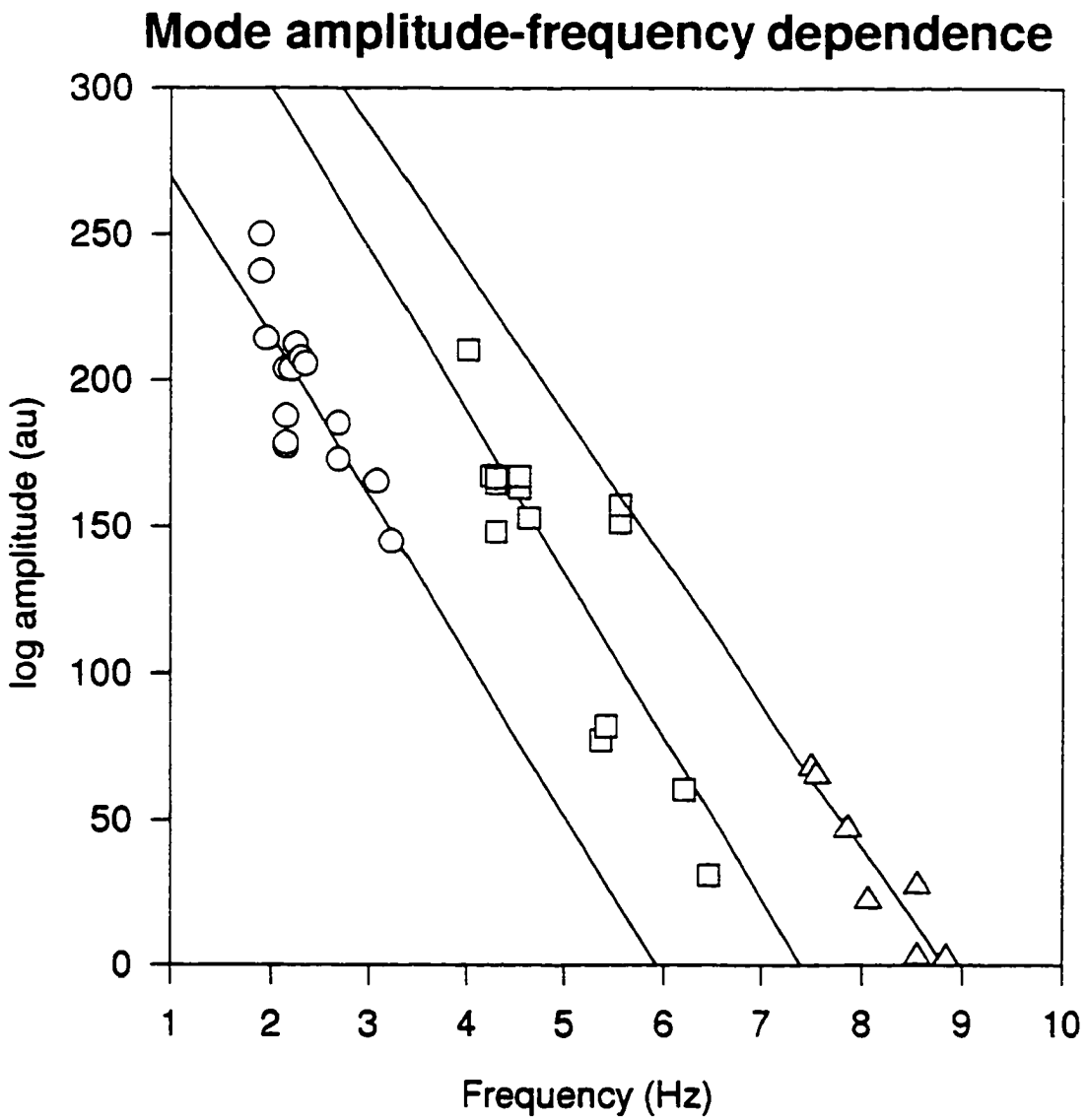

Figure 4.9 Frequency-amplitude dependence for tremor. The maximum amplitude of each peak or mode in the spectrogram is plotted against its frequency. The circles, squares, and triangles are amplitudes for the first, second, and third peaks in the spectra, respectively. The lines are least-squares regressions through data for each spectral peak.

We favor the "closed-closed" system for two reasons; first the "closed-closed" system has a pressure antinode at the top where degassing occurs as rhythmic pulses -- chugs -- that are coupled to the oscillating magma conduit and feed energy back into it. The frequency of chugs is similar to the fundamental mode of the tremor, about 2 Hz. The energy exchange may occur if each chug is triggered by a decompression wave; the gas release upward will cause a downward push or compression that is in phase with the reflected wave at the surface. Second, the "closed-closed" system has a transient lower boundary, which provides an explanation for the commonly observed abrupt loss of tremor (e.g. "A" in Figure 4.3). As degassing occurs, the bubble concentration will decrease and the bubble nucleation front will cease to act as a reflecting boundary sustaining strong resonance (strong tremor). The impedance contrast will be lost when the bubble concentrations are uniform across the former boundary. Complete degassing is not required: only enough to remove the impedance contrast. Figure 4.11 shows a qualitative model for this process. The bubble fraction, acoustic velocity, and acoustic impedance are shown for two time periods, the most gas-rich time directly after the whooshes (Figure 4.11a, b, c) and the most gas-poor time before the tremor stops (Figure 4.11d, e, f). The bubble fraction shown here assumes a simple parabolic bubble growth curve [e.g. *Sparks*, 1978] nucleating at a depth of 250 m (Figure 4.11a and d). The acoustic velocity (Figure 4.11b and e) was calculated following the formulation given in *Dibble* [1994]. The acoustic velocity is strongly dependent on the gas fraction and abruptly decreases as the first bubbles are nucleated. The velocity within the conduit varies from 2.5 km/s below the nucleation depth to less than 100 m/s just below the surface. The acoustic impedance, which is the product of the density and acoustic velocity of the magma, control the location and efficiency of the resonator reflecting boundaries. The impedance contrasts shown in Figure 4.11c and 4.11f are the ratio of acoustic impedance for two vertically

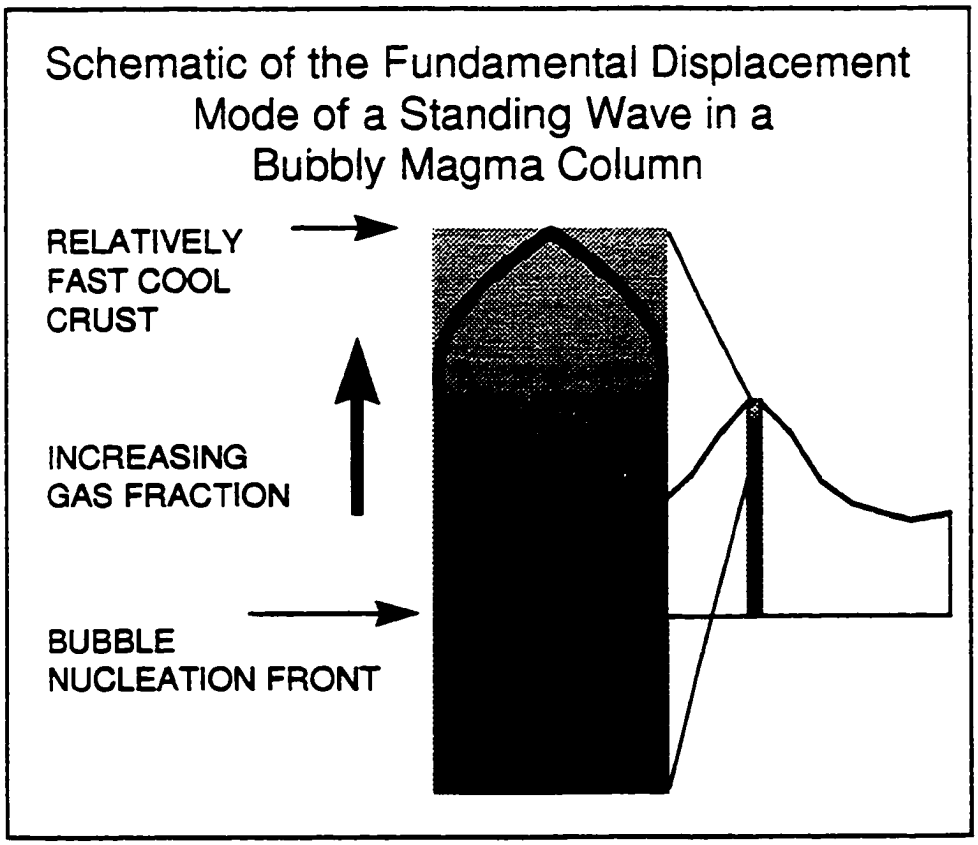

Figure 4.10 Schematic model of the fundamental displacement mode of a standing wave in a bubbly magma column. Velocity-controlled boundaries may consist of a very slow, gas-bubble-rich layer overlain by relatively cool, fast, crust at the top of the conduit, and the bubble nucleation front at the bottom, corresponding to a "closed-closed" system.

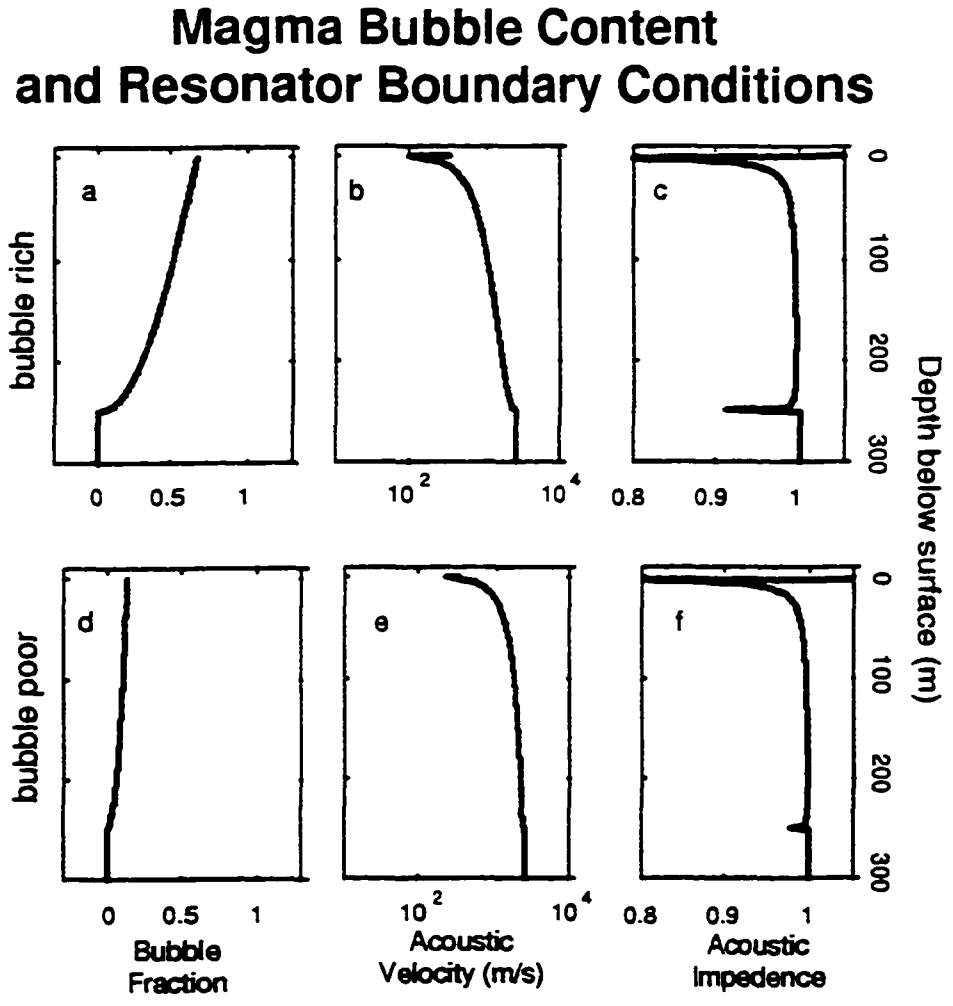

Figure 4.11 Numerical model of magma bubble content and resonator boundary conditions within the volcanic conduit. The bubble fraction, acoustic velocity, and acoustic impedance are shown for two time periods, gas-rich directly after the whooshes (a, b, and c) and gas-poor before the tremor stops (d, e, and f).

adjacent parcels of magma. Two strong boundaries are created at the surface and at the bubble nucleation depth (Figure 4.11c). The degassing process is modeled as a reduction in the bubble fraction throughout the conduit (Figure 4.11d); increasing the average acoustic velocity (Figure 4.11e) and dramatically reducing the impedance contrast at the lower boundary. The lower boundary then is no longer a competent reflector of energy and the tremor stops.

All the spectral peaks remain evenly spaced while they shift upward in frequency by up to 75%. Frequencies are lowest right after the whoosh, when the conduit is most gas-rich (i.e. slowest velocities), then shift upward as gas presumably is lost and the acoustic velocity increases. Additionally, when the tremor returns (e.g. at 800 seconds in Figure 4.3) it returns first with higher (gas poor) frequencies that gradually lower as gas content increases. The effect of bubbles on P-wave speeds in fluid has been shown by *Leet*, [1988] to agree with the observations here: a P-wave speed of 800 m/s in the magma implies a theoretical bubble concentration of 10^{-3}. We believe this value is too low, however, because of the shallow depths and because the magma contains abundant phenocrysts (up to 55%) so it may not behave as a theoretical two-phase fluid.

The polarization analyses show that both the particle motion incidence angle and the azimuth change systematically while the frequencies remain constant ("B" in Figure 4.3). This shows that either the source wave type is changing, that waves began to follow two different paths, or that there are two spatially distinct sources. Our temporary deployment did not collect sufficient data to definitively state which of the above hypotheses best explains this observation. The deployment of a small array of seismometers, to measure phase velocities for example, would help greatly in constraining the wave types and polarization effects due to shallow structure. We speculate that the depth of the source has changed, altering the path to the receiver. Small changes in incidence angle can cause dramatic changes in observed particle motion for waves incident near the critical angle. The change in the depth of the source would result from

uneven bubble concentrations within the conduit. The position of a resonator's displacement antinode depends on the acoustic velocity profile within the conduit (Figure 4.10). As bubble concentrations change during degassing the position of the displacement antinode, or strongest source of tremor, will shift (Figure 4.11b and e). The surface wave dispersion analysis suggests the presence of a 190 m thick layer with a substantially lower velocity within the volcanic structure. If the depth of the displacement antinode crosses this layer boundary we would expect to observe changes in the particle motions.

None of the new data presented here address the question of the energy source. We suggest that expanding gases provide most of the potential energy that drives the tremor and other events. The available power from 2 wt % water is about 6×10^6 J/s, whereas the strongest tremor has an energy release rate of about 8×10^5 J/s, for a seismic efficiency of 13 %.

4.4 Other Observations and Future Work

These data provide compelling arguments for a simple model of the source of volcanic tremor at this volcano. However, our model may apply only to this one type of signal. Tremor strikingly similar to that at Arenal has been observed at nine other volcanoes, including Semeru [*Schlindwein et al.*, 1995], Langila [*Mori et al.*, 1989], Merapi, Krakatau (R. Schick, writ. comm., 1994), Sakurajima [*Kamo et al.* 1977], Ruapehu [*Hurst*, 1992], Fuego, Pacaya (D. Harlow, writ. comm. 1984), and Karymsky (Gordeev, writ. comm. 1996). Future work is needed to test the model with additional instruments. This will allow us to better constrain the source locations, to determine the velocity structure, and to understand the evolution of the tremor source with time.

4.5 Acknowledgments

We are grateful to B. Melson, V. Barboza, and J. Barquero for many stimulating discussions and logistical support while in Costa Rica. We have collaborated with them fruitfully for 5 years. We thank G. Tytgat, M. Wyss, and M. Garcés for several technical discussions. We also thank B. Julian, J. Eichelberger, R. Hansen and two anonymous reviewers for their comments, which substantially improved this paper. This work was supported in part by the Alaska Volcano Observatory.

4.6 References

Aki, K., and R. Y. Koyanagi, Deep volcanic tremor and magma ascent mechanism under Kilauea, Hawaii. *J. Geophys. Res., 86*, 7095-7109, 1981.

Alvarado, G. E. y Barquero, R. Las senales sismicas del volcan Arenal (Costa Rica) y su relacion con las fases eruptivas (1968-1986), *Ciencia y Tecnologia*, 11, 15-35, 1987.

Barboza, V. and W. G. Melson, Correlacion entre las senales sismicas y los sonidos de las erupcions del Volcan Arenal, *Bull. de Vulcan. (Heredia, Costa Rica)*, 21, 8-12, 1990.

Barquero, R. Alvarado, G. E., and Matumoto, T., Arenal volcano (Costa Rica) premonitory seismicity, in *Volcanic seismology, IAVCEI proceedings in volcanology*, eds. Gasparini, P., R. Scarpa, and K. Aki, 3, 84-96, 1992.

Booth, D. C. and S. Crampin, Shear-wave polarization on a curved wavefront at an isotropic free surface, *Geophys. J. R. Astr. Soc.*, 83, 31-45, 1985.

Chouet, B. A., R. A. Page, C. D. Stephens, J. C. Lahr, and J. A. Power, Precursory swarms of long-period events at Reboubt Volcano (1989-1990), Alaska: Their origin and use as a forecasting tool, *J.Volcanol.Geotherm. Res.*, 62, 1994.

Dibble, R. R., Velocity modeling in the erupting magma column of Mount Erebus, Antarctica, in *Volcanological and Environmental Studies of Mount Erebus, Antarctica*, ed. P. R. Kyle, Antarctic Res. Ser., Am. Geophys. Union, Washington D. C., 66, 17-33, 1994.

Gordeev, E., Modeling of volcanic tremor as explosive point sources in a single-layered, elastic half-space, *J. Geophys. Res.*, 98, 19687-19703, 1993.

Julian, B. R., Volcanic tremor: Nonlinear excitation by fluid flow, *J. Geophys. Res.*, 99, 11,859-11,877, 1994.

Hagerty, M. T., S. Y. Schwartz, and J. M. Protti, Preliminary analysis of seismic observations at Arenal volcano, Costa Rica, *Volcanology and Seismology*, 1997 (in press).

Hurst, A. W., Stochastic simulation of volcanic tremor from Ruapehu, *J. Volcanol. Geotherm. Res.*, 51, 185-198, 1992.

Kamo, K., T. Furuzawa, and J. Akamatsu, Some natures of volcanic micro-tremors at the Sakurajima volcano, *Bull. Volcanol.* Soc. Japan, 22, 41-48, 1977.

Kedar, S., B. Sturtevant, and H. Kanamori, The origin of harmonic tremor at Old Faithful geyser, *Nature*, 379, 708-711, 1996.

Keilis-Borok, V. I., ed., *Seismic surface waves in a laterally inhomogeneous earth*, Kluwer Academic Publishers, Dordrecht, p. 293, 1989.

Leet, R. C., Saturated and subcooled hydrothermal boiling in groundwater flow channels as a source of harmonic tremor, *J. Geophys. Res.*, 93, 4835-4849, 1988.

McNutt, S. R., Volcanic tremor from around the world: 1992 update, *Acta Vulcanologica*, 5, 197-200, 1994.

McNutt, S. R., Observations and analysis of B-type earthquakes, explosions, and volcanic tremor at Pavlof Volcano, Alaska, *Bull. Seis. Soc. Am.*, 76, 153-175, 1986.

McNutt, S. R., Volcanic tremor, in: *Encyclopedia of Earth System Science*, 4, Academic Press, 417-425, 1992.

Melson, W. G., and R. Saenz, Volume, energy and cyclicity of eruptions at Arenal Volcano, Costa Rica, *Bull. Volcanol.*, 37, 416-437, 1973.

Melson, W. G., Alteration between acidic and basic magmas in major explosive eruptions of Arenal Volcano, Costa Rica, *Bol. de Vulconologia Costa Rica*, 14, 65-74, 1985.

Melson, W. G., Las erupiciones del Volcan Arenal 1 al 13 de April de 1989, *Bull. de Vulcan. (Heredia, Costa Rica)*, 20, 15-22, 1989.

Metaxian, J. P., P. Lesage, R. Barquero, A. Creusot-Eon, Caracteristicas espectrales de las senales sismicas y estimacion de Vp en la estructura superficial del volcan Arenal, *Bol. Obs. Vulc. Arenal*, 6, 23-44, 1993.

Montalbetti, J. F. and K. R. Kanasewich, Enhancement of teleseismic body phases with a polarization filter, *Geophys. J. R. Astr. Soc.*, 21, 119-129, 1970.

Morales, L. D., J. F. Soley, G. E. Alvarado, A. Borgia, G. Soto, Analisis espectral de algunas senales sismicas y su relacion con la actividad de los volcanes Arenal y Poas, Costa Rica, *Bol. Obs. Vulc. Arenal*, 1, 1-25, 1988.

Mori, J., H. Patia, C. McKee, C. Itikarai, P. Lowenstein, P. De Saint Ours, B. Talai, Seismicity associated with eruptive activity at Langila Volcano, Papua New Guinea, *J. Volcanol. Geotherm. Res.*, 38, 243-255, 1989.

Murase, T. and A. R. McBirney, Properties of some common igneous rocks and their melts at high temperatures, *Bull. Geol. Soc. Am.*, 84, 3563-3592, 1973.

Nuttli, O., The effect of the earth's surface on the S wave particle motion, *Bull. Seismol. Soc. Am.*, 51, 237-246, 1961.

Reagan, M. K, J. B. Gill, E. Malavassi, and M. O. Garcia, Changes in magma composition at Arenal volcano, Costa Rica, 1968-1985: Real-time monitoring of open-system differentiation, *Bull. Volcanol.* 49, 415-434, 1987.

Schlindwein, V., J. Wassermann, and F. Scherbaum, Spectral analysis of harmonic tremor signals at Mt. Semeru volcano, Indonesia, *Geophys. Res. Lett.*, 22, 1685-1688, 1995.

Sparks, R. S. J., The dynamics of bubble formation and growth in magmas: A review and analysis, *J. Volcanol. Geotherm. Res.* 3,1-37, 1978.

4.7 Appendix 4A

4.7.1 Calculation of theoretical dispersion curves for Love Waves

This appendix details how the theoretical dispersion curves were calculated for a layer over a half-space. The MATLAB source code to make these calculations is also listed. The following discussion and notation on dispersion of Love waves is primarily drawn from *Seismic surface waves in a laterally inhomogeneous earth* [*Keilis-Borok*, 1989]. A homogeneous layer overlying a homogeneous half-space for the case of a vertically varying medium given the parameters

$$b(z) = b_1, \qquad \rho(z) = \rho_1, \qquad \text{for } z \le Z;$$

$$b(z) = b_2, \qquad \rho(z) = \rho_2, \qquad \text{for } z > Z;$$

where b_1, ρ_1, and Z are the S-wave velocity, density, and thickness of the layer, respectively, and b_2 and ρ_2 are the S-wave velocity and density of the half-space. The phase velocity of Love waves obeys the dispersion relation

$$\tan(r_{\beta 1} Z) - \frac{b_2^2 \rho_2 r_{\beta 2}}{b_1^2 \rho_1 r_{\beta 1}} = 0 \qquad \text{(4A.1)}$$

where

$$r_{\beta 1} = \omega(\kappa^2 - 1)^{1/2}/(\kappa b_1),$$

$$r_{\beta 2} = \omega(1 - (b_1\kappa/b_2)^2)^{1/2}/(\kappa b_1),$$

$$\kappa = Ck_L/b_1.$$

For fixed frequency (ω), Equation 1 has one or more solutions and the fundamental mode can exist at any at any ω. The phase velocity for fundamental mode (Ck_L) can be numerically solved at a fixed ω. Figure 4A.1 shows a graphic representation of Equation 4A.1 and its solutions for several values of ω. Once the phase velocity as a function of frequency is determined, the group velocity then can be calculated. The group velocity obeys the relation

$$U_{kL} = \frac{b_1^2}{C_{kL}} \frac{\omega Z + \kappa^2 \Lambda b_1}{\omega Z + \Lambda b_1} \qquad (4A.2)$$

where

$$\Lambda = \frac{\rho_2 \kappa \cos^2(r_{\beta 1} Z)(b_2^2 / b_1^2 - 1)}{\rho_1 (\kappa^2 - 1)(1 - (b_1 \kappa / b_2)^2)^{1/2}}.$$

4.7.2 Source code

The following MATLAB code will calculate the phase and group velocity dispersion curves for Love waves for a single layer over a half-space; given the model parameters of layer thickness, layer and half-space S-wave velocities and densities.

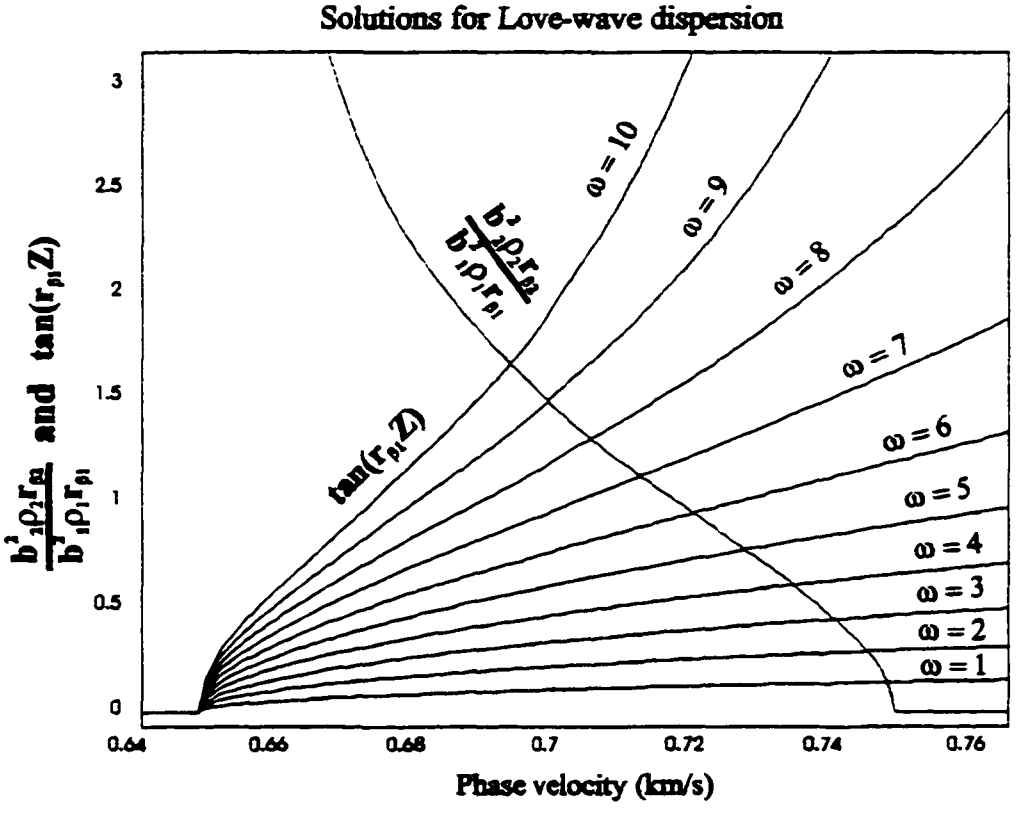

Figure 4A.1 Solutions to Equation 1, the dispersion relation for Love waves, for several frequencies. The phase velocity can read off this figure by projecting the intersection of these functions down to the abscissa.

```
%     Set model parameters
b1 = 0.650;              %  layer S-wave velocity (km/s)
b2 = 0.750;              %  half-space S-wave velocity (km/s)
rho1 = 2.0;              %  layer density (g/cm^3)
rho2 = 2.5;              %  half-space density (g/cm^3)
Z = 0.190;               %  layer thickness (km)

%     Run the calculations over range of phase velocities,
%     C (km/s) and frequencies w (Hz).
C = 0.1:0.01:1.5;
kap = C ./ b1;
w = 0.1:0.1:10;

for i = 1:length(w)
   %  Calculate the terms needed for Equation 1.
   rb1 = w(i) .* sqrt(kap.^2 - 1) ./ (kap .* b1);
   rb2 = w(i) .* sqrt(1 - (b1.*kap./b2).^2 ) ./ (kap .* b1);

   %  First term of Eq. 1
   y = tan(rb1*Z);

   %  Second term of Eq. 1
   x = (b2^2 .* rho2 .* rb2) ./ (b1^2 .* rho1 .* rb1);

   %  Find the zero crossings for each frequency.
   z(:,i) = abs(x)' - abs(y)';

   %  pind is the index of the smallest positive value.
   pind = length(find(z(:,i)>= 0));

   %  The phase velocity, Ckl at frequency w, is taken
   %  as the average between the smallest positive and negative
   %  values of the function z. This is not the exact zero of the
```

```
   %  function, but very close.
   CkL(i) = sum(C(pind:pind+1))/2;
end

%  Use the phase velocity to calculate the group
%  velocities.
%  Reassign values needed for equation 2.
kap = CkL ./ bl;
rbl = w .* sqrt(kap.^2 - 1) ./ (kap .* bl);
rb2 = w .* sqrt(1 - (bl.*kap./b2).^2 ) ./ (kap .* bl);


Clamda = (rho2.*kap.*cos(rbl.*Z(d)).^2 .*((b2^2/bl^2)-1)) ./ ...
         (rhol .* (kap.^2 - 1) .* (1 - bl.*kap/b2).^2).^0.5 );

%  Evaluate Equation 2 at the given frequencies.
Ukl = (bl^2./CkL).*(w .* Z + kap.^2 .* Clamda.*bl) ./ ...
      ( w .* Z(d) + Clamda .* bl);
%  Plot the results as a function of period.
semilogx(1./w,CkL,'.r',1./w,Ukl,'-b',T,U,'ok')
xlabel('period [s]');
ylabel('phase (red dots) and group (blue line) velocity [km/s]');
title('Love wave dispersion')
grid

%  Output the results to a text file.
out = [1./w' Ukl' CkL'];
save -ascii lovedisp.txt out
```

Chapter 5

Thesis Conclusions

5.0 General Conclusions

Results presented within this thesis investigated the patterns of occurrence and the underlying physical processes of two important seismological phenomena at volcanoes, earthquake swarms and volcanic tremor. Advancing towards the goal of eruption forecasting, several new contributions were made, including; the creation of the Global Volcanic Earthquake Swarm Database (Chapter 2); an understanding of the frequency-size scaling of volcanic tremor, (Chapter 3); and the placement of physical constraints on tremor source processes at Arenal volcano (Chapter 4). The swarm database has had the most immediate and direct contribution toward eruption forecasting, while the tremor studies have shed new insights on the processes underlying a ubiquitous seismic signal associated with the eruption of magma.

5.1 Volcanic Earthquake Swarms

The Global Volcanic Earthquake Swarm Database has provided a tool for evaluating potentially hazardous seismicity at volcanoes. The project accomplished this goal through the quantification of relevant parameters and the recognition of some precursory patterns.

In the past, basic parameters associated with volcanic earthquake swarms were alluded to, in only the most general terms. For example, in previous comparative studies of swarms, the duration of the swarms preceding eruptions was typically referred to as "lasting from days to months" [e.g. *Tokarev*, 1985; *Newhall and Dzurisin*, 1988]. The compilation of the database and

its analysis has described and quantified the distribution of this parameter, along with many others, for the first time.

The compilation of this large data set has exposed several new, general relationships between swarms and eruptions. For example, precursory swarms last longer than non-precursory swarms; somewhat longer swarms precede large eruptions; the size for the largest shock in a swarm is not a clear indicator of the likelihood of an eruption; and of precursory swarms, larger earthquakes often precede flank or large eruptions. In addition, the Generic Volcanic Earthquake Swarm Model [*McNutt and Benoit*, 1995] has also emerged from the database. This model outlines a series of processes and their associated seismicity throughout an eruption cycle and provides a framework in which to more fully evaluate seismic unrest.

These results and the information contained within the database have almost immediately proven their utility in volcanic hazard mitigation. During the March 1996 seismo-volcanic crisis at Akutan volcano the database proved to be valuable in repeatedly creating and evaluating possible eruptive scenarios. The outcome of the Akutan case study showed that an eruption was not likely. However, based on the magnitude data, if an eruption were to occur, a flank eruption was more likely then a summit eruption. Field observations conducted five months later showed extensive ground cracking suggesting that this forecast was indeed accurate.

At Akutan, only general likelihoods could be assessed. Future work with the database should subject these forecasts to more stringent rules. A probabilistic model could be created by merging the conceptual framework provided by the Generic Earthquake Swarm Model and the measured distributions of swarm parameters. The likelihood of various eruption scenarios then could be quantitatively assigned probabilities, which would be beneficial to the hazard response community. This model could be tested during the next crisis in real-time, then reevaluated, and improved.

Finally, the quantification of the swarm parameters, such as swarm duration and the magnitude of the largest earthquake, will provide constraints for theoretical models on the processes associated with the ascent and eruption of magma. Information on a variety of parameters can be supplied from the database. For example, an interesting future study may further investigate the relationship between the total moment released during a swarm and a volume change, as proposed by *McGarr* [1976]. A query could be designed to list the case studies where the total moment release and the total volume erupted was recorded. Although the database may not have all the parameters needed for a particular detailed study, it will provide a solid starting point for many studies.

5.2 Volcanic Tremor

5.2.1 The Amplitude Scaling of Volcanic Tremor

Volcanic tremor is a continuous seismic signal related to pressure fluctuations associated with the transport and degassing of magma. As such, it may provide a key to characterizing the size and type of eruptions. Given the importance of this signal, the remainder of this thesis was devoted to the processes underlying volcanic tremor. Two studies were conducted, the first revealed patterns in the occurrence of tremor, while the second focused on a detailed investigation of the tremor wavefield.

A fundamental property of any physical phenomena is the relationship between its frequency of occurrence and its size. For the first time, the frequency-size distribution of volcanic tremor was systematically investigated. This study revealed that that the frequency-size or

duration-amplitude distribution of volcanic tremor is well described by an exponential scaling function, not a power-law as noted for earthquakes. This observation was shown to hold for eight different volcanoes and is associated with a range of different volcanic phenomena. The significance of this finding is that the source processes involved in the generation of volcanic tremor are not scale-invariant like earthquakes, but scale bound. This type of scaling suggests that the tremor source has a fixed spatial geometry and is driven by variable excess pressures. Given this constraint, the scaling parameter or characteristic amplitude is then proportional to the tremor's source dimensions. This result provides a new and simple method to infer the relative dimensions of the tremor source.

Tremor associated with different types of volcanic activity shows variations in its characteristic amplitudes. For example, the strongest differences appear to be between tremor associated with magmatic and phreatic activity. This result is of particular importance with respect to hazard mitigation. The difference in this parameter may provide a useful monitoring discriminant between tremor associated with magmatic and phreatic eruptions.

The examination of the scaling properties of tremor has lead to an accessory finding. The hypothesis that tremor is composed of a series of low-frequency events, spaced closely in time, is a seldom contested concept. Synthetic experiments showed, however, that given the exponential scaling of the duration-amplitude distribution, tremor is <u>not</u> composed of a series of low-frequency events spaced closely in time.

Finally, the exponential scaling of tremor demonstrates that tremor source processes are fundamentally different from those of earthquakes and provides a fundamental observational constraint which future theoretical tremor source models need to reconcile.

Future work with the scaling of tremor will hopefully collect more data sets with accessory information on the source size to further constrain the link between the scaling parameters and the source dimensions.

5.2.2 The Tremor Source: A Case Study

The second tremor study examined the details of the tremor wavefield at Arenal volcano, Costa Rica. The tremor at Arenal provided a superb data set to study tremor source processes. The main advantages at Arenal were the high signal-to-noise ratio for tremor and the temporal variation in frequency, which can only be caused by source effects. A new tremor source model was developed and provided new constraints on shallow degassing processes occurring within the shallow conduit during eruptions. The model was developed on three primary observations, patterns in the spectra, rapid changes in polarization of the wavefield, and the abrupt cessation of the tremor.

The model suggests that the observed spectral patterns are the resonance modes of a 1-D, gas-charged, magma-filled conduit and the rapid changes in the spectra are due to degassing of the magma at shallow depths within the conduit. This "organ-pipe" model has been suggested previously [e.g. *Schick*, 1982; *McNutt*, 1986; *Mori*, 1989], but the Arenal case study documents perhaps the clearest example of this type of tremor recorded to date. The Arenal data have led to new ideas and constraints on the "organ-pipe" model. Among these are: the observed frequency changes are due to changes in gas content, not length; the realization that the resonator boundaries may be controlled by velocity contrasts within the conduit; evidence for source depth changes; and a model to explain how the tremor suddenly stops.

Although new ideas were generated from a limited single station deployment, a great deal more could be gained by revisiting Arenal. Future work is needed to test some of the components of the model with additional instruments. The deployment of a small array of seismometers, to measure phase velocities for example, would help greatly in constraining the wave types and polarization effects due to shallow structure. Finally, numerical modeling may yield new insights on the nature of this type of tremor source. For example, the mode structure within a resonator with a non-linear velocity structure can be calculated using the method of characteristics. The resulting synthetics then could be compared with existing data to refine the models of the acoustic velocity structure within the conduit.

5.3 References

McGarr, A., Seismic moments and volume change, *J. Geophys. Res.*, 81: 1487-1494, 1976.

McNutt, S. R., Observations and analysis of B-type earthquakes, explosions, and volcanic tremor at Pavlof Volcano, Alaska, *Bull. Seis. Soc. Amer.*, 76, 153-175, 1986.

McNutt, S. R. and J. P. Benoit, Generic Earthquake Swarm Model, (extended abs.), *Periodico di Mineralogia*, 64, 229-230, 1995.

Mori, J., H. Patia, C. McKee, C. Itikarai, P. Lowenstein, P. De Saint Ours, B. Talai, Seismicity associated with eruptive activity at Langila Volcano, Papua New Guinea, *J. Volcanol. Geotherm. Res.*, 38, 243-255, 1989.

Newhall, C. G., and D. Dzurisin, Historical unrest large calderas of the world, US Geol. Survey Bull. 1855, 1108 p., 1988.

Schick, R., G. Lombardo, G. Patane, Volcanic tremors and shocks associated with eruptions at Etna, (Sicily), September 1980, *J. Volc. Geotherm. Res.*, 14, 261-279, 1982.

Tokarev, P. I., The prediction of large explosions of andesitic volcanoes, *J. Geodynam.*, 3, 219-244, 1985.

IMAGE EVALUATION TEST TARGET (QA-3)

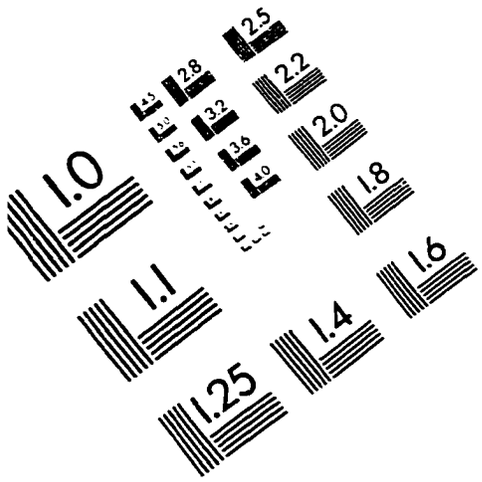

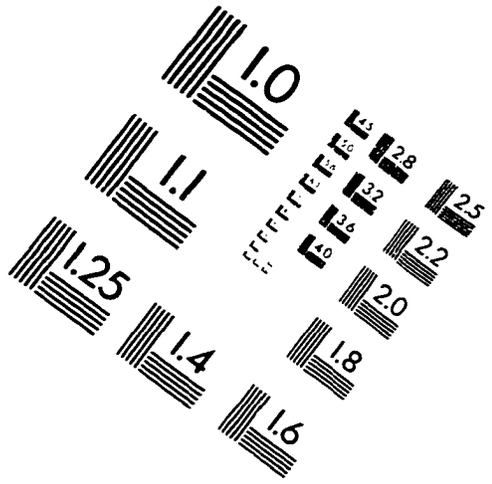

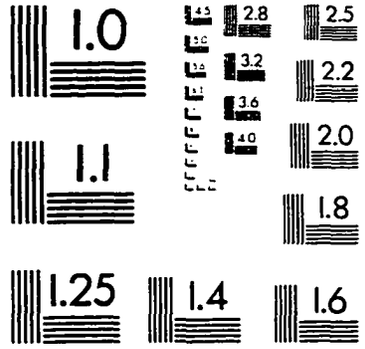

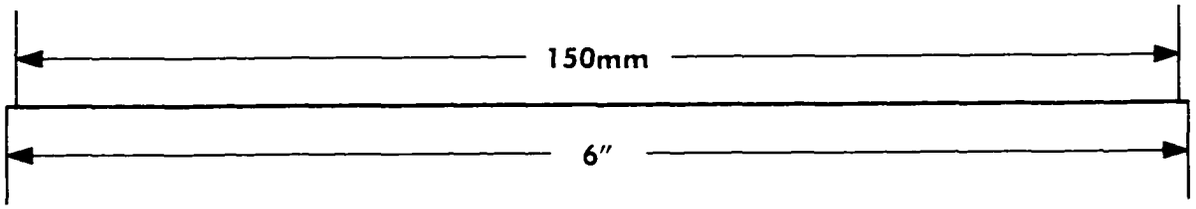

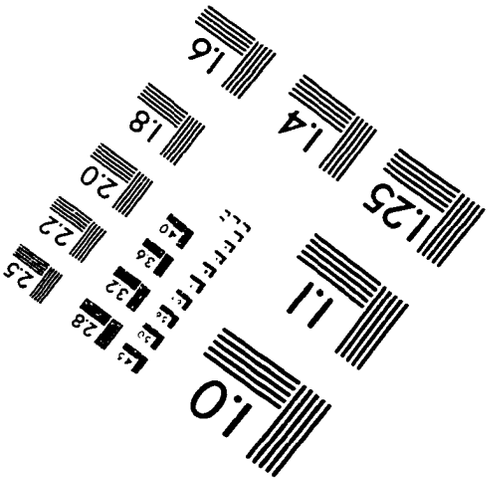

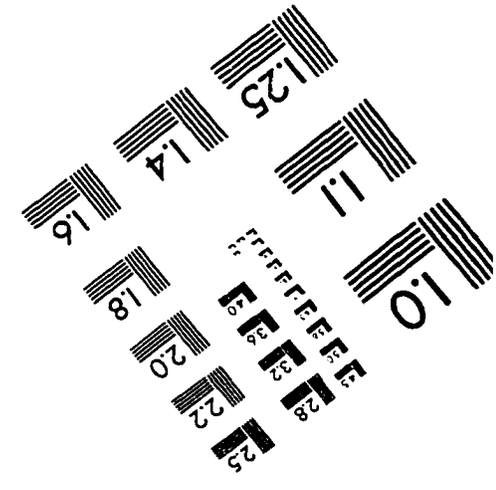

APPLIED IMAGE, Inc
1653 East Main Street
Rochester, NY 14609 USA
Phone: 716/482-0300
Fax: 716/288-5989